

**DYNAMICS OF PARTS ON NARROW TRACKS
USING THE MULTIBODY THEORY**

By

James Díaz González

A thesis submitted in partial fulfillment of the requirements for the degree of

MASTER of SCIENCE
in
MECHANICAL ENGINEERING

**UNIVERSITY OF PUERTO RICO
MAYAGÜEZ CAMPUS**

2004

Approved by:

Lourdes M. Rosario, Ph.D.
Chairperson

Date

Frederick Just-Agosto, Ph.D.
Member, Graduate Committee

Date

David Dooner, Ph.D.
Member, Graduate Committee

Date

Sonia M. Bartolomei Suárez, Ph.D.
Representative of Graduate Studies

Date

Paul Sundaram, Ph.D.
Director of the Mechanical Engineering Department

Date

Abstract

The vibratory feeder is used to feed parts in manufacturing processes. This work applied the multibody theory to describe the dynamic behavior of rectangular and cylindrical parts. The analysis studied the following cases: insulated part, part on the horizontal plane, and part on an inclined track. A new model was proposed to find the average transportation velocity to feed rectangular parts. The Coulomb friction and the Newtonian impact theories were used to describe the influence of the effects of the friction and part elasticity into the analysis. The multibody theory is complemented with the screw theory for the analysis of the cylindrical part on the horizontal plane. These results are employed in the simulation of the dynamic part. The simulation shows the importance of the friction coefficient in the dynamic of the part on the horizontal plane and on inclined plane. The results were compared with real data of other works. The results show correlation with this data.

Resumen

El alimentador vibratorio es usado para alimentar piezas industrialmente. Este trabajo usó la teoría de multicuerpos para describir el comportamiento dinámico de piezas rectangulares y cilíndricas. Para este análisis se estudiaron los siguientes casos: piezas aisladas, piezas sobre una superficie plana y piezas sobre un plano inclinado. Además se incluye un análisis completo de piezas rectangulares sobre el carril incluyendo para ello todos los parámetros geométricos del mismo. Se propuso un nuevo modelo para calcular la velocidad promedio de transporte de piezas. Las teorías de fricción de Coulomb y la de impacto de Newton fueron usadas para describir la influencia de la fricción y la elasticidad dentro del análisis. Se empleó la teoría del tornillo como complemento para el análisis de multicuerpos de la pieza cilíndrica sobre un plano horizontal. Estos resultados se simularon y se compararon con datos reales obtenidos en otros trabajos de investigación obteniéndose una buena correlación. La simulación muestra la importancia del coeficiente de fricción en la dinámica de piezas sobre un plano horizontal y sobre un plano inclinado.

Dedication

To God who guide me in all time of my life carried me every time higher.

To my parents, Jesús and Deris, who are my bigger treasure.

To my wife, Doris, for her support, for the good times and moments we shared together.

To my son, Jesús, for teaching me to be a father.

Acknowledgement

I acknowledge the guidance of my thesis advisor Dr Lourdes M. Rosario for her advice and support throughout the course of this study. I would like to thank the Mechanical Engineering Department, University of Puerto Rico Mayagüez Campus for giving me the opportunity to work in my master degree and supporting me economically during those years. I wish to express my gratitude to Dr. David Dooner for his interest in my research and his guidance.

Table of contents

ABSTRACT	ii
RESUMEN	iii
DEDICATION	iv
ACKNOWLEDGEMENT	v
CHAPTER 1 INTRODUCTION	1
1.1 JUSTIFICATION	2
1.2 OBJECTIVES	3
CHAPTER 2 LITERATURE REVIEW	4
2.1 MULTIBODY THEORY	6
2.1.1 CONTACT KINEMATICS	7
2.1.2 IMPACT NEWTON'S THEORY	8
2.2 SCREW THEORY	9
2.2.1 VECTOR REPRESENTATION	9
2.2.2 THE VELOCITY, MOMENTUM AND FORCE SCREWS	10
2.3 SUMMARY	12
CHAPTER 3 DYNAMIC ANALYSIS WITH MULTIBODY THEORY	13
3.1 INTRODUCTION	13
3.2 MODELING OF RECTANGULAR PARTS	13
3.2.1 INSULATE RECTANGULAR PART	14
3.2.2 RECTANGULAR PART ON THE HORIZONTAL PLANE	19
3.2.3 RECTANGULAR PART ON THE INCLINED PLANE	21
3.2.4 RECTANGULAR PART ON THE NARROW TRACK	23
3.2.5 CONTACT BETWEEN TWO RECTANGULAR PARTS	28

3.3 MODELING OF CYLINDRICAL PARTS	34
3.3.1 INSULATE CYLINDRICAL PART	34
3.3.2 CYLINDRICAL PART ON HORIZONTAL PLANE	39
3.3.3 CYLINDRICAL PART ON THE INCLINED PLANE	41
3.3.4 CONTACT BETWEEN TWO CYLINDRICAL PARTS	43
3.4 SUMMARY	50
<u>CHAPTER 4 DYNAMIC ANALYSIS WITH SCREW THEORY</u>	<u>51</u>
4.1 INTRODUCTION	51
4.2 WRENCH ANALYSIS	52
4.3 ANALYSIS DYNAMIC OF CYLINDRICAL PART USING SCREW THEORY	54
4.4 SUMMARY	59
<u>CHAPTER 5 CASES ANALYSIS</u>	<u>60</u>
5.1 INTRODUCTION	60
5.2 ANALYSIS OF CYLINDER ON THE PLANE SURFACE	61
5.3 ANALYSIS OF A RECTANGULAR PART ON THE NARROW TRACK	77
5.4 COMPARISON OF RESULTS	83
<u>CHAPTER 6 CONCLUSIONS AND RECOMMENDATIONS</u>	<u>85</u>
6.1 CONCLUSIONS	85
6.2 RECOMMENDATIONS	87
<u>BIBLIOGRAPHY</u>	<u>88</u>

List of figures

Figure 2.1 General orientations of two bodies.....	7
Figure 3.1 Coordinates and parameters of insulate parts.....	14
Figure 3.2 Free body diagram for the insulate part.....	14
Figure 3.3 Limit conditions for the rectangular part. Friction coefficient versus inclination angle.....	18
Figure 3.4 Axes and parameters of a rectangular part on the horizontal plane	19
Figure 3.5 Free body diagram of rectangular parts on horizontal plane.....	20
Figure 3.6 Rectangular part on inclined plane.....	22
Figure 3.7 Free body diagram of rectangular part on inclined plane.....	22
Figure 3.8 Part on the narrow track: (a) part, floor and wall, (b) plan view, (c) section view and (d) side view	24
Figure 3.9 Geometric dimensions of a rectangular part.....	24
Figure 3.10 Free body diagram of the rectangular part on the narrow track.	25
Figure 3.11 Vector diagram for the contact between two rectangular parts.	28
Figure 3.12 Vector diagram before impact (rectangular parts).....	29
Figure 3.13 Vector diagram after impact (rectangular parts).	29
Figure 3.14 (a) Position coordinates; (b) Free body diagram for contact edge;	35
Figure 3.15 Limit conditions for the cylindrical part: Friction coefficient versus inclination angle.....	38
Figure 3.16 Axes and parameters of cylindrical part on horizontal plane.....	39
Figure 3.17 Free body diagram of a cylindrical part on the horizontal plane.....	40

Figure 3.18 Axes and parameters of cylindrical part on inclined plane.	41
Figure 3.19 Free body diagram for a cylindrical part on inclined surface.....	42
Figure 3.20 Vector diagram for the contact between two rectangular parts.....	44
Figure 3.21 Contact forms between two cylindrical parts. Edge-plane, (b) Edge-curved surface, (c) plane-plane, (d) curved surface-curved surface and (e) Plane-curved surface.	45
Figure 3.22 Vector diagram before impact (cylindrical parts).	46
Figure 3.23 Vector diagram after impact (cylindrical parts).	46
Figure 4.1 External forces on a cylindrical part.....	52
Figure 4.2 Resultant wrench.	52
Figure 4.3 Coordinates frame of a cylindrical part in rolling.	54
Figure 4.4 Forces on a cylindrical part.	57
Figure 5.1 Acceleration in the x direction versus the excitation angles for cylindrical part on plane surface (surface).	61
Figure 5.2 Acceleration in the x direction versus the excitation angles for cylindrical part on plane surface (contour lines).	62
Figure 5.3 Acceleration in the x direction versus the excitation angle β and friction coefficient for cylindrical part on plane surface (surface).	63
Figure 5.4 Acceleration in the x direction versus the excitation angle β and friction coefficient for cylindrical part on plane surface (contour lines).	63
Figure 5.5 Acceleration in the x direction versus the frequency (f) and friction coefficient for cylindrical part on plane surface. Surface.	64
Figure 5.6 Acceleration in the x direction versus the frequency (f) and friction coefficient for cylindrical part on plane surface (contour lines).	65
Figure 5.7 Acceleration in the x direction versus the frequency (f) and vibration angle (β) for cylindrical part on plane surface (surface).	66
Figure 5.8 Acceleration in the x direction versus the frequency (f) and vibration angle (β) for cylindrical part on plane surface (contour lines).	66
Figure 5.9 Acceleration in the x direction versus the frequency (f) and vibration amplitude for cylindrical part on plane surface (surface).	67

Figure 5.10 Acceleration in the x direction versus the frequency (f) and vibration amplitude for cylindrical part on plane surface (contour lines).....	68
Figure 5.11 Acceleration in the y direction versus the excitation angles of the vibration force for cylindrical part on plane surface (surface).....	69
Figure 5.12 Acceleration in the y direction versus the excitation angles of the vibration force for cylindrical part on plane surface (contour lines).....	69
Figure 5.13 Acceleration in the y direction versus the excitation angle β and the friction coefficient for cylindrical part on plane surface (surface).....	70
Figure 5.14 Acceleration in the y direction versus the excitation angle β and the friction coefficient for cylindrical part on plane surface (contour lines).....	71
Figure 5.15 Acceleration in the y direction versus the excitation angle β and the frequency for cylindrical part on plane surface (surface).....	72
Figure 5.16 Acceleration in the y direction versus the excitation angle β and the frequency for cylindrical part on plane surface (contour lines).....	72
Figure 5.17 Acceleration in the y direction versus the frequency and the friction coefficient for cylindrical part on plane surface (surface).....	73
Figure 5.18 Acceleration in the y direction versus the frequency and the friction coefficient for cylindrical part on plane surface (contour lines).....	74
Figure 5.19 Angular acceleration versus the excitation angles α and β for cylindrical part on plane surface (surface).....	75
Figure 5.20 Angular acceleration versus the excitation angles α and β for cylindrical part on plane surface (contour lines).....	75
Figure 5.21 Acceleration in the y direction versus the excitation angles α and β for cylindrical part on plane surface.....	76
Figure 5.22 Transportation velocity versus frequency and amplitude of vibration.....	77
Figure 5.23 Transporting velocity versus inclination angle and vibration amplitude.	78
Figure 5.24 Transportation velocity versus frequency and excitation angle.....	79
Figure 5.25 Transportation velocity versus excitation angles.....	80
Figure 5.26 Transportation velocity versus excitation angles.....	81
Figure 5.27 Transportation velocity versus friction coefficient and frequency.....	82

Figure 5.28 Comparison of results for transportation velocity (Wolfsteiner and Pfeiffer).
..... 83

Figure 5.29 Comparison of results for the transportation velocity: B= Boothroyd (1992),
J= Proposed Model. 84

Nomenclature

α :	Excitation angle respect to x axis.
β :	Excitation angle respect to xy plane.
γ :	Inclination angle of the narrow around y axis.
δ :	Inclination angle of the narrow around x axis.
ε :	Restitution coefficient.
ε :	Dual number.
ζ :	Internal angle of part.
η :	Axis perpendicular to the center axis of the cylindrical part.
θ :	Rotation angle about z axis.
θ_A :	Rotation angle about z axis of part A.
θ_C :	Rotation angle about z axis of part C.
λ_N :	Normal force between two surfaces.
λ_T :	Friction force.
λ_{Tx} :	Friction force between two surfaces in the x direction.
λ_{Tx1} :	Friction force between two surfaces in the x direction with normal force λ_1 .
λ_{Tx2} :	Friction force between two surfaces in the x direction with normal force λ_2 .
λ_{Ty} :	Friction force between two surfaces in the y direction.
λ_{Tz1} :	Friction force between two surfaces in z direction with normal force λ_1 .
λ_{Tz2} :	Friction force between two surfaces in z direction with normal force λ_2 .
λ_1 :	Normal force between two surfaces in the point #1.
λ_2 :	Normal force between two surfaces in the point#2.
μ_k :	Kinetic friction coefficient.
μ_s :	Static friction coefficient.
ξ :	Inclination angle of part.
ς :	Axis parallel to the center axis of the cylindrical part.
σ :	Application angle of the normal force between the part and the bowl wall.
τ :	Parameter for to simplify the normal relative acceleration.

φ :	Rotation angle about x axis.
χ :	Parameter for to simplify the normal relative acceleration.
ω :	Angular frequency of vibration.
A_0 :	Vibration amplitude.
a_x :	Acceleration in the x direction.
a_y :	Acceleration in the y direction.
a_z :	Acceleration in z direction.
a :	Part width.
b :	Part high.
h :	Part length.
$[A_m]_n$:	Rotation matrix.
$[T_m]_n$:	Transformation matrix.
Λ_N :	Force impulsive.
$[M]$:	Mass matrix.
W_N :	Geometric matrix.
q :	Generalized coordinates vector.
q_E :	Generalized coordinates vector in expansion.
q_A :	Generalized coordinates vector in approximation.
F_x :	Forces in the x direction.
F_y :	Forces in the y direction.
F_z :	Forces in z direction.
m_p :	Part mass.
M_x :	Moments in the x direction.
M_y :	Moments in the y direction.
M_z :	Moments in z direction.
I :	Inertial moment of the part.
K :	Abbreviation.
\overrightarrow{AG} :	Position vector directed from point A to the mass center G.
G^{-1}_N :	Reduce mass of multibody system.
g :	Gravity acceleration.

g_N :	Relative distance in normal direction.
$\dot{\vec{g}}_{NA}$:	Relative velocity of approximation.
$\dot{\vec{g}}_{NE}$:	Relative velocity of approximation.
g_T :	Relative distance in tangential direction.
\vec{r}_1 :	Position vector of mass center of part #1
\vec{r}_2 :	Position vector of mass center of part #2
$\vec{r}_{1/2}$:	Relative position vector between parts 1 and 2.
$\ \vec{r}\ $:	Vector position magnitude.
$\ \vec{r}\ _{\max}$:	Maximum distance between two parts mass center.
$\ \vec{r}\ _{\min}$:	Minimum distance between two parts mass center.
r :	Cylindrical part radius.
R :	Feeder radius.
v :	Transportation velocity.
\vec{V} :	Linear velocity vector.
\hat{t} :	Unit vector tangent to surface.
\hat{p} :	Unit vector tangent to surface and perpendicular to \hat{t} .
\hat{n} :	Unit vector normal to surface.
x :	Fixed axis.
y :	Fixed axis.
z :	Fixed axis.
x_1 :	Mobile axis fixed to part 1.
y_1 :	Mobile axis fixed to part 1.
z_1 :	Mobile axis fixed to part 1.
$\hat{\$}$:	Screw.
$\hat{\$}_V$:	Velocity screw.

- $\hat{\$}_H$: Momentum screw.
- \bar{q} : Linear momentum vector.
- $\hat{\$}_N$: Derivate of the momentum screw.
- $\hat{\$}_P$: Screw cross product between velocity and momentum screw.
- $\hat{\$}_F$: Force screw.

CHAPTER 1

Introduction

The vibratory bowl feeder is used to feed parts industrially. It is able to guide, transport, store and orient the parts for their assembly. During this process the parts collide with the feeder's track and their walls. This collision can be studied under the multibody pattern assuming zero deformation or a rigid body model. This work will be based on this assumption for rectangular and cylindrical parts. The parts orientations are analyzed based on theories such as the Solid Angle and the Energy Barrier Methods. These theories are based in geometrical assumptions as areas and angles (Boothroyd, 1994). These theories are statically correct for simple part geometries but need to be adjusted for applications in the dynamic cases. This study complements these theories with a classic dynamic analysis.

The equations of motion for a multibody system can be derived using the Newtonian theory or Energy principle. The Newtonian theory advantage over the Energy principle is that it provides the accelerations and forces directly.

1.1 Justification

The multibody theory allows the development of kinematic and kinetic relationships of the interaction of interconnected bodies to describe their behavior in a combined and non-singular way. The multibody theory is a compact way to describe the dynamic behavior of interconnected bodies. The collision of bodies occurs when the interaction time of two or more bodies is short and the interaction forces are very large. This collision affects each of the parts that conform the group "multibody" differently. The collision of interconnected bodies is the physical phenomenon of the parts and bowl tracks, between parts and bowl walls or between parts. This theory will provide tools that will improve the design process of devices and parameters within the bowl.

For the study of this phenomenon, the first thing that should be specified is the frame or reference axes that describe the movement in an absolute or relative way. This frame can be of zero movement, called Newtonian frame, or permanent or intermittent movement, called relative movement frame. Newton's law of impact establishes that the relative speeds of the contact point determine the components of the impulsive force that can describe the movement after the collision.

Friction is fundamental for transportation dynamics. Consequently, an analysis will be done taking into account frictional effects. The main objective of this work is to dynamically simulate the parts with the help of the multibody and screw theories. This analysis is based in the dynamic behavior of the impact. It is convenient for the natural rest study including the impact effect. The result of the analysis will be a new description of physical phenomenon based in dynamic assumptions for the rectangular and cylindrical parts.

The spatial geometry and mechanical properties of the parts, requires an individual adaptation of the feeder parameters, such as orientating device geometries, inclination angles and frictional properties. Due to the complex mechanics of the feeding process the design of the feeders is currently performed by trial and error, Wolfsteiner and Pfeiffer (2000). The current dynamic theories about feeding process, propose a two-dimensional model, Boothroyd (1992). The two-dimensional model does not include the centripetal effects caused by the wall curvature. A three-dimensional dynamic model for rectangular and cylindrical parts allows a theoretical investigation and an improvement in the properties of the feeder.

1.2 Objectives

The research objectives of this work are:

- To develop a numerical analysis of the dynamic behavior of rectangular and cylindrical parts in the feeder based on the multibody theory.
- To make a kinematic study of cylindrical parts using the screw theory.
- To study the dynamics of the parts on the bowl track considering the combined part - track as a multibody system.

CHAPTER 2

Literature Review

The multibody dynamics is studied from the impact and direct contact perspective. The analysis can be made with force or energy methods. The formulation of multibody dynamics with rigid contacts can be the theoretical basis to develop new sophisticated models of contact-impact laws.

Andreas and Casini (1999) modeled the case of three blocks assembled with deformable contact. First, they described the pattern from the rigid perspective and with the deformable formulation. They proposed a model of contact force that is appropriate for the study of the multibody dynamics with restricted unilateral contact. In the second part they showed the application of this proposed model for the trilith (the simplest scheme of a colonnade to a temple) to half-sine-wave pulse and to horizontal harmonic ground motion. According to this model they identified three motion areas: rest, stable motion and collapse.

Chang and Huston (2001) presented a computational procedure for the analysis of impact in multibody systems by combining the Newtonian theory of impact and dynamic of the multibody. Their work is applicable to the design and analysis of couplers, latches, docking mechanisms and grippers. They considered the collision between two multibody system and the internal collisions for the same multibody system. They also provided a method to find velocity changes during impact and to determine impulse at the point of contact and the motion after the collision. The procedure is applicable to the collision decoupled multibody system and for collisions of bodies within a single constrained multibody system.

Gerstmayr and Schöberl (2002) combined the dynamics of multibody systems and numerical analysis techniques to study the field of 3D deformable multibody dynamics. Two analysis methods were used: (i) the finite element for small deformation and (ii) the Lagrangian description of the deformation including large deformation, displacements and rotations. The formulation is capable to treat small nonlinear effects like geometric stiffening by introducing additional rotational degrees of freedom for every single body. Small deformation means that its value is less or equal to the two percent of yield deformation and large deformation is on the contrary.

Pennock and Meehan (2002) used the geometric relationships between the velocity screw and momentum screw to describe the kinetic of rigid body. They defined the centripetal screw, and they explained the significance of this screw in a study of the dynamics of a rigid body. The method presented in this paper will prove useful in a dynamic analysis of closed-loop spatial mechanism and multi-rigid body open-chain system.

Huang and Wang (2003) utilized Dimentberg's definition of pitch to demonstrate that all possible screws for displacing a line from one position to another can indeed form a screw system of the third order. Two different approaches are taken: one uses the concept of a screw triangle, and the other is based on analytical geometry. They demonstrated that, by using Dimentberg's definition of pitch, the displacement screws can indeed form a screw system of the third order. The screw system derived in this paper can be useful in applications where only certain line elements of a rigid body are of interest. These applications include the displacements of a cylindrical joint and light source.

Pennock and Oncu (1992) applied screw theory to the dynamic analysis of a rigid body in general spatial motion. This research placed emphasis upon the geometric interpretation of the velocity, the momentum, and the force screw. The dynamic state of motion of the rigid body is described by a dual vector equation, referred to as the dual Euler equation. The geometric approach presented in this paper proves useful in the graphical representation of the dynamics of a rigid body.

2.1 Multibody Theory

The parts motion is composed of translations and rotations around an axis. The Kardan angles for three elementary rotations are given, Pfeiffer and Glocker (1996):

$$A_\alpha = \begin{pmatrix} 1 & 0 & 0 \\ 0 & \cos(\alpha) & -\sin(\alpha) \\ 0 & \sin(\alpha) & \cos(\alpha) \end{pmatrix}; A_\beta = \begin{pmatrix} \cos(\beta) & 0 & \sin(\beta) \\ 0 & 1 & 0 \\ -\sin(\beta) & 0 & \cos(\beta) \end{pmatrix}; A_\gamma = \begin{pmatrix} \cos(\gamma) & -\sin(\gamma) & 0 \\ \sin(\gamma) & \cos(\gamma) & 0 \\ 0 & 0 & 1 \end{pmatrix} \quad (2.1)$$

where the transformation from B to R is $A_{RB} = A_\gamma A_\beta A_\alpha$

The sequence is $B \xrightarrow{A_\alpha} B_1 \xrightarrow{A_\beta} B_2 \xrightarrow{A_\gamma} R$

The equation motion for rigid body systems without unilateral constraint is

$$\left\{ \begin{pmatrix} \dot{\mathbf{p}} \\ \dot{\mathbf{L}} \end{pmatrix} - \begin{pmatrix} \mathbf{E} & \mathbf{0} \\ \tilde{\mathbf{r}}_{S_A} & \mathbf{E} \end{pmatrix} \begin{pmatrix} \mathbf{F}_A \\ \mathbf{M}_A \end{pmatrix} - \begin{pmatrix} \mathbf{E} & \mathbf{0} \\ \tilde{\mathbf{r}}_{S_P} & \mathbf{E} \end{pmatrix} \begin{pmatrix} \mathbf{F}_P \\ \mathbf{M}_P \end{pmatrix} \right\}_i = \mathbf{0}$$

$i = 1, \dots, n,$ (2.2)

with

$$\begin{pmatrix} \dot{\mathbf{p}} \\ \dot{\mathbf{L}} \end{pmatrix} = \begin{pmatrix} m \mathbf{E} & \mathbf{0} \\ \mathbf{0} & \mathbf{I}_s \end{pmatrix}_i \begin{pmatrix} \dot{\mathbf{v}}_s \\ \dot{\boldsymbol{\Omega}} \end{pmatrix}_i + \begin{pmatrix} \mathbf{0} \\ \tilde{\boldsymbol{\Omega}} \mathbf{I}_s \boldsymbol{\Omega} \end{pmatrix}_i$$

where $\dot{\mathbf{p}}$ and $\dot{\mathbf{L}} \in \mathbb{R}^3$ respectively

The subscript s denotes the center of mass of the rigid body under consideration, \mathbf{I}_s is the inertial matrix, \mathbf{E} is the identity matrix, \mathbf{M}_P is moments vector, $\boldsymbol{\Omega}$ is the angular velocities vector, \mathbf{F} is the force vector and $\tilde{\mathbf{r}}$ is the position vector.

2.1.1 Contact Kinematics

The characteristic vectors for the contact point of the two bodies are shown in figure 2.1. The Vectors \mathbf{t} and \mathbf{n} are perpendicular vectors. Therefore, $\mathbf{n}_i \cdot \mathbf{t}_i = 0$.

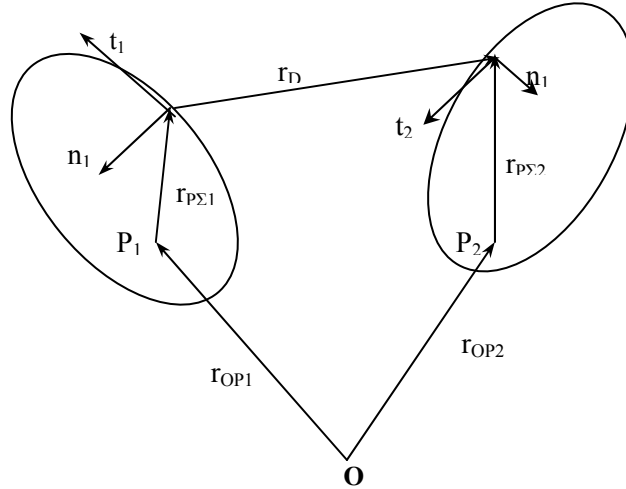


Figure 2.1 General orientations of two bodies

The distance between bodies g_N is

$$\begin{aligned} \mathbf{g}_N(\mathbf{q}, t) &= r_D \mathbf{n}_2 = -r_D \mathbf{n}_1 \\ \text{if} & \\ \mathbf{n}_1 &= -\mathbf{n}_2; \mathbf{t}_1 = -\mathbf{t}_2; \mathbf{b}_1 = \mathbf{b}_2 \end{aligned} \quad (2.3)$$

2.1.2 Impact Newton's theory

The impact theory formulated for Newton is a relation that describes the energy loss factor of impact, Pfeiffer and Glocker (1996). The energy loss factor is called the coefficient of restitution ε . This coefficient is

$$\begin{aligned} \dot{\mathbf{g}}_{NE} &= -\bar{\varepsilon}_N \dot{\mathbf{g}}_{NA} \\ \bar{\varepsilon}_N &= \text{diag}\{\varepsilon_{Ni}\} \end{aligned} \quad (2.4)$$

Where $\dot{\mathbf{g}}_{NE}$ and $\dot{\mathbf{g}}_{NA}$ are the relative velocities before and after the impact respectively.

The range value for the restitution coefficient is $0 \leq \varepsilon \leq 1$. The expression for the impact force is:

$$\Lambda_N = -G_N^{-1} (E + \bar{\varepsilon}) \dot{\mathbf{g}}_{NA} \quad (2.5)$$

The term G_N^{-1} corresponds to the reduced mass of the multibody system, Λ_N is the impulsive force in normal direction, and E is the identity matrix. The Coulomb friction equation is a linear approximation of the relationship between the friction force and the normal contact force. The Coulomb friction is given by

$$\lambda_{Ti} = -\mu_i \lambda_{Ni} \text{sing}(\dot{\mathbf{g}}_{Ti}) ; \lambda_{Ni} \geq 0 \quad (2.6)$$

Where μ_i is the coefficient of friction of the i th sliding contact, λ_{Ni} is the corresponding normal force which is assumed to act only as a compressive force ($\lambda_{Ni} \geq 0$), and the sing function includes the opposite direction of relative velocity respect to the friction force.

2.2 Screw Theory

The Screw is associated with motion. However; it can be associated with other physical quantities like the load on a body. The Screw was defined by Sir Robert Stawell Ball in 1990 as follows: “A screw is a straight line with which a definite magnitude termed the pitch is associated.” Screw is a geometrical element that has the parameter h attached to it. This parameter h is called the pitch of the screw. The pitch measures linear advancement along the axis per unit rotation about the axis.

Screw theory is based on two fundamental theorems, Lipkin and Duffy (2002):

1. *Chasles' theorem*. Rigid-body motion is equivalent to *twist on a screw*, i.e. a rotation along a unique axis and a translation parallel to the axis.
2. *Poinsot's theorem*. Rigid-body action is equivalent to a *wrench on a screw*, i.e. a force along a unique line and a couple parallel to the line.

2.2.1 Vector Representation

A screw quantity is represented using a pair of vectors. Let ω be the angular velocity of the body about the screw axis of the twist. Points on the axis, such as A , have a parallel linear velocity $v_A = h \cdot \omega$, where h is the pitch of the screw. If point A is known, then the vector pair (ω_A, v_A) is sufficient uniquely to specify the twist. Similarly, let f be the force on the body along the screw axis of the wrench. Points on the axis, such as A , have a parallel net moment $m_A = h \cdot f$, where h is the pitch of the screw. If point A is known, then the vector pair (f, m_A) is sufficient uniquely to specify the wrench.

It is also sufficient to specify the twist or wrench using the linear velocity or net moment of any other point P on the body:

$$\begin{aligned}(\omega; v_p) &= (\omega; r_p \times \omega + h\omega) \\(f; m_p) &= (f; r_p \times f + hf)\end{aligned}\tag{2.7}$$

Where r_p is vector from P to axis. All screw quantities can be expressed as scalar multiples of a screw $(\mathbf{S}; \mathbf{S}^o)$, so for a twist and a wrench.

$$\begin{aligned}\omega(\mathbf{S}; \mathbf{S}^o) &= \omega(\mathbf{S}; r_p \times \mathbf{S} + h\mathbf{S}) \\f(\mathbf{S}; \mathbf{S}^o) &= f(\mathbf{S}; r_p \times \mathbf{S} + h\mathbf{S})\end{aligned}\tag{2.8}$$

Where \mathbf{S} is a unit vector along the screw axis, ω is called the amplitude of the twist and f is called the intensity of the wrench. The pitch and perpendicular vector a screw axis are given by:

$$\begin{aligned}h &= \frac{\mathbf{S} \cdot \mathbf{S}^o}{\mathbf{S} \cdot \mathbf{S}} \\r_{\perp} &= \frac{\mathbf{S} \times \mathbf{S}^o}{\mathbf{S} \cdot \mathbf{S}}\end{aligned}\tag{2.9}$$

A pure rotation has $h=0$ since all points long the axis are stationary. A pure force has $h=0$ since all moments about the axis are zero. A pure translation has $h=\infty$ and a pure couple has $h=\infty$.

2.2.2 The velocity, momentum and force screws

The velocity of a rigid body is completely specified, by the angular velocity vector $\vec{\omega}$, and the linear velocity vector \vec{V}_A of an arbitrary point A fixed in the body, Pennock and Oncu (1992).

The screw velocity is then

$$\hat{\$}_{\hat{V}_A} = (\vec{\omega}; \vec{V}_A) = \vec{\omega} + \varepsilon \vec{V}_A \quad (2.10)$$

the dual operator is defined as ε where $\varepsilon^2=0$, and has the dimension $[L]^{-1}$.

The linear momentum vector of the mass center of the rigid body can be written as:

$$\vec{q} = m(\vec{V}_A + \vec{\omega} \times \overline{AG})$$

where m is the mass of the body and \overline{AG} is the position vector directed from point A to the mass center G. The angular momentum vector, about the arbitrary point A fixed in the body, can be written as:

$$\vec{H}_A = [I_A] \vec{\omega} + m(\overline{AG} \times \vec{V}_A) \quad (2.11)$$

where $[I_A]$ is the (3x3) inertia matrix referred to point A.

The momentum screw is defined as the combination of linear and angular momentum vectors, Pennock and Oncu (1992).

$$\hat{\$}_{\hat{H}_A} = (\vec{q}; \vec{H}_A) = \vec{q} + \varepsilon \vec{H}_A \quad (2.12)$$

The cross product of the velocity screw and the momentum screw is other screw which will, henceforth, be denoted as

$$\hat{\$}_{\hat{P}_A} = \hat{\$}_{\hat{V}_A} \otimes \hat{\$}_{\hat{H}_A} \quad (2.13)$$

the cross product of the equation 2.13 is a special operation between screws. This operation can be derived as the cross product between two dual vectors:

$$\$1 \otimes \$2 = (s_1 + \varepsilon \cdot s_1^o) \times (s_2 + \varepsilon \cdot s_2^o) = s_1 \times s_2 + \varepsilon (s_1 \times s_2^o - s_2 \times s_1^o) \quad (2.14)$$

The resultant external force vector and the resultant external moment can be combined into the force screw

$$\hat{\$}_{F_A} = (\vec{F}; \vec{M}_A) = \vec{F} + \varepsilon \vec{M}_A$$

The dual Euler equation can be written as

$$\hat{\$}_{F_A} = \hat{\$}_{N_A} + \hat{\$}_{P_A} \quad (2.15)$$

where $\hat{\$}_{N_A}$ is the time rate of change of the momentum screw.

$$\hat{\$}_{N_A} = \dot{\$}_{H_A}$$

2.3 Summary

The necessary equations for describe the rigid body dynamic were given in this chapter. The dual Euler equation is the screw form used to describe the rigid body motion. These equations will be used in next chapter to describe the motion of rectangular and cylindrical parts on a surface.

CHAPTER 3

Dynamic Analysis with Multibody Theory

3.1 Introduction

Modeling mechanical systems requires engineering intuition and of a lot of practical imagination. The modeling process requires appropriate assumptions based on the physical nature of the problem. This chapter is divided in physical conditions for rectangular and cylindrical parts. The physical conditions are insulating the part, part on horizontal plane, part on inclined plane and interaction of the two parts. The goal of this chapter is to study the interaction of the rectangular and cylindrical parts using multibody theory. A complete mathematical formulation with a description of the physical phenomenon is provided in this chapter.

3.2 Modeling of Rectangular Parts

Rectangular parts are prisms with all the plane faces perpendicular or parallel to the motion surface. The rectangular parts are analyzed with five degrees of freedom for contact type point-surface, three degrees of freedom for contact type surface-surface and four degrees of freedom for contact type line-surface. The interaction of the parts with the bowl surfaces are the restrictions for its motion.

3.2.1 Insulate Rectangular Part

An Insulate Rectangular Part (IRP) is when the interaction between the parts is zero, but the interaction between part and bowl is not zero. This analysis is made in two dimensions.

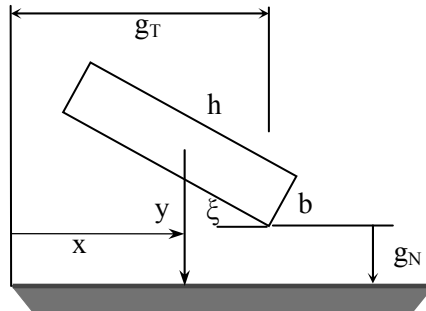


Figure 3.1 Coordinates and parameters of insulate parts.

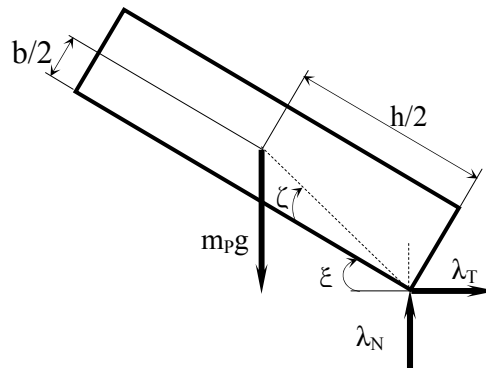


Figure 3.2 Free body diagram for the insulate part.

The generalized coordinates for this motion are $q = (x, y, \xi)$. The figure 3.1 shows the position and orientation coordinates for this IRP. The variables x and y are the horizontal and vertical positions, respectively, of mass center with respect to the fixed frame while h and b represent the length and high of the part, respectively. Figure 3.2 shows the free body diagram for an insulate part. The vectors λ_T and λ_N are the impulsive forces in the tangential and normal directions respectively.

Based on the Newton's second law:

$$\begin{aligned}
 \sum F_x : \quad m_p \ddot{x} &= \lambda_T \\
 \sum F_y : \quad m_p \ddot{y} &= \lambda_N - m_p g \\
 \sum M_0 : \quad I_{\xi} \ddot{\xi} &= -\lambda_N \left(\frac{\sqrt{h^2 + b^2}}{2} \right) \cos(\xi + \zeta) - \lambda_T \left(\frac{\sqrt{h^2 + b^2}}{2} \right) \sin(\xi + \zeta)
 \end{aligned} \tag{3.1}$$

From the geometry: $\zeta = \arctan\left(\frac{b}{h}\right)$

The goal of this section is to find the distance between the contact point and a plane surface (g_N, g_T) and its time derivatives (\dot{g}_N, \dot{g}_T) and (\ddot{g}_N, \ddot{g}_T). The distance g is:

$$g_N = y - \frac{1}{2} \sqrt{b^2 + h^2} \sin(\zeta + \xi) \tag{3.2}$$

$$g_T = x + \frac{1}{2} \sqrt{b^2 + h^2} \cos(\zeta + \xi)$$

Differentiating 3.2 with respect to t :

$$\dot{g}_N = \dot{y} - \frac{\sqrt{b^2 + h^2}}{2} \dot{\xi} \cos(\zeta + \xi) \tag{3.3}$$

$$\dot{g}_T = \dot{x} - \frac{\sqrt{b^2 + h^2}}{2} \dot{\xi} \sin(\zeta + \xi)$$

Differentiating 3.3 with respect to t

$$\ddot{g}_N = \ddot{y} - \frac{\sqrt{b^2 + h^2}}{2} \ddot{\xi} \cos(\zeta + \xi) + \frac{\sqrt{b^2 + h^2}}{2} \dot{\xi}^2 \sin(\zeta + \xi) \tag{3.4}$$

$$\ddot{g}_T = \ddot{x} - \frac{\sqrt{b^2 + h^2}}{2} \ddot{\xi} \sin(\zeta + \xi) - \frac{\sqrt{b^2 + h^2}}{2} \dot{\xi}^2 \cos(\zeta + \xi)$$

Equations 3.1 and 3.2 describe the contact state. The rectangular part has contact and can slide to right. Contact means that the distance (g_N) and the relative velocity in normal direction (\dot{g}_N) are zero.

The sliding condition occurs if $\dot{g}_T \geq 0$. Applying 2.6 it is obtained:

$$\begin{aligned} \lambda_T &= -\mu \lambda_N \text{sing}(\dot{g}_T) \\ \text{If } \dot{g}_T &\geq 0 \text{ then} \\ \lambda_T &= -\mu \lambda_N \end{aligned} \quad (3.5)$$

The term $\text{sing}(\dot{g}_T)$ is the sign function. Equations 3.1, 3.4 and 3.5 provide six equations for the six unknown accelerations ($\ddot{x}, \ddot{y}, \ddot{\xi}, \ddot{g}_N, \ddot{g}_T$) and forces (λ_N, λ_T).

Substituting 3.1 in 3.4 the relative accelerations are:

$$\begin{aligned} \ddot{g}_N &= \frac{\lambda_N}{m_p} \left(1 + \frac{b^2 + h^2}{4I} m_p \cos^2(\zeta + \xi) - \frac{\mu(h^2 + b^2)}{4I} m_p \sin(\zeta + \xi) \cos(\zeta + \xi) \right) \\ &\quad + \frac{\sqrt{b^2 + h^2}}{2} \dot{\xi}^2 \sin(\zeta + \xi) - g \end{aligned} \quad (a) \quad (3.6)$$

$$\begin{aligned} \ddot{g}_T &= \frac{\lambda_N}{m_p} \left(\mu + \frac{b^2 + h^2}{4I} m_p \cos(\zeta + \xi) \sin(\psi + \xi) - \frac{\mu(h^2 + b^2)}{4I} m_p \sin^2(\zeta + \xi) \right) \\ &\quad - \frac{\sqrt{b^2 + h^2}}{2} \dot{\xi}^2 \cos(\zeta + \xi) \end{aligned} \quad (b)$$

To simplify the analysis, equation 3.6a can be represented by:

$$\begin{aligned} \tau &= \frac{1}{m_p} \left(1 + \frac{b^2 + h^2}{4I} m_p \cos^2(\zeta + \xi) - \frac{\mu(b^2 + h^2)}{4I} m_p \sin(\zeta + \xi) \cos(\zeta + \xi) \right) \\ \chi &= g \left(\frac{1}{2g} \sqrt{b^2 + h^2} \dot{\xi}^2 \sin(\zeta + \xi) - 1 \right) \end{aligned}$$

The equation 3.6a is a linear equation with two unknowns: \ddot{g}_N and λ_N . The system is in contact if the normal force is compressive and the normal acceleration is zero ($\lambda_N \geq 0; \ddot{g}_N = 0$) or if ($\lambda_N = 0; \ddot{g}_N \geq 0$). Then, contact exists if $\ddot{g}_N \geq 0; \lambda_N \geq 0; \ddot{g}_N \lambda_N = 0$

Then $\ddot{g}_N = \tau\lambda_N + \chi$; $\ddot{g}_N \geq 0$; $\lambda_N \geq 0$; and $\ddot{g}_N\lambda_N = 0$. τ and χ may have positive or negative values depending on the parameters μ , ξ and ξ^2 . The normal relative acceleration is in linear form. The signs of τ and χ values generate the following cases of study.

Case I $\tau > 0$

- (i) If $\chi > 0$: The solution for this case is:

$$\ddot{g}_N = \chi > 0; \lambda_N = 0$$

Because the second possibility would contradict the condition $\lambda_N \geq 0$

$\left(\ddot{g}_N = 0, \lambda_N = -\frac{\chi}{\tau} < 0 \right)$. This case corresponds to separation of the body.

- (ii) If $\chi < 0$: The solution for this case is:

$$\ddot{g}_N = 0; \lambda_N = -\frac{\chi}{\tau} > 0$$

This situation corresponds to continual sliding.

Summarizing, for $\tau > 0$ the solution only is separation or continual sliding of the part.

Case II $\tau < 0$

- (i) If $\chi > 0$: The solution for this case is:

$$\ddot{g}_N = \chi > 0 \text{ and } \lambda_N = 0$$

This is a solution, but now τ is negative and thus a second solution can be found

$$\ddot{g}_N = 0; \text{ and } \lambda_N = -\frac{\chi}{\tau} > 0$$

These solutions are continual sliding and separation as case I.

(ii) If $\chi < 0$: The solution for this case is:

$$\ddot{g}_N = 0 \text{ and } \lambda_N = -\frac{\chi}{\tau} < 0$$

or

$$\ddot{g}_N = \chi < 0 \text{ and } \lambda_N = 0$$

In this case, sliding and separation are contradictory to the equation of motion and the contact law; thus the solution does not exist.

For the special case when $\tau = 0$ the solution boundary is obtained. This boundary limits the regions of positive and negative values depending on the friction coefficient μ and the part angle ξ . The boundary function is given by:

$$\mu = \frac{1 + 3 \cos^2(\zeta + \xi)}{3 \sin(\zeta + \xi) \cos(\zeta + \xi)} \quad (3.7)$$

The equation 3.7 is obtained with $I = \frac{m_p}{12}(b^2 + h^2)$. The figure 3.3 is generated plotting $\mu(\xi)$. This figure shows the lines for $\tau = 0$. The region above these lines correspond $\tau < 0$ and the region below these lines correspond to $\tau > 0$.

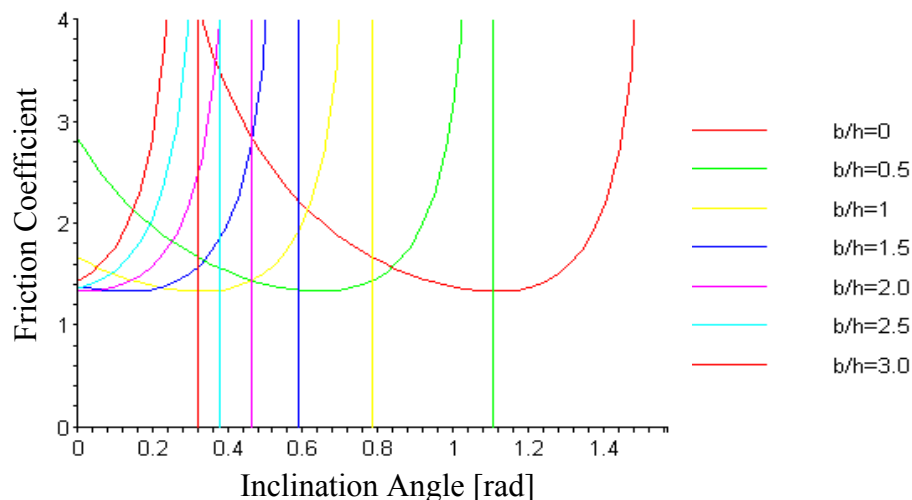


Figure 3.3 Limit conditions for the rectangular part. Friction coefficient versus inclination angle.

From figure 3.3, $\mu < 4/3$ the values of τ are always positive. If the coefficient of friction is chosen small enough ($<4/3$), then it will always provide a unique solution.

3.2.2 Rectangular Part on the Horizontal Plane

In this section a study of the physical behavior of rectangular parts on the horizontal plane will be presented. Figure 3.4 shows a drawing of a basic rectangular part with the relevant parameters for the analysis of rectangular parts on the horizontal plane. U_x represents the part displacement in the x direction; U_y represents the part displacement in the y direction; θ represents the part rotation about the z direction. It is assumed that in the x and y directions there no rotation and in the z direction there is no translation.

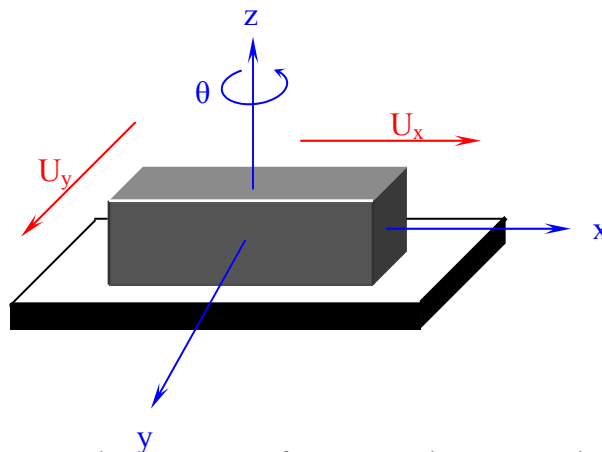


Figure 3.4 Axes and parameters of a rectangular part on the horizontal plane

A free body diagram for the rectangular part on horizontal plane is shown in Figure 3.5. λ_{Tx} and λ_{Ty} are components of the friction force, λ_N is the normal force and $m_p A_0 \omega^2$ represents the vibration force. Where m_p is the part mass, A_0 is the vibration amplitude and w is the angular frequency of vibration. The excitation angles of the vibration force are α and β .

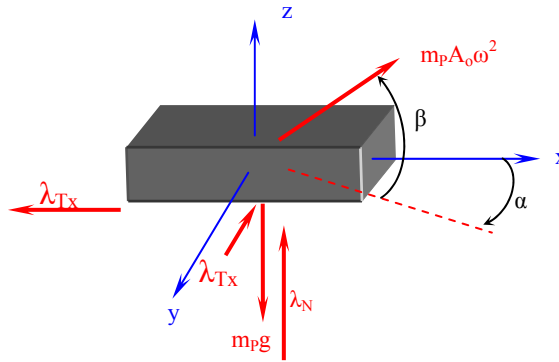


Figure 3.5 Free body diagram of rectangular parts on horizontal plane

The motion in this condition has generalized coordinates given by:

$$q = \begin{Bmatrix} x \\ y \\ z \\ \theta \end{Bmatrix}$$

where x , y and z represent the mass center position and θ is the rotation about the z axis.

Based on the Newton's second law

$$\begin{aligned} \sum F_x : m_p A_o \omega^2 \cos(\beta) \cos(\alpha) - \lambda_{Tx} &= m_p \ddot{x} \\ \sum F_y : m_p A_o \omega^2 \cos(\beta) \sin(\alpha) - \lambda_{Ty} &= m_p \ddot{y} \\ \sum F_z : m_p A_o \omega^2 \sin(\beta) - m_p g + \lambda_N &= m_p \ddot{z} \end{aligned} \quad (3.8)$$

Replacing the equation 2.6 in 3.8 it is obtained:

$$\begin{Bmatrix} \ddot{x} \\ \ddot{y} \\ \ddot{z} \end{Bmatrix} = A_o \omega^2 \begin{Bmatrix} \cos(\alpha) \cos(\beta) \\ \sin(\alpha) \cos(\beta) \\ \sin(\beta) \end{Bmatrix} - \frac{\lambda_N}{m_p} \begin{Bmatrix} \mu_k \\ \mu_k \\ \frac{m_p g}{\lambda_N} - 1 \end{Bmatrix} \quad (3.9)$$

The equation 3.9 is the force matrix form of the motion of rectangular part on the horizontal plane. This equation does not include the rotation about the z axis. The rotation matrix is symbolized by $[A_m]_n$, where n is the rotation axis and m is the angle.

Then $[A_m]_n$ is:

$$[A_\theta]_z = \begin{bmatrix} \cos(\theta) & \sin(\theta) & 0 \\ -\sin(\theta) & \cos(\theta) & 0 \\ 0 & 0 & 1 \end{bmatrix}$$

The rotation about z is:

$$\begin{Bmatrix} \ddot{x}' \\ \ddot{y}' \\ \ddot{z}' \end{Bmatrix} = [A_\theta]_z \begin{Bmatrix} \ddot{x} \\ \ddot{y} \\ \ddot{z} \end{Bmatrix}$$

The apostrophe means that the accelerations are given in rotate coordinates. The result of this matrix multiplication is given by equation 3.10.

$$\begin{Bmatrix} \ddot{x}' \\ \ddot{y}' \\ \ddot{z}' \end{Bmatrix} = A_o \omega^2 \begin{bmatrix} \cos(\alpha) \cos(\beta) \cos(\theta) + \sin(\alpha) \cos(\beta) \sin(\theta) \\ -\cos(\alpha) \cos(\beta) \sin(\theta) + \sin(\alpha) \cos(\beta) \cos(\theta) \\ \sin(\beta) \end{bmatrix} - \frac{\lambda_N}{m_p} \begin{bmatrix} \mu_x \cos(\theta) + \mu_y \sin(\theta) \\ -\mu_x \sin(\theta) + \mu_y \cos(\theta) \\ \frac{m_p g}{\lambda_N} - 1 \end{bmatrix} \quad (3.10)$$

3.2.3 Rectangular Part on the Inclined Plane

The figure 3.6 shows the geometric parameters of rectangular part on the inclined plane. The angle θ is the rotation angle about the z axis. The angles β and α are the directions of the vibration force. The angle γ is the inclination of the plane.

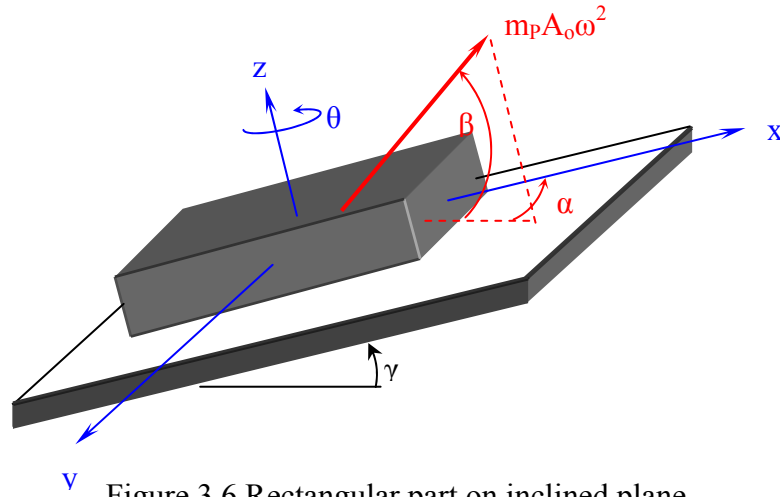


Figure 3.6 Rectangular part on inclined plane.

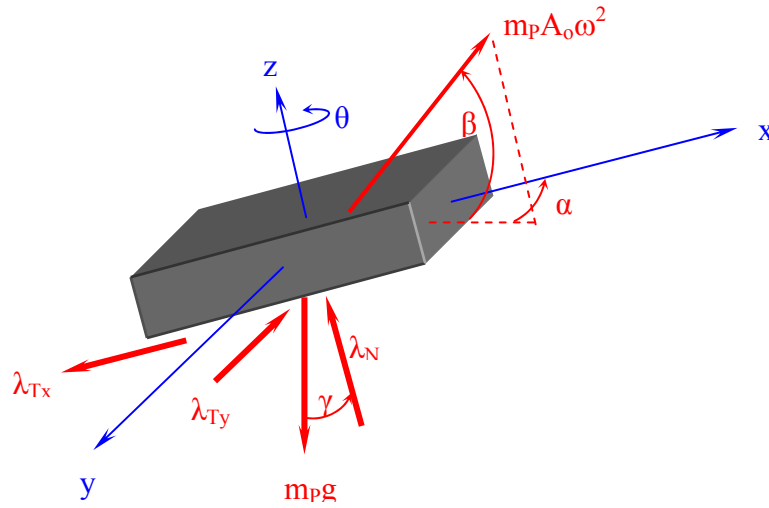


Figure 3.7 Free body diagram of rectangular part on inclined plane.

The figure 3.7 shows the free body diagram for a rectangular part on the inclined plane. The friction forces are λ_{Tx} and λ_{Ty} . The normal force is λ_N . The Coulomb friction equation was used for this analysis.

For the Newton second law, it is obtained:

$$\begin{aligned}
 \sum F_x &: A_o \omega^2 m_p \cos(\beta) \cos(\alpha) - \lambda_{Tx} - m_p g \sin(\gamma) = m_p \ddot{x} \\
 \sum F_y &: A_o \omega^2 m_p \cos(\beta) \sin(\alpha) - \lambda_{Ty} = m_p \ddot{y} \\
 \sum F_z &: A_o \omega^2 m_p \sin(\beta) - m_p g \cos(\gamma) + \lambda_N = m_p \ddot{z}
 \end{aligned} \tag{3.11}$$

The equation 3.11 be write in matrix form

$$\begin{bmatrix} \ddot{x} \\ \ddot{y} \\ \ddot{z} \end{bmatrix} = A_o \omega^2 \begin{bmatrix} \cos(\alpha) \cos(\beta) \\ \sin(\alpha) \cos(\beta) \\ \sin(\beta) \end{bmatrix} - \frac{\lambda_N}{m_p} \begin{bmatrix} \mu_x + \frac{m_p g \sin(\gamma)}{\lambda_N} \\ \mu_y \\ \frac{m_p g \cos(\gamma)}{\lambda_N} - 1 \end{bmatrix}$$

Now the rotation about z is made: $\begin{Bmatrix} \ddot{x}' \\ \ddot{y}' \\ \ddot{z}' \end{Bmatrix} = [A_\theta]_Z \begin{Bmatrix} \ddot{x} \\ \ddot{y} \\ \ddot{z} \end{Bmatrix}$

The result of this matrix multiplication is given by:

$$\begin{bmatrix} \ddot{x}' \\ \ddot{y}' \\ \ddot{z}' \end{bmatrix} = A_o \omega^2 \begin{bmatrix} \cos(\theta) \cos(\alpha) \cos(\beta) + \sin(\theta) \sin(\alpha) \cos(\beta) \\ -\sin(\theta) \cos(\alpha) \cos(\beta) + \cos(\theta) \sin(\alpha) \cos(\beta) \\ \sin(\beta) \end{bmatrix} \quad (3.12)$$

$$- \frac{\lambda_N}{m_p} \begin{bmatrix} \mu_x \cos(\theta) + \frac{m_p g}{\lambda_N} \cos(\theta) \sin(\gamma) + \mu_y \sin(\theta) \\ -\mu_x \sin(\theta) - \frac{m_p g}{\lambda_N} \sin(\theta) \sin(\gamma) + \mu_y \cos(\theta) \\ \frac{m_p g}{\lambda_N} \cos(\gamma) - 1 \end{bmatrix}$$

The equation 3.12 describes the body accelerations with respect to the mobile frame, fixed to the body. This equation is formed by the sum of two vectors: the first vector represented the vibrational effects and the second vector is the frictional and gravitational effects.

3.2.4 Rectangular Part on the Narrow Track

The figure 3.8 shows the rectangular part upward the track. The rectangular part has contact with the track floor and wall. The figure 3.9 shows the dimensions used for this analysis.

The contact between the part and the track wall move the action line of the normal force to a part corner because this contact generates a moment about of the mass center.

From figure 3.8b and by geometry:

$$\sigma = \arcsin\left(\frac{h}{2R}\right)$$

where R is the bowl radius.

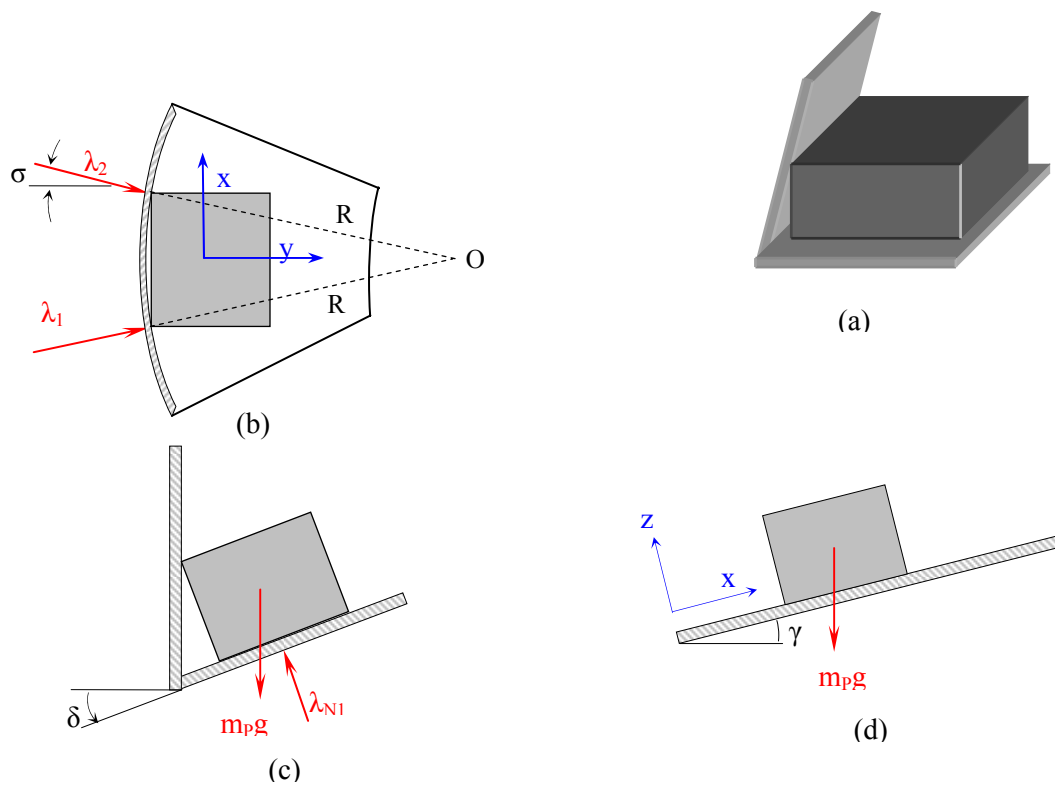


Figure 3.8 Part on the narrow track: (a) part, floor and wall, (b) plan view, (c) section view and (d) side view

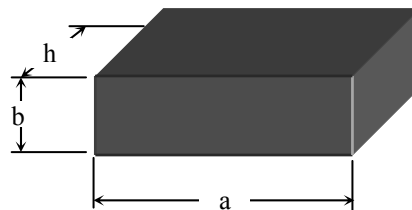


Figure 3.9 Geometric dimensions of a rectangular part.

The figure 3.10 shows the free body diagram of the part on the narrow track. The forces λ_1 and λ_2 are the normal forces of the contact between the part and track wall. The frictions forces are: λ_{Tx1} , λ_{Tx2} , λ_{Tz} and λ_{Ty} orientated as it shows in the figure. The angles γ and δ are the inclination angles of the track about y and x axis respectively showed in the figure 3.8d and 3.8c respectively.

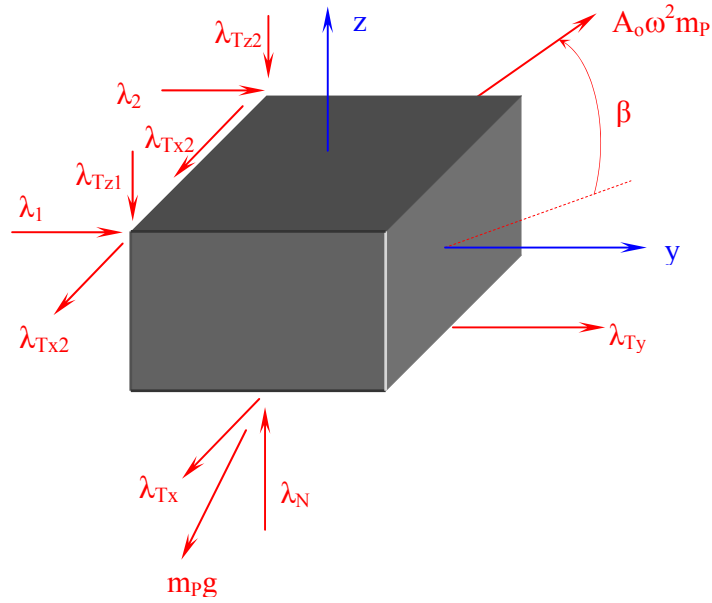


Figure 3.10 Free body diagram of the rectangular part on the narrow track.

The a_x , a_y and a_z are the accelerations in x, y and z directions. Based on the second Newton law and employing the transformation matrix given in the equation 2.1, it is written

$$\begin{aligned}
 m_P \begin{Bmatrix} a_x \\ a_y \\ a_z \end{Bmatrix} &= \begin{Bmatrix} 1 & 0 & 0 \\ 0 & \cos(\delta) & \sin(\delta) \\ 0 & -\sin(\delta) & \cos(\delta) \end{Bmatrix} \begin{Bmatrix} \cos(\gamma) & 0 & \sin(\gamma) \\ 0 & 1 & 0 \\ -\sin(\gamma) & 0 & \cos(\gamma) \end{Bmatrix} \begin{Bmatrix} 0 \\ 0 \\ -mg \end{Bmatrix} \\
 &+ \begin{Bmatrix} 0 \\ \lambda_1 \cos(\sigma) + \lambda_2 \cos(\sigma) \\ \lambda_N \end{Bmatrix} + A_o \omega^2 m_p \begin{Bmatrix} \cos(\beta) \cos(\alpha) \\ \cos(\beta) \sin(\alpha) \\ \sin(\beta) \end{Bmatrix} + \begin{Bmatrix} -\lambda_{Tx} - \lambda_{Tx1} - \lambda_{Tx2} \\ \lambda_{Ty} \\ -\lambda_{Tz1} - \lambda_{Tz2} \end{Bmatrix}
 \end{aligned} \tag{3.13}$$

The sum of moments about the center gives the following equations:

$$\begin{aligned}
 \sum M_{ox} &= \lambda_1 \cos(\sigma) \left(\frac{b}{2} \right) + \lambda_2 \cos(\sigma) \left(\frac{b}{2} \right) - \lambda_{Tz1} \left(\frac{a}{2} \right) - \lambda_{Tz2} \left(\frac{a}{2} \right) - \lambda_{Ty} \left(\frac{b}{2} \right) = 0 \\
 \sum M_{oy} &= \lambda_{Tz1} \left(\frac{h}{2} \right) - \lambda_{Tz2} \left(\frac{h}{2} \right) + \lambda_{Tx1} \left(\frac{b}{2} \right) + \lambda_{Tx2} \left(\frac{b}{2} \right) - \lambda_{Tx} \left(\frac{b}{2} \right) = 0 \\
 \sum M_{oz} &= \lambda_1 \cos(\sigma) \left(\frac{h}{2} \right) - \lambda_2 \cos(\sigma) \left(\frac{h}{2} \right) + \lambda_{Tx1} \left(\frac{a}{2} \right) + \lambda_{Tx2} \left(\frac{a}{2} \right) = 0
 \end{aligned} \tag{3.14}$$

By the Coulomb friction equation it can be written as:

$$\begin{aligned}
 \lambda_{Tx1} &= \lambda_1 \mu_k \cos(\sigma) \\
 \lambda_{Tx2} &= \lambda_2 \mu_k \cos(\sigma) \\
 \lambda_{Tz1} &= \lambda_1 \mu_s \cos(\sigma) \\
 \lambda_{Tz2} &= \lambda_2 \mu_s \cos(\sigma)
 \end{aligned} \tag{3.15a}$$

Replacing the equations 3.14 and 3.15a into of the equation 3.13 it is obtained:

$$\begin{aligned}
 \lambda_1 &= \lambda_2 \left(\frac{h - \mu_k a}{h + \mu_k a} \right) \\
 \lambda_N &= \frac{\lambda_2 \cos(\sigma)}{\mu_k b} \left[\left(\frac{h - \mu_k a}{h + \mu_k a} \right) (\mu_s h + \mu_k b) - (\mu_s h - \mu_k b) \right] \\
 \lambda_{Ty} &= \frac{\lambda_2 \cos(\sigma)}{b} \left[\left(\frac{h - \mu_k a}{h + \mu_k a} + 1 \right) (b - \mu_s a) \right]
 \end{aligned} \tag{3.15b}$$

The acceleration a_y is the acceleration in radial direction. Therefore, a_y is the centripetal acceleration. The centripetal acceleration is a function of the velocity; this acceleration can be expressed as:

$$a_y = \frac{v^2}{R}$$

where v is the velocity of the part and R is the radius of the bowl.

Replacing the equations 3.15a and 3.15b into of the equation 3.13 and solving for λ_2 in function of the velocity

$$\lambda_2 = \frac{m_p b(\mu_k a + h)(A_0 \omega^2 \cos(\beta) \sin(\alpha) + g \cos(\gamma) \sin(\delta))}{2 \cos(\sigma) h(\mu_s a - 2b)} - \frac{m_p b(h + \mu_k a)}{2 \cos(\sigma) h R(\mu_s a - 2b)} v^2 \quad (3.16)$$

Replacing the equation 3.16 into the equation 3.13 it is obtained for a_x

$$a_x = A_0 \omega^2 \cos(\beta) (\cos(\alpha) + \mu_k \sin(\alpha)) + g (\mu_k \cos(\gamma) \sin(\delta) - \sin(\gamma)) - \frac{\mu_k}{R} v^2$$

Simplifying this equation with the following abbreviations

$$K = A_0 \omega^2 \cos(\beta) (\cos(\alpha) + \mu_k \sin(\alpha)) + g (\mu_k \cos(\gamma) \sin(\delta) - \sin(\gamma))$$

where K is a parameters that depend of the friction and track inclinations angles.

The acceleration in the x direction can be written as:

$$a_x = K - \frac{\mu_k}{R} v^2 \quad (3.17)$$

The equation 3.17 shows that the acceleration in the x direction is not constant and is function of the part velocity.

The differential equation for a part with variable acceleration in term of the velocity and displacement, is given by:

$$a_x \cdot dx = v \cdot dv$$

Replacing the equation 3.17 into of this differential equation and solving for the velocity it is obtained the equation 3.18.

$$v = \frac{\sqrt{-\mu_k \cdot K \cdot R \cdot \left(e^{\frac{-2\mu_k x}{R}} - 1 \right)}}{\mu_k} \quad (3.18)$$

The equation 3.18 represents the transportation velocity of the part. This model is a model in three-dimensional analysis. The equation 3.18 is the final result for this section.

3.2.5 Contact Between Two Rectangular Parts

The contact of two rectangular parts can be of three types. The first contact is between plane surface and plane surface. The second contact is between plane surface and a line. The third contact is between a line and a line. In this section only the second contact is analyzed because is the most frequent.

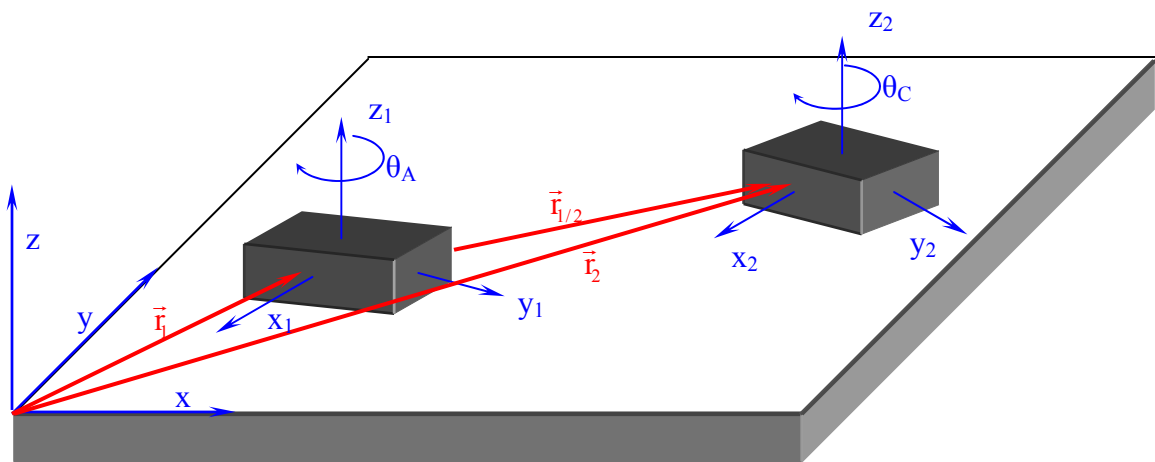


Figure 3.11 Vector diagram for the contact between two rectangular parts.

The figure 3.11 shows the vectors set used for the analysis of this situation. In the contact between two rectangular parts can occur:

$$\|\vec{r}_{1/2}\|_{\max} = \sqrt{h^2 + a^2}$$

$$\|\vec{r}_{1/2}\|_{\min} = a, \text{ if } a < h$$

$$\|\vec{r}_{1/2}\|_{\min} = h, \text{ if } a > h$$

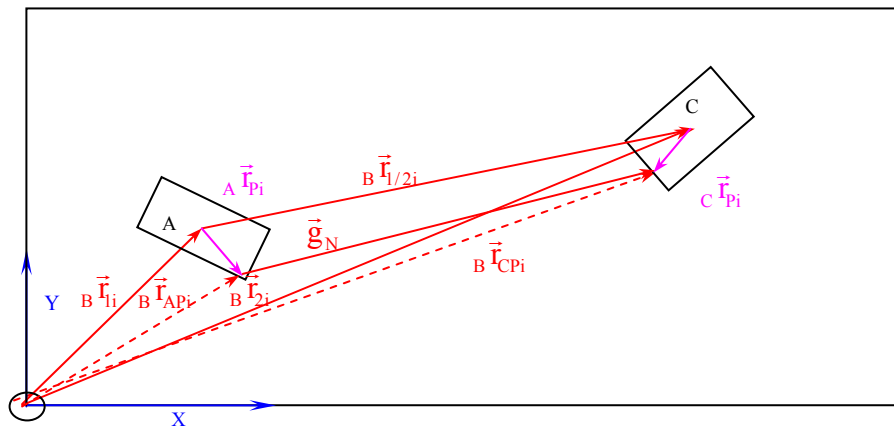


Figure 3.12 Vector diagram before impact (rectangular parts).

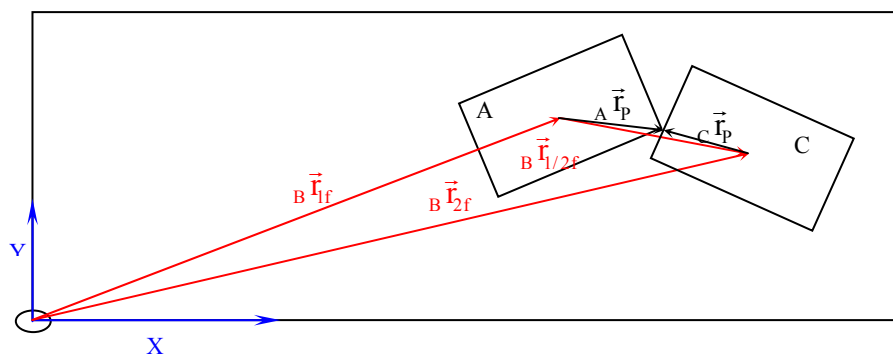


Figure 3.13 Vector diagram after impact (rectangular parts).

The figures 3.12 and 3.13 show the conditions before and after impact respectively. The subscript B represented the fixed frame (x, y, z). The subscripts A and C represented the mobile frames fixed to bodies A and C respectively. The vectors are given by:

$$\begin{aligned} {}_B \vec{r}_{1i} &= \begin{pmatrix} x_1 \\ y_1 \\ 0 \end{pmatrix}_i ; & {}_B \vec{r}_{2i} &= \begin{pmatrix} x_2 \\ y_2 \\ 0 \end{pmatrix}_i ; & {}_B \vec{r}_{1f} &= \begin{pmatrix} x_1 \\ y_1 \\ 0 \end{pmatrix}_f ; & {}_B \vec{r}_{2f} &= \begin{pmatrix} x_2 \\ y_2 \\ 0 \end{pmatrix}_f \\ {}_B \vec{r}_{1/2i} &= \begin{pmatrix} x_2 - x_1 \\ y_2 - y_1 \\ 0 \end{pmatrix}_i ; & {}_B \vec{r}_{1/2f} &= \begin{pmatrix} x_2 - x_1 \\ y_2 - y_1 \\ 0 \end{pmatrix}_f ; & {}_B \vec{r}_{Pf} &= \begin{pmatrix} x_p \\ y_p \\ 0 \end{pmatrix}_f \end{aligned}$$

In the initial and final positions, the vector equations are respectively given by

$${}_B \vec{r}_{1/2i} + {}_C \vec{r}_{CP} - {}_A \vec{r}_{AP} = \vec{g}_N \quad (3.19)$$

$${}_B \vec{r}_{1/2f} + {}_C \vec{r}_{CP} - {}_A \vec{r}_{AP} = 0$$

Equation 3.19 can be written by its components:

$$\vec{g}_N = \begin{pmatrix} x_2 - x_1 \\ y_2 - y_1 \\ 0 \end{pmatrix}_B + \begin{pmatrix} x_{CP} \\ y_{CP} \\ 0 \end{pmatrix}_C - \begin{pmatrix} x_{AP} \\ y_{AP} \\ 0 \end{pmatrix}_A$$

Equation 3.19 can not be solved in this form because its terms are given in different reference frames. It is necessary to apply a coordinate transformation. The transformation matrix is symbolized by $[T_n]_m$, where n is the rotation axis and m is the translation vector. The vector equations are:

$$\begin{aligned} {}_C r_{pi} &= [T_z]_{r_C} \cdot {}_B r_{CPi} \quad \text{then,} \quad {}_B r_{CPi} = [T_z]_{r_C}^{-1} \cdot {}_C r_{CPi} \\ {}_A r_{Pi} &= [T_z]_{r_A} \cdot {}_B r_{APi} \quad \text{then,} \quad {}_B r_{APi} = [T_z]_{r_A}^{-1} \cdot {}_A r_{APi} \end{aligned}$$

The result is

$${}^B r_{CPi} = \begin{bmatrix} \cos(\theta_C) & -\sin(\theta_C) & 0 & x_2 \\ \sin(\theta_C) & \cos(\theta_C) & 0 & y_2 \\ 0 & 0 & 1 & 0 \\ 0 & 0 & 0 & 1 \end{bmatrix} \begin{bmatrix} x_{CP} \\ y_{CP} \\ 0 \\ 1 \end{bmatrix}_i = \begin{bmatrix} x_{CP} \cos(\theta_C) - y_{CP} \sin(\theta_C) + x_2 \\ x_{CP} \sin(\theta_C) + y_{CP} \cos(\theta_C) + y_2 \\ 0 \\ 1 \end{bmatrix}_i$$

$${}^B r_{APi} = \begin{bmatrix} \cos(\theta_A) & -\sin(\theta_A) & 0 & x_1 \\ \sin(\theta_A) & \cos(\theta_A) & 0 & y_1 \\ 0 & 0 & 1 & 0 \\ 0 & 0 & 0 & 1 \end{bmatrix} \begin{bmatrix} x_{AP} \\ y_{AP} \\ 0 \\ 1 \end{bmatrix}_i = \begin{bmatrix} x_{AP} \cos(\theta_A) - y_{AP} \sin(\theta_A) + x_1 \\ x_{AP} \sin(\theta_A) + y_{AP} \cos(\theta_A) + y_1 \\ 0 \\ 1 \end{bmatrix}_i$$

Then, the relative distance between the contacts points can be written as:

$$\bar{g}_N = \begin{bmatrix} x_{CP} \cos(\theta_C) - x_{AP} \cos(\theta_A) - y_{CP} \sin(\theta_C) + y_{AP} \sin(\theta_A) + x_2 - x_1 \\ x_{CP} \sin(\theta_C) - x_{AP} \sin(\theta_A) + y_{CP} \cos(\theta_C) - y_{AP} \cos(\theta_A) + y_2 - y_1 \\ 0 \\ 1 \end{bmatrix} \quad (3.20)$$

Differentiating the equation 3.20 it found the relative velocity between two bodies. This derivate is given in Cartesian coordinates in the equation 3.21a.

$$\dot{\bar{g}}_N = \begin{bmatrix} \dot{x}_{CP} \cos(\theta_C) - x_{CP} \sin(\theta_C) \dot{\theta}_C - \dot{x}_{AP} \cos(\theta_A) + x_{AP} \sin(\theta_A) \dot{\theta}_A - \dot{y}_{CP} \sin(\theta_C) - y_{CP} \cos(\theta_C) \dot{\theta}_C \\ \quad + \dot{y}_{AP} \sin(\theta_A) + y_{AP} \cos(\theta_A) \dot{\theta}_A + \dot{x}_2 - \dot{x}_1 \\ \dot{x}_{CP} \sin(\theta_C) - x_{CP} \cos(\theta_C) \dot{\theta}_C - \dot{x}_{AP} \sin(\theta_A) - x_{AP} \cos(\theta_A) \dot{\theta}_A + \dot{y}_{CP} \cos(\theta_C) - y_{CP} \sin(\theta_C) \dot{\theta}_C \\ \quad - \dot{y}_{AP} \cos(\theta_A) + y_{AP} \sin(\theta_A) \dot{\theta}_A + \dot{y}_2 - \dot{y}_1 \\ 0 \end{bmatrix} \quad (3.21a)$$

The equation 3.21a can be separated in two terms

$$\dot{\mathbf{g}}_N = \underbrace{\begin{bmatrix} \cos(\theta_C) & \sin(\theta_C) \\ -\cos(\theta_A) & -\sin(\theta_A) \\ -\sin(\theta_C) & -\cos(\theta_C) \\ \sin(\theta_A) & -\cos(\theta_A) \\ (-x_{CP} \sin(\theta_C) - y_{CP} \cos(\theta_C)) & (-x_{CP} \cos(\theta_C) - y_{CP} \sin(\theta_C)) \\ (x_{AP} \sin(\theta_A) + y_{AP} \cos(\theta_A)) & (-x_{AP} \cos(\theta_A) + y_{AP} \sin(\theta_A)) \\ 1 & 0 \\ -1 & 0 \\ 0 & 1 \\ 0 & -1 \end{bmatrix}}_{W_N^T} \underbrace{\begin{bmatrix} \dot{x}_{CP} \\ \dot{x}_{AP} \\ \dot{y}_{CP} \\ \dot{y}_{AP} \\ \dot{\theta}_C \\ \dot{\theta}_A \\ \dot{x}_2 \\ \dot{x}_1 \\ \dot{y}_2 \\ \dot{y}_1 \end{bmatrix}}_{\dot{\mathbf{q}}} \quad (3.21b)$$

The generalized coordinates given in the equation 3.21b can be reduced with a constrain on contact point. This constrain is to consider that the body A always impacts at one of its four corner. The constrain equations are:

$$\begin{aligned} x_{AP} &= x_1 + \frac{1}{2} \sqrt{a^2 + h^2} \cos(\theta_A); & \dot{x}_{AP} &= \dot{x}_1 - \frac{1}{2} \sqrt{a^2 + h^2} \sin(\theta_A) \dot{\theta}_A \\ y_{AP} &= y_1 + \frac{1}{2} \sqrt{a^2 + h^2} \sin(\theta_A); & \dot{y}_{AP} &= \dot{y}_1 + \frac{1}{2} \sqrt{a^2 + h^2} \cos(\theta_A) \dot{\theta}_A \end{aligned} \quad (3.22)$$

Replacing the equation 3.22 into 3.21 a relationship for the relative velocity is obtained

$$\delta q_N = \underbrace{\begin{bmatrix} -(\cos(\theta_A)+1) & 1 & \sin(\theta_A) & 0 & \cos(\theta_C) & -\sin(\theta_C) & \left(\sqrt{a^2+h^2}\sin(2\theta_A)+x_1\sin(\theta_A)+y_1\cos(\theta_A)\right) & -(x_{CP}\sin(\theta_C)+y_{CP}\cos(\theta_C)) \\ -\sin(\theta_A) & 0 & -(\cos(\theta_A)+1) & 1 & \sin(\theta_C) & \cos(\theta_C) & \left(-2\sqrt{a^2+h^2}\sin(2\theta_A)-x_1\cos(\theta_A)+y_1\sin(\theta_A)\right) & -(x_{CP}\cos(\theta_C)+y_{CP}\sin(\theta_C)) \end{bmatrix}}_{W_N^T} \underbrace{\begin{bmatrix} \dot{x}_1 \\ \dot{x}_2 \\ \dot{y}_1 \\ \dot{y}_2 \\ \dot{x}_{CP} \\ \dot{y}_{CP} \\ \dot{\theta}_A \\ \dot{\theta}_C \end{bmatrix}}_{\dot{q}}$$

The contact equation is given by $[M](\dot{q}_E - \dot{q}_A) - W_N \Lambda_N = 0$, with $\Lambda_N = \lim_{t_E \rightarrow t_A} \int_{t_A}^{t_E} \lambda_N dt$

Where $[M]$ is the mass matrix and \dot{q}_E and \dot{q}_A the derivatives of the generalized coordinates at expansion and approximation respectively.

$$[M] = \begin{bmatrix} m_P & 0 & 0 & 0 & 0 & 0 & 0 & 0 \\ 0 & m_P & 0 & 0 & 0 & 0 & 0 & 0 \\ 0 & 0 & m_P & 0 & 0 & 0 & 0 & 0 \\ 0 & 0 & 0 & m_P & 0 & 0 & 0 & 0 \\ 0 & 0 & 0 & 0 & m_P & 0 & 0 & 0 \\ 0 & 0 & 0 & 0 & 0 & m_P & 0 & 0 \\ 0 & 0 & 0 & 0 & 0 & 0 & \frac{1}{12}m_P(b^2+h^2) & 0 \\ 0 & 0 & 0 & 0 & 0 & 0 & 0 & \frac{1}{12}m_P(b^2+h^2) \end{bmatrix}, \quad \dot{q}_E - \dot{q}_A = \begin{bmatrix} \dot{x}_{1E} - \dot{x}_{1A} \\ \dot{x}_{2E} - \dot{x}_{2A} \\ \dot{y}_{1E} - \dot{y}_{1A} \\ \dot{y}_{2E} - \dot{y}_{2A} \\ \dot{x}_{CPE} - \dot{x}_{CPA} \\ \dot{y}_{CPE} - \dot{y}_{CPA} \\ \dot{\theta}_{AE} - \dot{\theta}_{AA} \\ \dot{\theta}_{CE} - \dot{\theta}_{CA} \end{bmatrix}$$

Based on the impact Newton theory, it is obtained:

$$\dot{\vec{g}}_{NE} = -\varepsilon \dot{\vec{g}}_{NA}$$

And

$$\vec{g}_{NE} - \vec{g}_{NA} = W_N^T (\dot{q}_E - \dot{q}_A) \quad (3.23)$$

Since

$$\Lambda_N = (1 - \varepsilon) \cdot \left[W_N^T \cdot [M]^{-1} \cdot W_N \right]^{-1} \cdot \dot{\vec{g}}_{NA} \quad (3.24)$$

The equation 3.24 is the final result for this section.

3.3 Modeling of Cylindrical Parts

The cylindrical parts have two surface types: one curve surface and two plane surfaces. The part curve surface has two different effects on its motion. These effects are a rolling effect if the motion is perpendicular to the cylinder axis and a stick-sliding effect if the motion direction is parallel to cylinder axis.

3.3.1 Insulate Cylindrical Part

When a cylindrical part is in free fall, the contact can occur only of three forms:

1. Contact between the cylindrical edge and the plane surface (point-surface).
2. Contact between two plane surfaces (surface-surface).
3. Contact between the curved surface and the plane surface (line-surface).

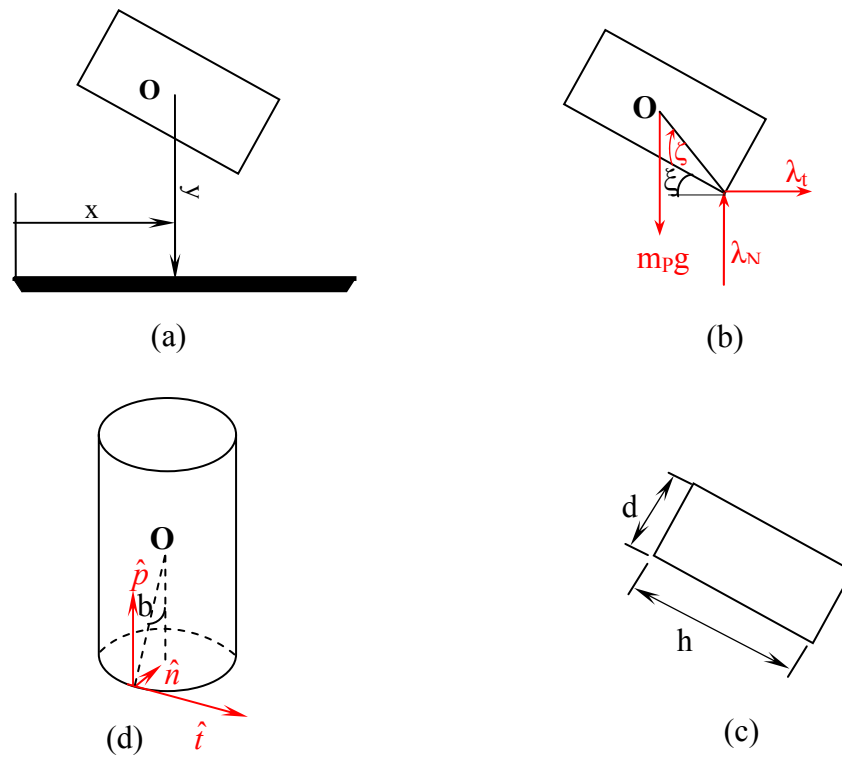


Figure 3.14 (a) Position coordinates; (b) Free body diagram for contact edge; (c) dimensions; (d) 3D parameters

The figure 3.14 shows the parameters that will be used for the analysis of this section. The figure 3.14a shows the 2D position coordinates of the cylinder mass center. The figure 3.14b is the free body diagram of cylinder in contact with the plane surface. This contact is considered in the cylinder edge, the other contact type is analyzed later. The figure 3.14d shows the three-dimensional parameter in the contact point. The figure 3.14e shows the cylinder dimensions diameter and high. By geometry it is obtained:

$$b = \frac{\sqrt{d^2 + h^2}}{2} \quad \text{and} \quad \zeta = \arctan\left(\frac{d}{h}\right) \quad (3.25)$$

By the second Newton law the kinetic equations for this case are

$$\begin{aligned}\sum F_x : m_p \ddot{x} &= \lambda_T \\ \sum F_y : m_p \ddot{y} &= \lambda_N - m_p g \\ \sum M_O : I \ddot{\xi} &= -\lambda_N b \cos(\zeta + \xi) - \frac{1}{2} \lambda_T b \sin(\zeta + \xi)\end{aligned}\tag{3.26}$$

Replacing the equation 3.25 into the equation 3.26 for the third equation:

$$I \ddot{\xi} = -\frac{1}{2} \lambda_N \sqrt{d^2 + h^2} \cos(\xi + \zeta) - \frac{1}{2} \lambda_T \sqrt{d^2 + h^2} \sin(\xi + \zeta)\tag{3.27}$$

The goal is to found the relative distance g_N and its derivates:

$$\bar{g}_N = y - \frac{\sqrt{d^2 + h^2}}{2} \sin(\zeta + \xi)\tag{3.28}$$

The equation 3.28 has the following derivates:

$$\dot{\bar{g}}_N = \dot{y} - \frac{1}{2} \dot{\xi} \sqrt{d^2 + h^2} \sin(\xi + \zeta)\tag{3.29}$$

$$\ddot{\bar{g}}_N = \ddot{y} - \frac{1}{2} \ddot{\xi} \sqrt{d^2 + h^2} \cos(\xi + \zeta) + \frac{1}{2} \dot{\xi}^2 \sqrt{d^2 + h^2} \sin(\xi + \zeta)$$

In the tangential direction the relative distance is:

$$\bar{g}_T = x + \frac{\sqrt{d^2 + h^2}}{2} \cos(\xi + \zeta)\tag{3.30}$$

The derivates of the equation 3.30 are:

$$\dot{\bar{g}}_T = \dot{x} - \frac{\sqrt{d^2 + h^2}}{2} \dot{\xi} \sin(\xi + \zeta)\tag{3.31}$$

$$\ddot{\bar{g}}_T = \ddot{x} - \frac{\sqrt{d^2 + h^2}}{2} \ddot{\xi} \cos(\xi + \zeta) - \frac{\sqrt{d^2 + h^2}}{2} \dot{\xi}^2 \sin(\xi + \zeta)$$

The equation 3.31 completely describes the condition of proximity from the body to surface. The body slides if the tangential relative velocity is larger than zero. The body is in contact with surface if g_N is zero. Then by the condition for contact and sliding

$$\begin{aligned} \lambda_T &= -\mu\lambda_N \text{sig}(\dot{g}_T) \\ \text{if } \dot{g}_T > 0 \text{ then} & \\ \lambda_T &= -\mu\lambda_N \end{aligned} \quad (3.32)$$

Solving the equations 3.26 for \ddot{x} , \ddot{y} and $\ddot{\xi}$, and replacing into 3.29 and 3.31, it is obtained:

$$\begin{aligned} \ddot{g}_N &= \frac{\lambda_N}{m_p} \left(1 + \frac{d^2 + h^2}{4I} m_p \cos^2(\xi + \zeta) - \frac{m_p \mu}{4I} (h^2 + d^2) \sin(\xi + \zeta) \cos(\xi + \zeta) \right) \\ &\quad + \frac{\sqrt{d^2 + h^2}}{2} \dot{\xi}^2 \sin(\xi + \zeta) - g \end{aligned} \quad (a) \quad (3.33)$$

$$\begin{aligned} \ddot{g}_T &= \frac{\lambda_N}{m_p} \left(\mu + \frac{d^2 + h^2}{4I} m_p \sin(\xi + \zeta) \cos(\xi + \zeta) - \frac{m_p \mu}{4I} (h^2 + d^2) \cos^2(\xi + \zeta) \right) \\ &\quad - \frac{\sqrt{d^2 + h^2}}{2} \dot{\xi}^2 \cos(\xi + \zeta) \end{aligned} \quad (b)$$

Now the equation 3.33a is written using the following abbreviations:

$$\begin{aligned} \tau &= \frac{1}{m_p} \left(1 + \frac{d^2 + h^2}{4I} m_p \cos^2(\xi + \zeta) - \frac{m_p \mu}{4I} (h^2 + d^2) \sin(\xi + \zeta) \cos(\xi + \zeta) \right) \\ \chi &= \frac{\sqrt{d^2 + h^2}}{2} \dot{\xi}^2 \sin(\xi + \zeta) - g \end{aligned}$$

Then, $\ddot{g}_N = \tau\lambda_N + \chi$; $\ddot{g}_N \geq 0$; $\lambda_N \geq 0$; and $\ddot{g}_N \lambda_N = 0$. τ and χ may have positive or negative

values depending on the parameters μ , ξ and $\frac{\sqrt{d^2 + h^2}}{2g} \dot{\xi}^2$. This result and conclusions

are equal to the results obtained in the section 3.2.1.

The boundary condition ($\tau=0$) is

$$\mu = \frac{4I + m_p \cos(\xi + \zeta)^2 (d^2 + h^2)}{m_p \sin(\xi + \zeta) \cos(\xi + \zeta) (d^2 + h^2)} \quad (3.34)$$

For a cylinder $I = \frac{m_p}{12} \left(\frac{3}{4} d^2 + h^2 \right)$

Replacing this value into the equation 3.34 it is obtained

$$\mu = \frac{3d^2 + 4h^2 + 12 \cos^2(\xi + \zeta) (d^2 + h^2)}{12 \sin(\xi + \zeta) \cos(\xi + \zeta) (d^2 + h^2)}$$

The figure 3.15 is the plot of $\mu(\xi)$. This figure shows the lines for $\tau=0$. The region above these lines correspond $\tau < 0$ and the region below this lines correspond $\tau > 0$.

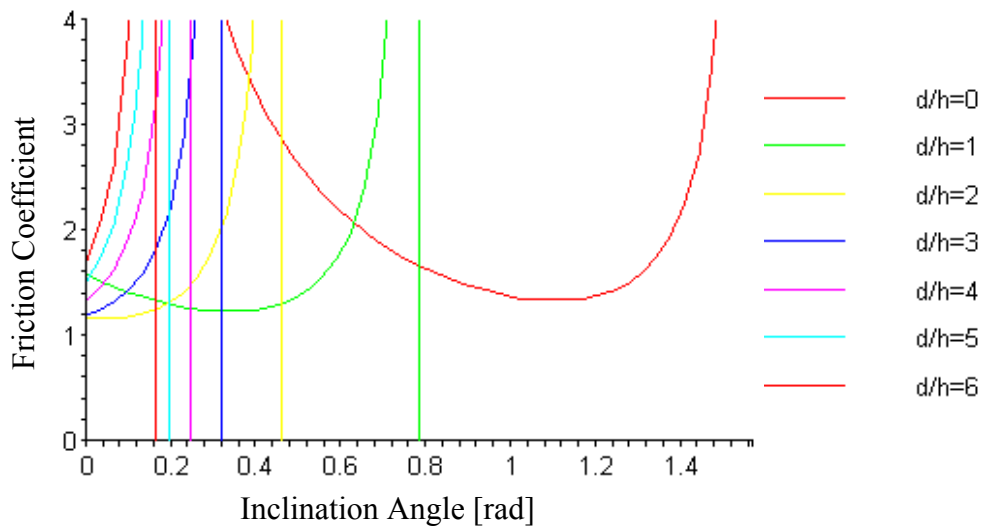


Figure 3.15 Limit conditions for the cylindrical part: Friction coefficient versus inclination angle.

From figure 3.15, when $\mu < 1.2$ the values of τ are always positive. If the coefficient of friction is chosen small enough, then the solution is unique.

3.3.2 Cylindrical Part on Horizontal Plane

In this section the physical phenomenon of cylindrical parts on the horizontal plane is analyzed. Figure 3.16 shows the situation when a part lies on its side and the horizontal plane is vibrating. The angle θ value is considered to be zero because this angle is consequence of the eccentricity in the part. In this study the eccentricity is assumed zero since the analysis focus on the part with uniform cylindrical confection.

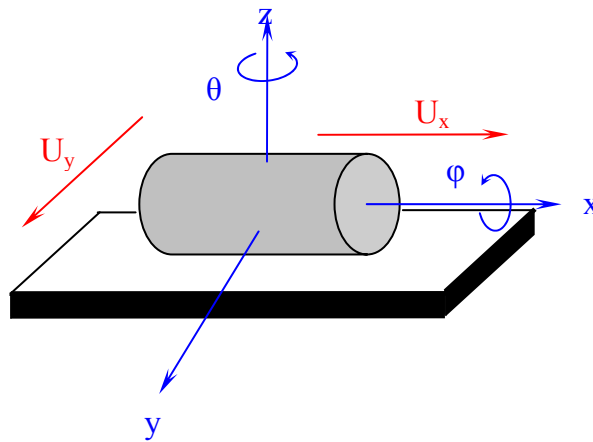


Figure 3.16 Axes and parameters of cylindrical part on horizontal plane.

For this case the generalized coordinates are:

$$q = \begin{Bmatrix} x \\ y \\ z \\ \phi \end{Bmatrix}$$

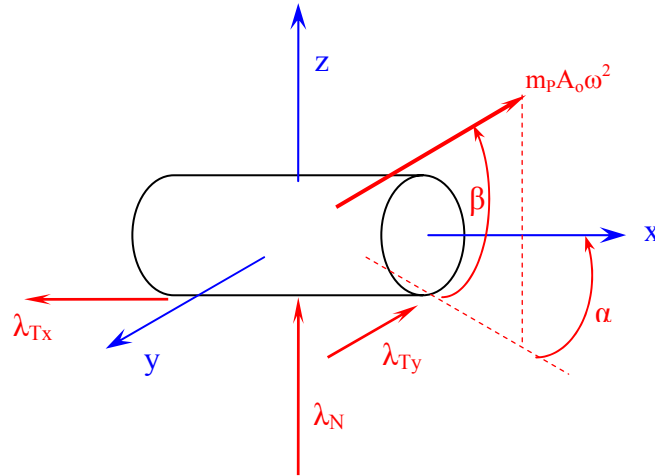


Figure 3.17 Free body diagram of a cylindrical part on the horizontal plane.

The figure 3.17 shows the free body diagram of cylindrical part on horizontal plane. The term $m_p A_o \omega^2$ represent the vibration force, where m_p is the part mass, A_o is the amplitude of vibration and ω is the angular frequency. The angles β and α represent the orientation and direction of this force. The forces λ_N , λ_{Tx} and λ_{Ty} are the normal force, tangential force in the x direction and tangential force in the y direction respectively.

Applying the second Newton law the kinetic equations are:

$$\begin{aligned}
 \sum F_x : m_p A_o \omega^2 \cos(\beta) \cos(\alpha) - \lambda_{Tx} &= m_p \ddot{x} \\
 \sum F_y : m_p A_o \omega^2 \cos(\beta) \sin(\alpha) - \lambda_{Ty} &= m_p \ddot{y} \\
 \sum F_z : -m_p g + m_p A_o \omega^2 \sin(\beta) + \lambda_N &= m_p \ddot{z} \\
 \sum M_x : \frac{m_p A_o \omega^2 d \cos(\beta) \sin(\alpha)}{2} &= I \ddot{\theta}_x
 \end{aligned} \tag{3.35}$$

Rewriting the equations 3.35 in matrix form:

$$\begin{Bmatrix} \ddot{x} \\ \ddot{y} \\ \ddot{z} \\ \ddot{\theta}_x \end{Bmatrix} = A_o \omega^2 \begin{Bmatrix} \cos(\beta) \cos(\alpha) \\ \cos(\beta) \sin(\alpha) \\ \sin(\beta) \\ \frac{m_p \cos(\beta) \sin(\alpha)}{2I} \end{Bmatrix} - \frac{\lambda_N}{m_p} \begin{Bmatrix} \mu \\ \mu \\ \frac{g m_p}{\lambda_N} - 1 \\ 0 \end{Bmatrix}$$

Assuming \ddot{z} equal zero and resolving for equations 3.35:

$$\begin{Bmatrix} \ddot{x} \\ \ddot{y} \\ \ddot{\theta}_x \end{Bmatrix} = A_o \omega^2 \begin{Bmatrix} \cos(\beta) \cos(\alpha) \\ \cos(\beta) \sin(\alpha) \\ \frac{4 \cos(\beta) \sin(\alpha)}{d} \end{Bmatrix} - \begin{Bmatrix} \mu(g - A_o \omega^2 \sin(\beta)) \\ \mu(g - A_o \omega^2 \sin(\beta)) \\ 0 \end{Bmatrix} \quad (3.36)$$

Equation 3.36 is the final result for this section. This equation defines the accelerations of the cylindrical part on the horizontal surface.

3.3.3 Cylindrical Part on the Inclined Plane

Figure 3.18 shows the case the parameters and axis for the study. The angles α and β represent the direction of the vibration force. The angle γ is the inclination of surface respect to horizontal line. The term $m_p A_o \omega^2$ is the magnitude of this force, where m_p is the part mass, A_o is the vibration amplitude and w is the angular frequency. The angles ϕ and θ are the possible part rotations about X and Z axis respectively. The angle θ value is considered to be equal to zero because it is not eccentric part.

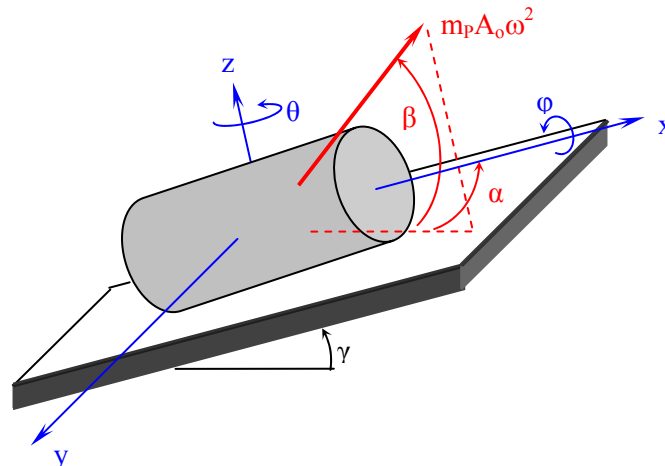


Figure 3.18 Axes and parameters of cylindrical part on inclined plane.

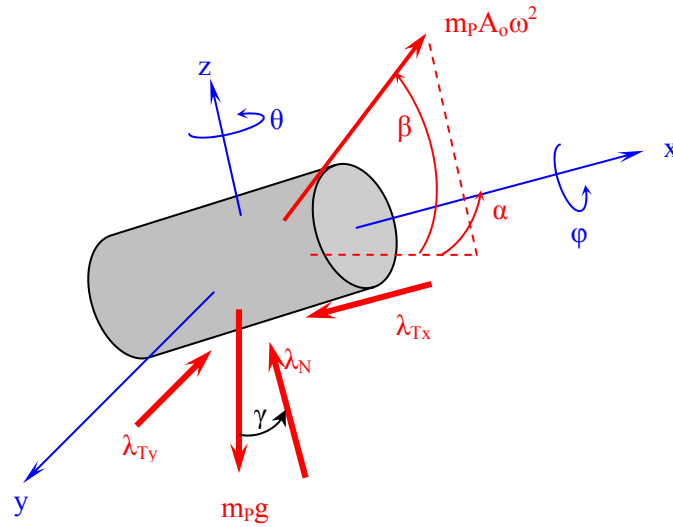


Figure 3.19 Free body diagram for a cylindrical part on inclined surface

The figure 3.19 shows the free body diagram for a cylindrical part on the inclined plane. This diagram shows the directions of the vibration force (α and β) and the rotations about the axis x and z (ϕ and θ). The friction and normal forces are represented by λ_{Tx} , λ_{Ty} and λ_N (tangential friction force in direction of axis x , tangential friction force in direction of axis Z and normal force respectively).

Based on the Newton second law the kinetic equations are:

$$\begin{aligned}
 \sum F_x &: A_o w^2 m_p \cos(\beta) \cos(\alpha) - \lambda_{Tx} - m_p g \sin(\gamma) = m_p \ddot{x} \\
 \sum F_y &: A_o w^2 m_p \cos(\beta) \sin(\alpha) - \lambda_{Ty} = m_p \ddot{y} \\
 \sum F_z &: A_o w^2 m_p \sin(\beta) - m_p g \cos(\gamma) + \lambda_N = m_p \ddot{z} \\
 \sum M_x &: \frac{d}{2} A_o w^2 m_p \cos(\beta) \sin(\alpha) = I \ddot{\phi}
 \end{aligned} \tag{3.37}$$

From equations 3.37 it is obtained the following matrix form:

$$\begin{Bmatrix} \ddot{x} \\ \ddot{y} \\ \ddot{z} \\ \ddot{\phi} \end{Bmatrix} = A_o w^2 \underbrace{\begin{Bmatrix} \cos(\beta) \cos(\alpha) \\ \cos(\beta) \sin(\alpha) \\ \sin(\beta) \\ \frac{d}{2I} m_p \cos(\beta) \sin(\alpha) \end{Bmatrix}}_{\text{Vibration Effect}} + \frac{1}{m_p} \underbrace{\begin{Bmatrix} -\lambda_{Tx} - m_p g \sin(\gamma) \\ -\lambda_{Ty} \\ -m_p g \cos(\gamma) + \lambda_N \\ 0 \end{Bmatrix}}_{\text{Gravitational Field and Friction effects}} \quad (3.38)$$

The equation 3.38 is constituted by two parts. The first part represents the effects of the vibration force. The second part represents the effects of gravity and friction, represented by gravity acceleration and friction coefficients. Assuming that the friction coefficients are equal for different directions and applying the Coulomb friction equation in the equation 3.38, it is obtained:

$$\begin{Bmatrix} \ddot{x} \\ \ddot{y} \\ \ddot{z} \\ \ddot{\phi} \end{Bmatrix} = A_o w^2 \begin{Bmatrix} \cos(\beta) \cos(\alpha) \\ \cos(\beta) \sin(\alpha) \\ \sin(\beta) \\ \frac{d}{2I} m_p \cos(\beta) \sin(\alpha) \end{Bmatrix} - \frac{\lambda_N}{m_p} \begin{Bmatrix} \mu + \frac{g}{\lambda_N} m_p \sin(\gamma) \\ \mu \\ \frac{g}{\lambda_N} m_p \cos(\gamma) - 1 \\ 0 \end{Bmatrix}$$

3.3.4 Contact Between Two Cylindrical Parts

The figure 3.20 shows the vector diagram the physical situation and vector configuration for this analysis. For this case the contact can occur of five forms:

1. Contact between the cylinder edge and the plane surface of other cylinder.
2. Contact between the cylinder edge and the curve surface of the other cylinder.

3. Contact between the plane surface of one part and the plane surface of the other part.
4. Contact between the curved surface of one part and the curved surface of the other part.
5. Contact between the plane surface and the curved surface.

The two first forms are of point type, because the cylinder has contact only in one point. The third form is of planar type because the contact is in a plane. The fourth and fifth forms are of linear type because the contact is in a line. These situations are illustrated in the figure 3.21.

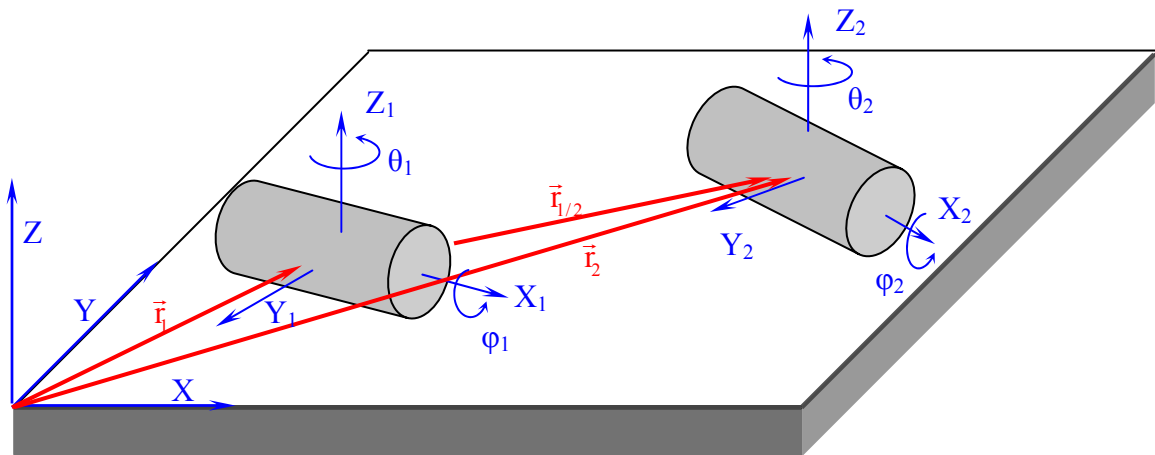


Figure 3.20 Vector diagram for the contact between two rectangular parts.

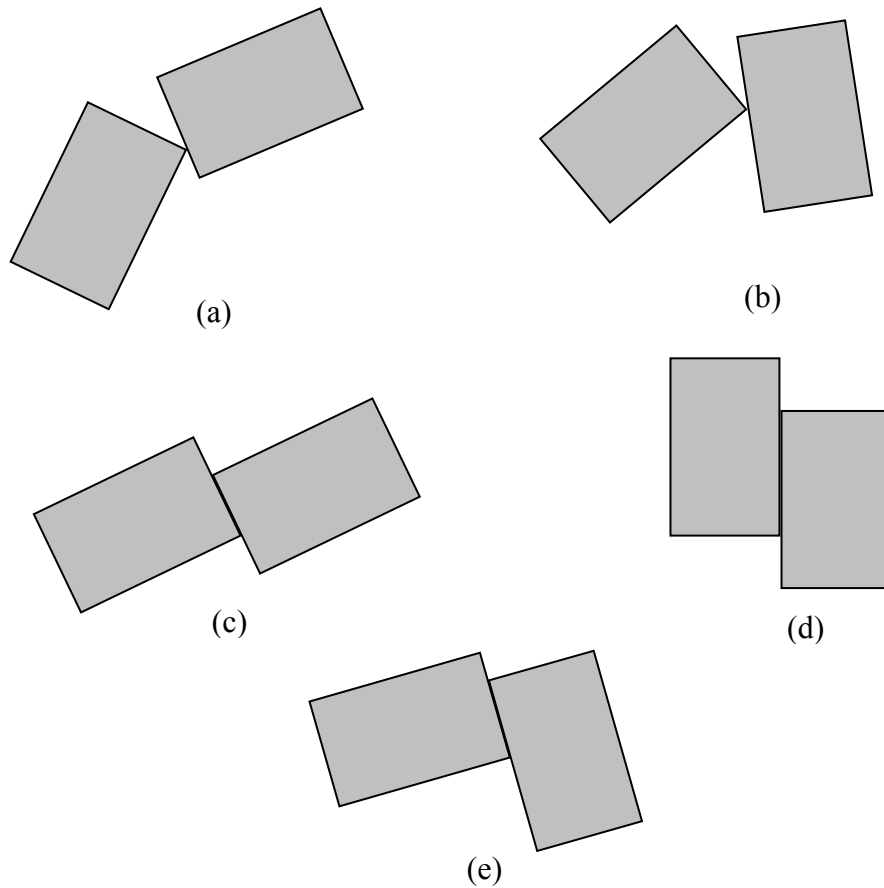


Figure 3.21 Contact forms between two cylindrical parts. Edge-plane, (b) Edge-curved surface, (c) plane-plane, (d) curved surface-curved surface and (e) Plane-curved surface.

The contact form determines the motion freedom degrees. Edge-plane is the motion of a point on a plane. Therefore, this motion has five freedom degrees. Edge-curved surface (b) contact has four freedom degrees because the motion is a point on a line. Plane-plane (c) contact has three freedom degrees because the motion is a plane on other plane. Curved surface-curved surface (d) contact is the motion of a line on other line. Therefore, has two freedom degrees. Plane-curved surface (e) contact has four freedom degrees because the motion is a line on a plane.

The figures 3.22 and 3.23 show the vectors that are used for the dynamic analysis. The subscript “B” means that the vector is observed from fixed frame. With respect to figure 3.20 it is obtained.

$${}^B\vec{r}_{1i} = \begin{pmatrix} x_1 \\ y_1 \\ 0 \end{pmatrix}_i ; \quad {}^B\vec{r}_{2i} = \begin{pmatrix} x_2 \\ y_2 \\ 0 \end{pmatrix}_i$$

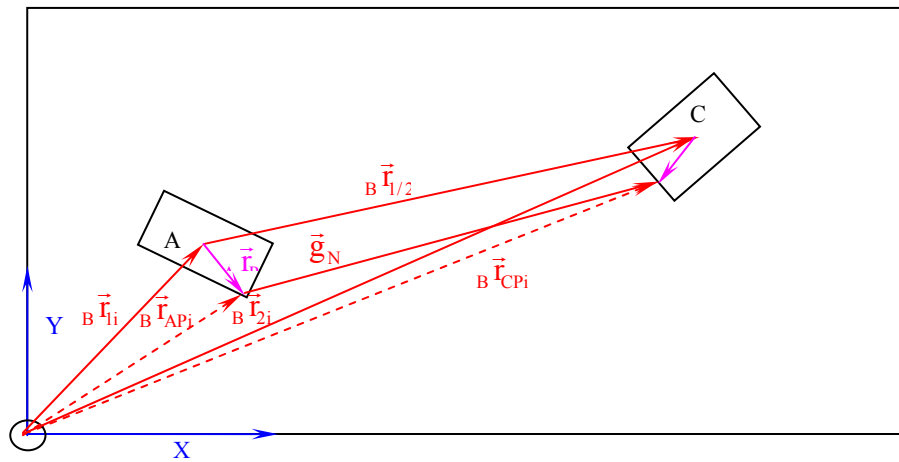


Figure 3.22 Vector diagram before impact (cylindrical parts).

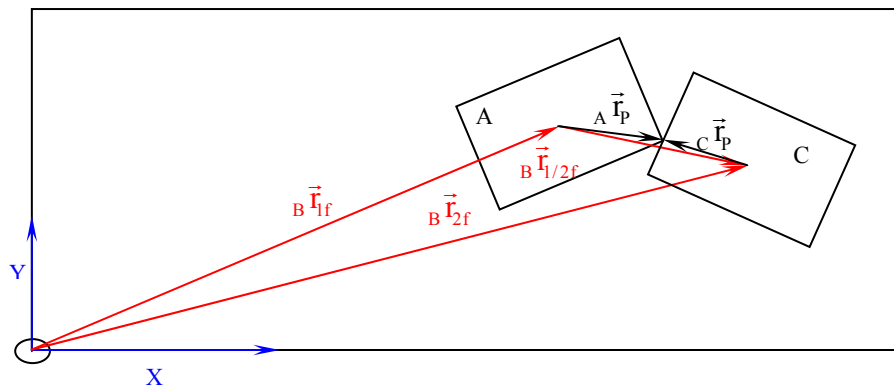


Figure 3.23 Vector diagram after impact (cylindrical parts).

Based on the figure 3.23 it is obtained:

$${}^B\vec{r}_{\frac{1}{2}i} + {}^C\vec{r}_{PCi} = {}^A\vec{r}_{PAi} + \vec{g}_N$$

then

$$\vec{g}_N = {}^B\vec{r}_{\frac{1}{2}i} + {}^C\vec{r}_{PCi} - {}^A\vec{r}_{PAi}$$

(3.39)

The rotations matrices are $[A_x]_\varphi$ and $[A_z]_\theta$. These matrices are in homogenous coordinates.

$$[A_x]_\varphi = \begin{bmatrix} 1 & 0 & 0 & 0 \\ 0 & \cos(\varphi_c) & -\sin(\varphi_c) & 0 \\ 0 & \sin(\varphi_c) & \cos(\varphi_c) & 0 \\ 0 & 0 & 0 & 1 \end{bmatrix}$$

$$[A_z]_\theta = \begin{bmatrix} \cos(\theta_c) & \sin(\theta_c) & 0 & 0 \\ -\sin(\theta_c) & \cos(\theta_c) & 0 & 0 \\ 0 & 0 & 1 & 0 \\ 0 & 0 & 0 & 1 \end{bmatrix}$$

The transformation matrix is:

$$[T]_C = \begin{bmatrix} \cos(\theta_c) & \sin(\theta_c)\cos(\varphi_c) & -\sin(\theta_c)\sin(\varphi_c) & -x_2 \\ -\sin(\theta_c) & \cos(\theta_c)\cos(\varphi_c) & -\cos(\theta_c)\sin(\varphi_c) & -y_2 \\ 0 & \sin(\varphi_c) & \cos(\varphi_c) & 0 \\ 0 & 0 & 0 & 1 \end{bmatrix}$$

With this matrix it obtains the vector respect fixed frame for the part C:

$${}_B\vec{r}_{CPi} = \begin{bmatrix} x_{cp} \cos(\theta_c) + y_{cp} \sin(\theta_c) \cos(\varphi_c) - x_2 \\ -x_{cp} \sin(\theta_c) + y_{cp} \cos(\theta_c) \cos(\varphi_c) - y_2 \\ y_{cp} \sin(\varphi_c) \\ 1 \end{bmatrix} \quad (3.40)$$

The transformation matrix of the part A is obtained by the same way that the transformation matrix of part C and is given by:

$$[T]_A = \begin{bmatrix} \cos(\theta_A) & \sin(\theta_A)\cos(\varphi_A) & -\sin(\theta_A)\sin(\varphi_A) & -x_1 \\ \sin(\theta_A) & \cos(\theta_A)\cos(\varphi_A) & \cos(\theta_A)\sin(\varphi_A) & -y_1 \\ 0 & \sin(\varphi_A) & \cos(\varphi_A) & 0 \\ 0 & 0 & 0 & 1 \end{bmatrix}$$

With this matrix it obtains the vector respect fixed frame for the part C:

$${}^B\vec{r}_{Api} = \begin{bmatrix} \cos(\theta_A)x_{Ap} + \sin(\theta_A)\cos(\varphi_A)y_{Ap} - x_1 \\ -x_{Ap}\sin(\theta_A) + y_{Ap}\cos(\theta_A)\cos(\varphi_A) - y_1 \\ y_{Ap}\sin(\varphi_A) \end{bmatrix} \quad (3.41)$$

The relative distance is obtained from the equations 3.40 and 3.41:

$$\vec{g}_N = \begin{pmatrix} x_{cp}\cos(\theta_c) + y_{cp}\sin(\theta_c)\cos(\varphi_c) - x_2 - \cos(\theta_A)x_{Ap} - y_{Ap}\sin(\theta_A)\cos(\varphi_A) + x_1 \\ -x_{cp}\sin(\theta_c) + y_{cp}\cos(\theta_c)\cos(\varphi_c) - y_2 + x_{Ap}\sin(\theta_A) - y_{Ap}\cos(\theta_A)\cos(\varphi_A) + y_1 \\ \sin(\varphi_c)y_{cp} - y_{Ap}\sin(\varphi_A) \end{pmatrix} \quad (3.42)$$

The relative velocity is obtained differentiating the equation 3.42

$$\dot{\mathbf{g}}_N = \underbrace{\begin{bmatrix}
 -\cos(\theta_A) & -\sin(\theta_A)\cos(\varphi_A) & \cos(\theta_c) & \sin(\theta_c)\cos(\varphi_c) & 1 & -1 & 0 & 0 & \sin(\theta_A)x_{cp} - \cos(\theta_A)\cos(\varphi_A)y_{Ap} \\
 & & & & & & & -\sin(\theta_c)x_{cp} + \cos(\theta_c)\cos(\varphi_c)y_{cp} & \sin(\theta_A)\sin(\varphi_A)y_{Ap} & -\sin(\theta_c)\sin(\varphi_c)y_{cp} \\
 \sin(\theta_A) & -\cos(\theta_A)\cos(\varphi_A) & -\sin(\theta_c) & \cos(\theta_c)\cos(\varphi_c) & 0 & 0 & 1 & -1 & \cos(\theta_A)x_{cp} + \sin(\theta_A)\cos(\varphi_A)y_{Ap} \\
 & & & & & & & -\cos(\theta_c)x_{cp} - \sin(\theta_c)\cos(\varphi_c)y_{cp} & \cos(\theta_A)\sin(\varphi_A)y_{Ap} & -\cos(\theta_c)\sin(\varphi_c)y_{cp} \\
 0 & -\sin(\varphi_A) & 0 & \cos(\varphi_c) & 0 & 0 & 0 & 0 & 0 & 0 \\
 & & & & & & & 0 & -\sin(\varphi_A) & \cos(\varphi_c)
 \end{bmatrix}}_{W^T} \underbrace{\begin{bmatrix}
 \dot{x}_{Ap} \\
 \dot{y}_{Ap} \\
 \dot{x}_{cp} \\
 \dot{y}_{cp} \\
 \dot{x}_1 \\
 \dot{x}_2 \\
 \dot{y}_1 \\
 \dot{y}_2 \\
 \dot{\theta}_A \\
 \dot{\theta}_c \\
 \dot{\varphi}_A \\
 \dot{\varphi}_c
 \end{bmatrix}}_{\dot{\mathbf{q}}} \quad (3.43)$$

The mass matrix for the cylinder part respect to the rotation axis is given by a diagonal matrix. This matrix contained the displacements mass and rotations mass.

The rotations mass are the inertia moments (I) respect to the rotation axis.

$$I_x = \frac{1}{16} m_p d^2, \quad \text{and} \quad I_z = \frac{1}{12} m_p \left(\frac{3}{4} d^2 + h^2 \right)$$

$$[M] = \begin{bmatrix} m_p & 0 & 0 & 0 & 0 & 0 & 0 & 0 & 0 & 0 & 0 & 0 \\ 0 & m_p & 0 & 0 & 0 & 0 & 0 & 0 & 0 & 0 & 0 & 0 \\ 0 & 0 & m_p & 0 & 0 & 0 & 0 & 0 & 0 & 0 & 0 & 0 \\ 0 & 0 & 0 & m_p & 0 & 0 & 0 & 0 & 0 & 0 & 0 & 0 \\ 0 & 0 & 0 & 0 & m_p & 0 & 0 & 0 & 0 & 0 & 0 & 0 \\ 0 & 0 & 0 & 0 & 0 & m_p & 0 & 0 & 0 & 0 & 0 & 0 \\ 0 & 0 & 0 & 0 & 0 & 0 & m_p & 0 & 0 & 0 & 0 & 0 \\ 0 & 0 & 0 & 0 & 0 & 0 & 0 & m_p & 0 & 0 & 0 & 0 \\ 0 & 0 & 0 & 0 & 0 & 0 & 0 & 0 & I_x & 0 & 0 & 0 \\ 0 & 0 & 0 & 0 & 0 & 0 & 0 & 0 & 0 & I_x & 0 & 0 \\ 0 & 0 & 0 & 0 & 0 & 0 & 0 & 0 & 0 & 0 & I_z & 0 \\ 0 & 0 & 0 & 0 & 0 & 0 & 0 & 0 & 0 & 0 & 0 & I_z \end{bmatrix}$$

Replacing these matrices into the equation 3.24 it is obtained the final result for the contact of two cylindrical parts.

$$\Lambda_N = (1 - \varepsilon) \cdot \left[W_N^T \cdot [M]^{-1} \cdot W_N \right]^{-1} \cdot \dot{\tilde{g}}_{NA} \quad (3.44)$$

3.4 Summary

In this chapter the multibody theory was employed for the analysis of the dynamic behavior of rectangular and cylindrical parts. The cases studied were: insolate part, part on horizontal plane, part on inclined plane and contact between two parts. The obtained equations describe the phenomenon of interaction and contact for parts on the bowl. The results obtained in this chapter will be used for different parameters.

CHAPTER 4

Dynamic Analysis with Screw Theory

4.1 Introduction

In this chapter the screw theory is used to evaluate the friction forces on the cylindrical part; this analysis provides a complete description of the dynamic behavior. The Coulomb friction equation is the linear relationship between the normal force and friction force. This equation is correct for the maximums static and kinetic friction forces. In the case of the rolling motion of a cylinder, the friction forces are not necessarily maxima. For this case, the friction force must be found so that the dynamic analysis is complete. This chapter begins with a reduction of forces to a wrench based on Poinot's theorem (Lipkin and Duffy, 2002). This analysis is only for the case of rolling on the horizontal plane. The analysis of the spatial motion of the rigid body is based on the dual Euler equation 2.14, which completely describes the dynamic state of the rigid body.

4.2 Wrench analysis

The goal of this section is to analyze the cylinder part dynamic behavior. This is accomplished by reducing the external forces and moments acting about a cylindrical part to a wrench. Figure 3.17 shows the free body diagram of a cylindrical part. The first step is placed at the center all the external forces with its generated moment (M_{Tx} and M_{Ty}) showed in figure 4.1.

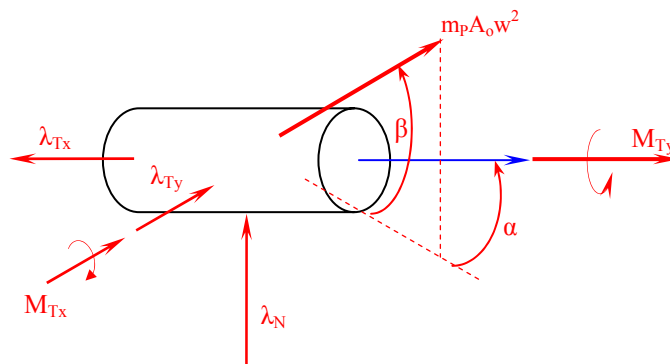


Figure 4.1 External forces on a cylindrical part.

The figure 4.2 shows the resultant wrench ($\hat{\$}_R$) and the position vector respect to part center.

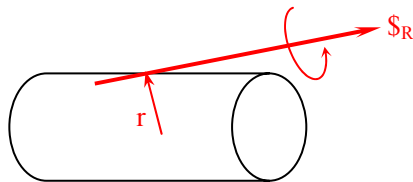


Figure 4.2 Resultant wrench.

The wrench direction is the resultant force direction. The resultant moment magnitude on resultant force axis is

$$M_1 = \frac{\vec{F}_R \cdot \vec{M}_R}{|\vec{F}_R|^2} \quad (4.1)$$

where M_R is the resultant moment vector and F_R is the resultant force vector

From the equation 4.1 the wrench can be written as

$$\hat{\$}_R = (\vec{F}_R; \vec{r} \times \vec{F}_R + h\vec{F}_R) = \vec{F}_R + \mathcal{E}(\vec{r} \times \vec{F}_R + h\vec{F}_R) \quad (4.2)$$

The condition is considered for M_1 to be the unique resultant moment about the body

$$\vec{r} \times \vec{F}_R = -\vec{M}_2 \quad (4.3)$$

The moments M_1 and M_2 are the rectangular components of the resultant moment M_R , where M_1 and M_2 are parallel and perpendicular to the screw axis respectively.

$$\vec{M}_1 + \vec{M}_2 = \vec{M}_R \quad (4.4)$$

Substituting the equations 4.1 and 4.3 into the equation 4.4 it is obtained

$$\vec{r} \times \vec{F}_R = -\vec{M}_R + \frac{\vec{F}_R \cdot \vec{M}_R}{|\vec{F}_R|^2} \vec{F}_R \quad (4.5)$$

The unknown is r ; applying the cross product in both side of the equation 4.5 by F_R it is obtained:

$$(\vec{r} \times \vec{F}_R) \times \vec{F}_R = \left(-\vec{M}_R + \frac{\vec{F}_R \cdot \vec{M}_R}{|\vec{F}_R|^2} \vec{F}_R \right) \times \vec{F}_R$$

The triple cross product is equal to

$$(\vec{r} \times \vec{F}_R) \times \vec{F}_R = (\vec{F}_R \cdot \vec{r}) \vec{F}_R - (\vec{F}_R \cdot \vec{F}_R) \vec{r}$$

but the dot product between F_R and r is equal to zero. F_R and r are perpendicular, then

$$(\vec{r} \times \vec{F}_R) \times \vec{F}_R = -(\vec{F}_R \cdot \vec{F}_R) \vec{r}$$

Replacing this result and solving for \vec{r} it is obtained

$$\vec{r} = \frac{\vec{M}_R \times \vec{F}_R}{\vec{F}_R \cdot \vec{F}_R} \quad (4.6)$$

Then, the wrench can be written as:

$$\hat{\$} = \left(\vec{F}_R; \vec{r} \times \vec{F}_R + \frac{\vec{F}_R \cdot \vec{M}_R}{|\vec{F}_R|^2} \vec{F}_R \right) \quad (4.7)$$

4.3 Analysis dynamic of cylindrical part using screw theory

A part is considered cylindrical when the ratio $L/D > 0.8$, where L is the length and D is the diameter. If the ratio $L/D < 0.8$ then the part is a disc (Boothroyd 1989).

The figure 4.3 shows the cylindrical part on the horizontal plane with two coordinates frame. The first frame is the fixed frame with center in the rolling point. The second frame is fixed to body with the center in the figure center.

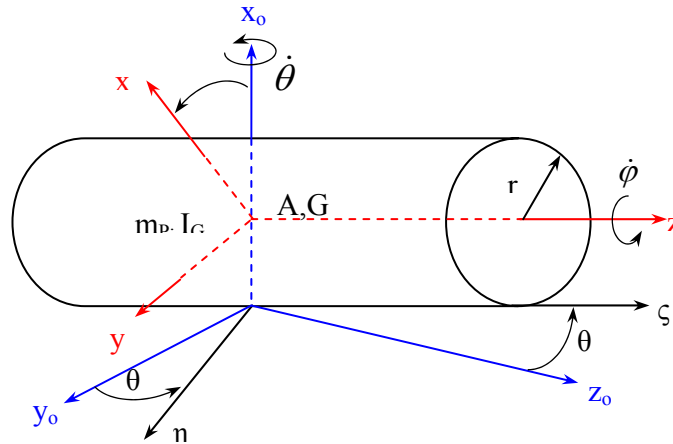


Figure 4.3 Coordinates frame of a cylindrical part in rolling.

The screw velocity referred to point A and expressed in the body frame is

$$\hat{\$}_{V_A} = \begin{bmatrix} \dot{\theta} \cos(\varphi) \\ -\dot{\theta} \sin(\varphi) \\ \dot{\varphi} \end{bmatrix} + \epsilon r \begin{bmatrix} \dot{\varphi} \sin(\varphi) \\ \dot{\varphi} \cos(\varphi) \\ 0 \end{bmatrix}$$

where

$$\vec{\omega} = \begin{bmatrix} \dot{\theta} \cos(\varphi) \\ -\dot{\theta} \sin(\varphi) \\ \dot{\phi} \end{bmatrix} \quad \text{and} \quad \vec{V}_A = r \begin{bmatrix} \dot{\phi} \sin(\varphi) \\ \dot{\phi} \cos(\varphi) \\ 0 \end{bmatrix}$$

The vectors $\vec{\omega}$ and \vec{V}_A are the angular and linear velocities respectively. The momentum screw defined in the equation 2.11 is equal to

$$\hat{\$}_{H_A} = \vec{q} + \boldsymbol{\varepsilon} \vec{H}_A$$

The vector \vec{q} is the linear momentum equal to

$$\vec{q} = m_p \left(\vec{V}_A + \vec{\omega} \times \overline{AG} \right)$$

The angular moment is defined by

$$\vec{H}_A = [I_A] \vec{\omega} + m_p \left(\overline{AG} \times \vec{V}_A \right)$$

but the vector \overline{AG} is equal to zero because A and G are in the same position. Then the vectors \vec{q} and \vec{H}_A are equal to:

$$\vec{q} = m_p \vec{V}_A$$

and

$$\vec{H}_A = [I_A] \vec{\omega}$$

(4.8)

The inertial matrix $[I_A]$ is equal to:

$$[I_A] = \begin{bmatrix} \frac{1}{12} m_p (3r^2 + L^2) & 0 & 0 \\ 0 & \frac{1}{12} m_p (3r^2 + L^2) & 0 \\ 0 & 0 & \frac{1}{2} m_p r^2 \end{bmatrix} = \frac{m_p r^2}{12} \begin{bmatrix} 3 + \left(\frac{L}{r}\right)^2 & 0 & 0 \\ 0 & 3 + \left(\frac{L}{r}\right)^2 & 0 \\ 0 & 0 & 6 \end{bmatrix}$$

From the equation 4.8, the momentum screw can be written as:

$$\hat{\$}_{H_A} = m_p r \begin{bmatrix} \dot{\varphi} \sin(\varphi) \\ \dot{\varphi} \cos(\varphi) \\ 0 \end{bmatrix} + \boldsymbol{\varepsilon} \frac{m_p r^2}{12} \begin{bmatrix} \left(3 + \left(\frac{L}{r}\right)^2\right) \dot{\theta} \cos(\varphi) \\ -\left(3 + \left(\frac{L}{r}\right)^2\right) \dot{\theta} \sin(\varphi) \\ 6\dot{\varphi} \end{bmatrix} \quad (4.9)$$

The cross screw product of the velocity screw and the momentum screw is the screw

$\hat{\$}_P$:

$$\hat{\$}_P = \hat{\$}_{V_A} \otimes \hat{\$}_{H_A} = m r \begin{bmatrix} -\dot{\varphi}^2 \cos(\varphi) \\ \dot{\varphi}^2 \sin(\varphi) \\ \dot{\theta} \dot{\varphi} \end{bmatrix} + \boldsymbol{\varepsilon} \left(\frac{1}{12} m_p r^2\right) \begin{bmatrix} -\dot{\theta} \dot{\varphi} \sin(\varphi) \left(3 - \frac{L^2}{r^2}\right) \\ -\dot{\theta} \dot{\varphi} \cos(\varphi) \left(3 - \frac{L^2}{r^2}\right) \\ 0 \end{bmatrix} \quad (4.10)$$

Differentiating equation 4.9 it is obtained:

$$\begin{aligned} \frac{d}{dx}(\hat{\$}_{H_A}) &= \dot{\hat{q}} + \boldsymbol{\varepsilon} \dot{\hat{H}}_A = \hat{\$}_{N_A} \\ &= m_p r \begin{bmatrix} \ddot{\varphi} \sin(\varphi) + \dot{\varphi}^2 \cos(\varphi) \\ \ddot{\varphi} \cos(\varphi) - \dot{\varphi}^2 \sin(\varphi) \\ 0 \end{bmatrix} \\ &\quad + \boldsymbol{\varepsilon} \left(\frac{1}{12} m_p r^2\right) \begin{bmatrix} \left(3 + \frac{L^2}{r^2}\right) \ddot{\theta} \cos(\varphi) - \left(3 + \frac{L^2}{r^2}\right) \dot{\theta} \dot{\varphi} \sin(\varphi) \\ -\left(3 + \frac{L^2}{r^2}\right) \ddot{\theta} \sin(\varphi) - \left(3 + \frac{L^2}{r^2}\right) \dot{\theta} \dot{\varphi} \cos(\varphi) \\ 6\ddot{\varphi} \end{bmatrix} \end{aligned} \quad (4.11)$$

Based on the Euler dual equation

$$\hat{\$}_{F_A} = \hat{\$}_{N_A} + \hat{\$}_{P_A} \quad (4.12)$$

$$= m_p r \begin{bmatrix} \ddot{\varphi} \sin(\varphi) \\ \ddot{\varphi} \cos(\varphi) \\ \dot{\theta} \dot{\varphi} \end{bmatrix} + \varepsilon \left(\frac{1}{12} m_p r^2 \right) \begin{bmatrix} \left(3 + \frac{L^2}{r^2} \right) \ddot{\theta} \cos(\varphi) - 6 \dot{\theta} \dot{\varphi} \sin(\varphi) \\ - \left(3 + \frac{L^2}{r^2} \right) \ddot{\theta} \sin(\varphi) - 6 \dot{\theta} \dot{\varphi} \cos(\varphi) \\ 6 \ddot{\varphi} \end{bmatrix}$$

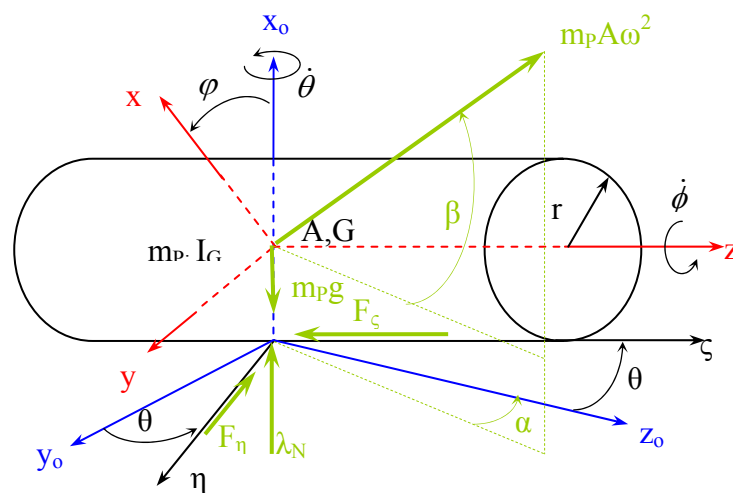


Figure 4.4 Forces on a cylindrical part.

Figure 4.4 shows the free body diagram of the cylindrical part on the horizontal plane. The forces F_η and F_ζ are the friction forces about η and ζ direction respectively. The force λ_N is the normal force between the two surfaces. The angles α and β are the vibration force directions. This set of forces and generate moments are referred and expressed in the body frame in the equation 4.13.

$$\hat{\$}_{F_A} = \begin{bmatrix} -F_\eta \sin(\varphi) + m_p A \omega^2 \cos(\beta) \sin(\alpha + \theta) \sin(\varphi) \\ \quad + (\lambda_N - m_p g + m_p A \omega^2 \sin(\beta) \cos(\varphi)) \\ -F_\eta \cos(\varphi) + m_p A \omega^2 \cos(\beta) \sin(\alpha + \theta) \cos(\varphi) \\ \quad - (\lambda_N - m_p g + m_p A \omega^2 \sin(\beta) \sin(\varphi)) \\ -F_\zeta + m_p A \omega^2 \cos(\beta) \cos(\alpha + \theta) \end{bmatrix} + \boldsymbol{\varepsilon} r \begin{bmatrix} -F_\zeta \sin(\varphi) \\ -F_\zeta \sin(\varphi) \\ F_\eta \end{bmatrix} \quad (4.13)$$

Equating the real and dual part of the equations 4.12 and 4.13 the following equations 4.14 are obtained:

$$\begin{aligned} -F_\eta \sin(\varphi) + m_p A \omega^2 \cos(\beta) \sin(\alpha + \theta) \sin(\varphi) \\ + (\lambda_N - m_p g) \cos(\varphi) + m_p A \omega^2 \sin(\beta) \cos(\varphi) = m_p r \ddot{\varphi} \sin(\varphi) \end{aligned} \quad (a)$$

$$\begin{aligned} -F_\eta \cos(\varphi) + m_p A \omega^2 \cos(\beta) \sin(\alpha + \theta) \cos(\varphi) \\ - (\lambda_N - m_p g) \sin(\varphi) - m_p A \omega^2 \sin(\beta) \sin(\varphi) = m_p r \ddot{\varphi} \cos(\varphi) \end{aligned} \quad (b)$$

$$-F_\zeta + m_p A \omega^2 \cos(\beta) \cos(\alpha + \theta) = m_p r \dot{\theta} \dot{\varphi} \quad (c)$$

$$-r F_\zeta \sin(\varphi) = \frac{1}{12} m_p r^2 \left[\left(3 + \frac{h^2}{r^2} \right) \ddot{\theta} \cos(\varphi) - 6 \dot{\theta} \dot{\varphi} \sin(\varphi) \right] \quad (d)$$

$$-r F_\zeta \cos(\varphi) = -\frac{1}{12} m_p r^2 \left[\left(3 + \frac{h^2}{r^2} \right) \ddot{\theta} \sin(\varphi) + 6 \dot{\theta} \dot{\varphi} \cos(\varphi) \right] \quad (e)$$

$$r F_\eta = \frac{1}{2} m_p r^2 \ddot{\varphi} \quad (f)$$

Equations 4.14a-4.14f are the necessary and sufficient relations for the description of the rolling cylinder. Manipulating equations 4.14a-4.14c, the components of the friction force and the normal reaction may be expressed, respectively, as:

$$F_\eta = m_p A \omega^2 \cos(\beta) \sin(\alpha + \theta) - m_p r \ddot{\varphi} \quad (4.15)$$

$$F_{\zeta} = m_p A \omega^2 \cos(\beta) \cos(\alpha + \theta) - m_p r \dot{\phi} \dot{\theta} \quad (4.16)$$

$$\lambda_N = m_p g - m_p A \omega^2 \sin(\beta) \quad (4.17)$$

Then manipulating equations 4.14d-4.14f, and with the aid of equations 4.15-4.17, the second order kinematic constraints imposed on the cylinder may expressed in the equations 4.18-4.20

$$\ddot{\theta} = 0 \quad (4.18)$$

$$\ddot{\phi} = \frac{2}{3r} A \omega^2 \cos(\beta) \sin(\alpha + \theta) \quad (4.19)$$

$$\dot{\theta} = \frac{2}{3r \dot{\phi}} A \omega^2 \cos(\beta) \cos(\alpha + \theta) \quad (4.20)$$

The obtained result suggests that if the sum of angles α and θ is equal to 90 degrees then the sliding does not occur and only rolling occurs.

4.4 Summary

In this chapter, the screw theory was employed for the analysis of the dynamic behavior of cylindrical parts. The case studied were part on horizontal plane. The obtained equations in this chapter will be modeled for different parameters. The equations are more general than in the chapter 3 because they take into consideration the rotation in the vertical axis. The direction of the axis was different to the chapter 3 by ease, but this does not change the result.

CHAPTER 5

Cases Analysis

5.1 Introduction

This chapter includes the results obtained from the results of chapters three and four. The first case in the analysis is the cylinder on the plane surface, because is the more interesting case. The variable parameters are the frequency, friction coefficient and vibration direction. The responses studied are the accelerations about different directions and the contact force. The objective is the comparison of some simulation results and some results obtained in previous works. This comparison required some assumptions such as to change of accelerations to velocities assumed an effective distance of the vibration force. These assumptions are necessary because the vibration forces are pulsed on the part due to the part jumps.

In this analysis the motion parameters such as frequency (f), vibration amplitude (A_0), friction coefficient (μ), excitation angles (α and β) and track inclination angles (γ and δ) will be changed to analyze the accelerations and transportation velocity behavior. These motion parameters are chosen for typical values from other experimental works done by Boothroyd (1992) and Wolfsteiner and Pfeiffer (2000). Some contour line graphics will be included for better visualization of the physical behavior.

5.2 Analysis of Cylinder on the plane surface

The analysis is based on the axes and excitation angles as shown in figure 3.17 shows in chapter 3. The figure 5.1 shows the acceleration in the x direction. The parameters values used are: $f=60\text{Hz}$, $A_0=5 \times 10^{-4}\text{m}$, $g=9.8\text{m/s}^2$ and $\mu=0.5$. This figure shows the maxima region for values of α form 0° to 20° and β from 8° to 45° . For these values it is obtained the maximum efficiency in the rate of part transporting.

Figure 5.2 shows surface contour lines of the figure 5.1. This figure shows the change in the acceleration versus the orientation parameters of vibration. The acceleration values are smaller for angles values out of maximum interval, and then the interval is an absolute maximum interval.

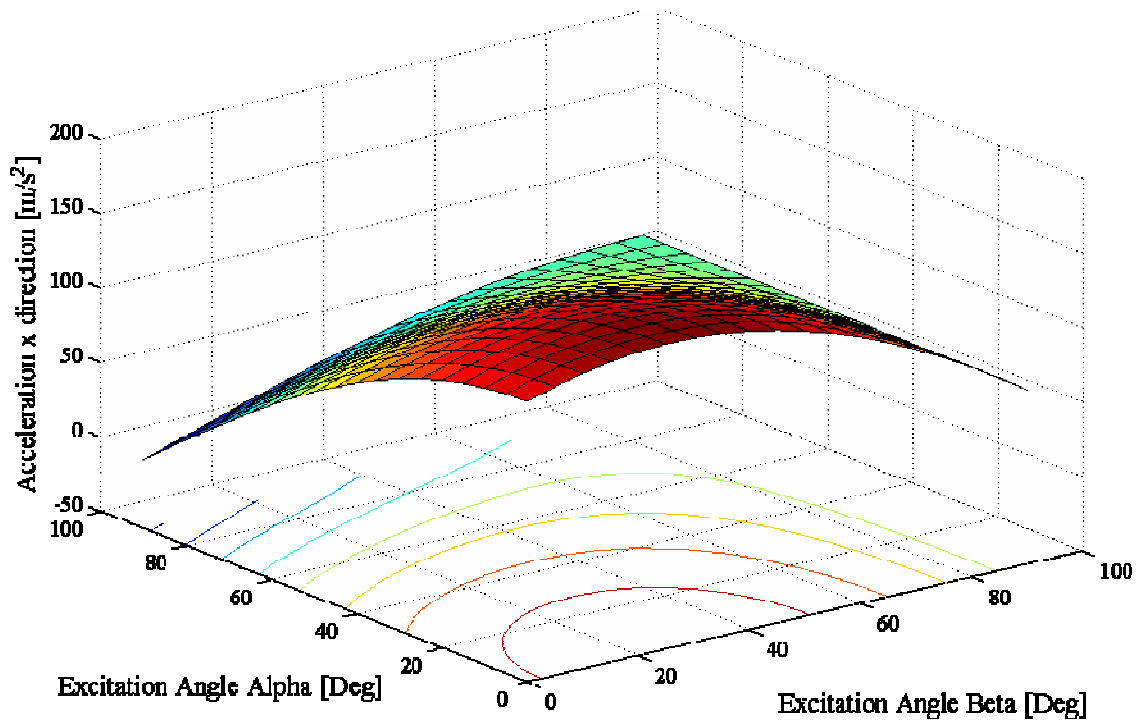


Figure 5.1 Acceleration in the x direction versus the excitation angles for cylindrical part on plane surface (surface).

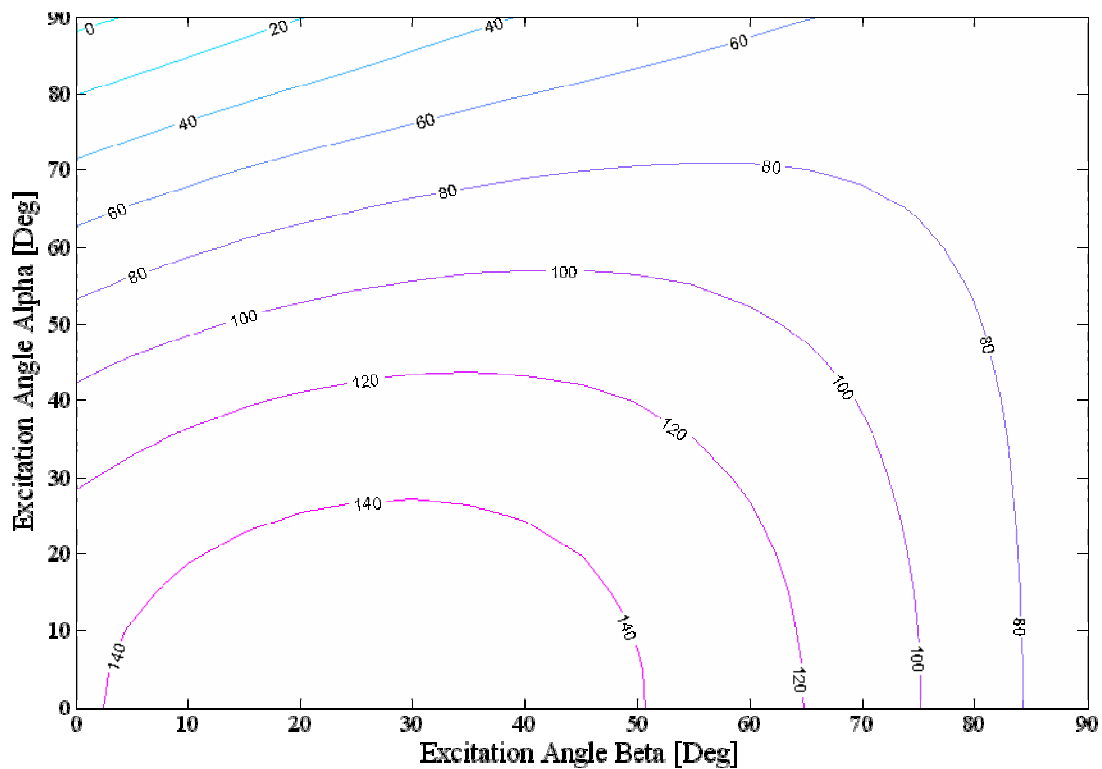


Figure 5.2 Acceleration in the x direction versus the excitation angles for cylindrical part on plane surface (contour lines).

The figure 5.3 shows the acceleration in the x direction as function of the friction coefficient and the elevation angle of the vibration force. The figure 5.4 shows the contour lines of the surface. The used parameters for this analysis are: $f=60\text{Hz}$, $\alpha=16^\circ$, $A_o=5 \times 10^{-4}\text{m}$ and $g=9.8\text{m/s}^2$. The friction coefficient increases if the acceleration increases; this is observed in the figure 5.3 and 5.4. A non-proportionality behavior out of the maximum interval for the β angle is showed.

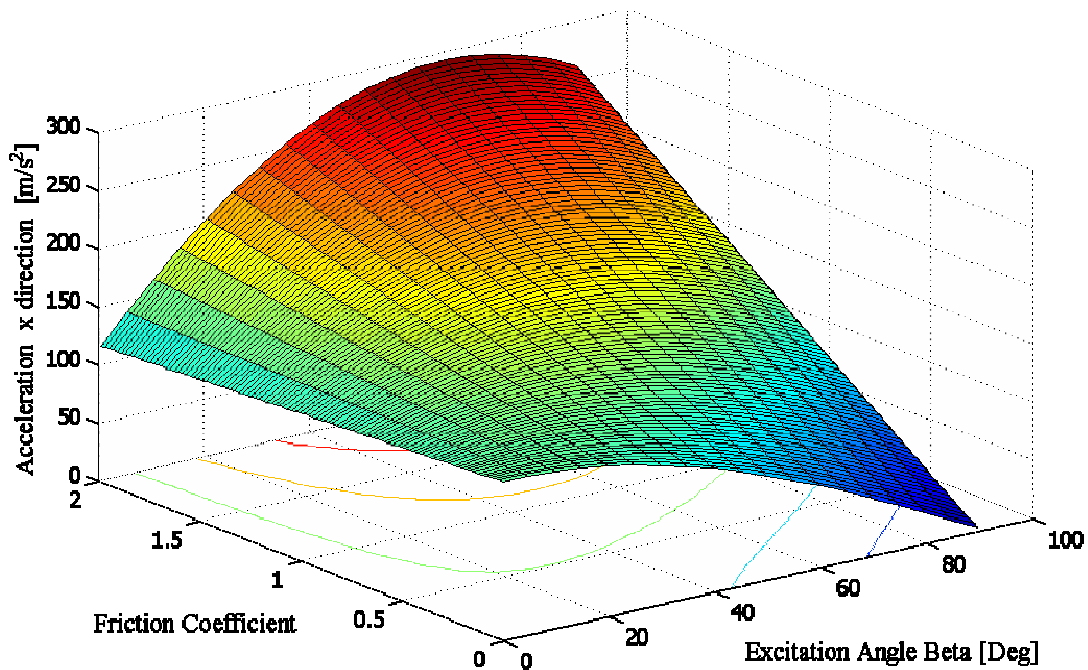


Figure 5.3 Acceleration in the x direction versus the excitation angle β and friction coefficient for cylindrical part on plane surface (surface).

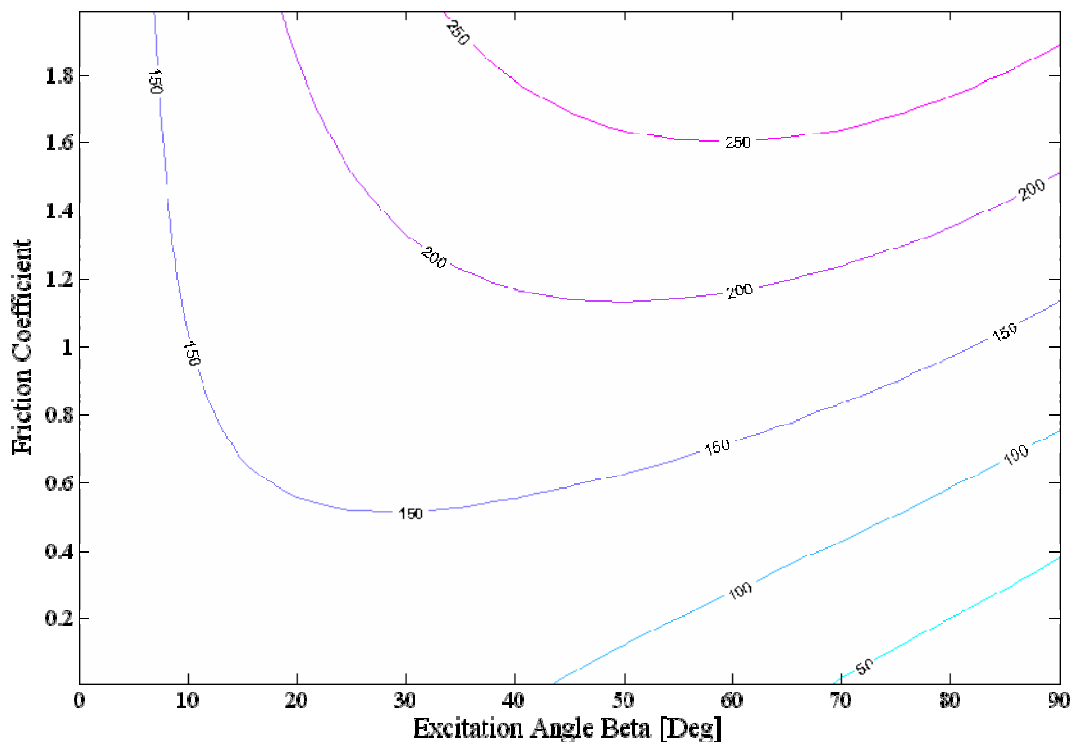


Figure 5.4 Acceleration in the x direction versus the excitation angle β and friction coefficient for cylindrical part on plane surface (contour lines).

Acceleration in the x direction versus the friction coefficient and frequency of vibration is shown in the figure 5.5. The contour lines are shown in the figure 5.6. The used parameters for these graphics are: $\alpha=16^\circ$, $\beta=20^\circ$, $A_o=5 \times 10^{-4}m$ and $g=9.8m/s^2$. The frequency effect in the acceleration is greater than the friction coefficient effect. In the study range the friction effect is linear but the frequency effect is parabolic. The friction effect is significant for $\mu > 0.2$ and in a range for the frequency of 50-80Hz.

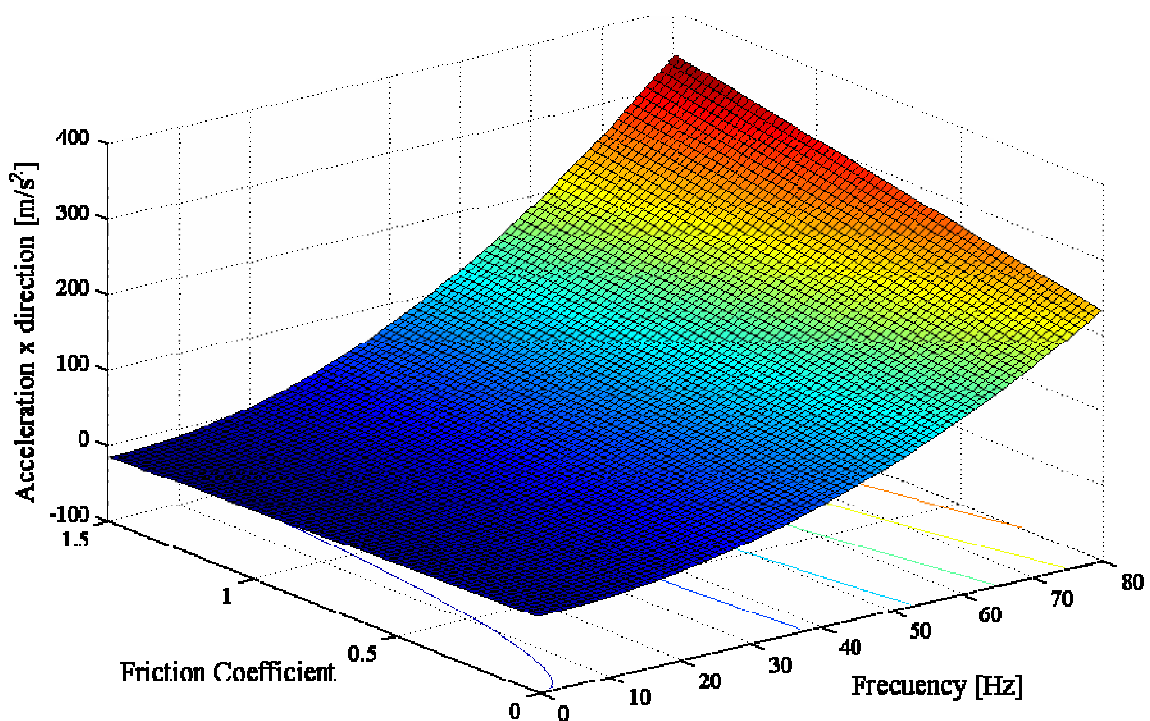


Figure 5.5 Acceleration in the x direction versus the frequency (f) and friction coefficient for cylindrical part on plane surface. Surface.

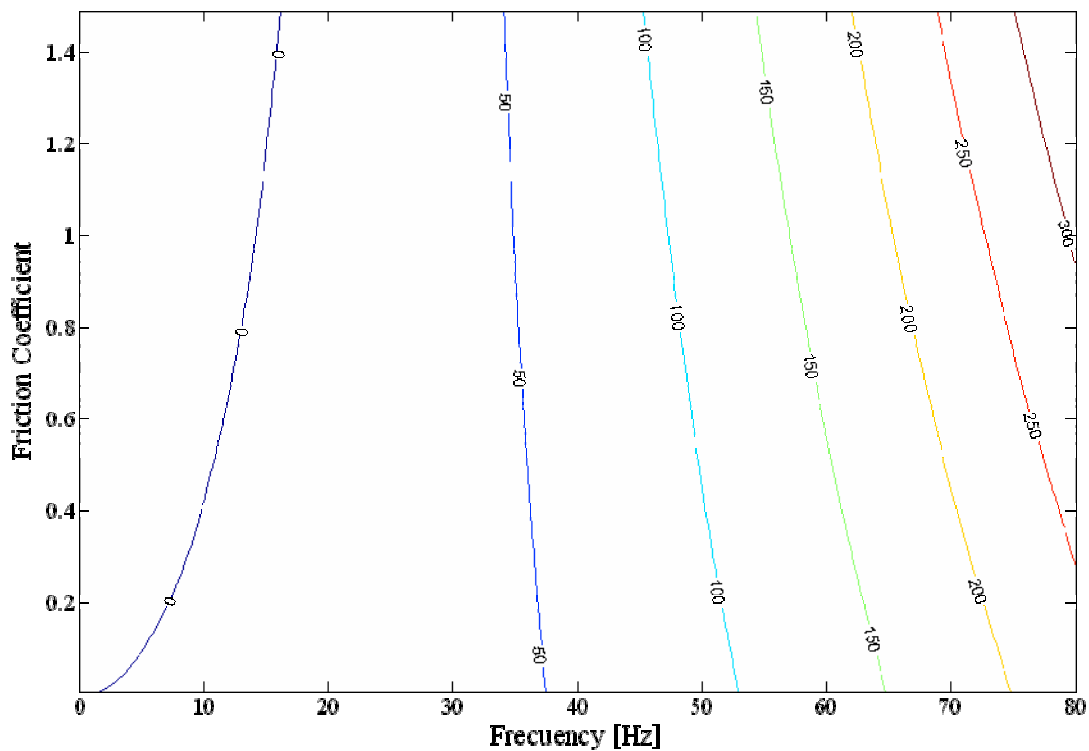


Figure 5.6 Acceleration in the x direction versus the frequency (f) and friction coefficient for cylindrical part on plane surface (contour lines).

The acceleration in the x direction versus the frequency and vibration angle β is shown in the figures 5.7 and 5.8. These figures show that an increase of acceleration agree with a increase in frequency. The used parameters for these graphics are: $\alpha=16^\circ$, $A_o=5 \times 10^{-4} m$, $\mu=0.5$ and $g=9.8 m/s^2$. The frequency effect is more significant and the excitation angle effect is significant in the high frequency region. The result agrees with the proposed model because the vibration force is modeled proportional to the square of the frequency and vibration amplitude.

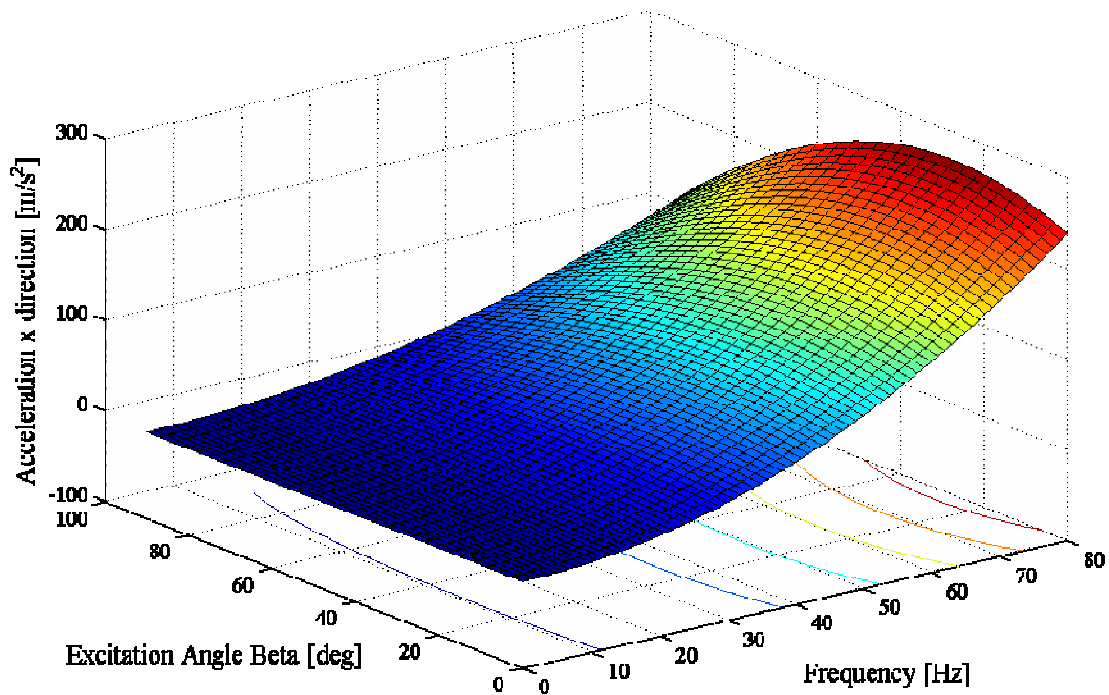


Figure 5.7 Acceleration in the x direction versus the frequency (f) and vibration angle (β) for cylindrical part on plane surface (surface).

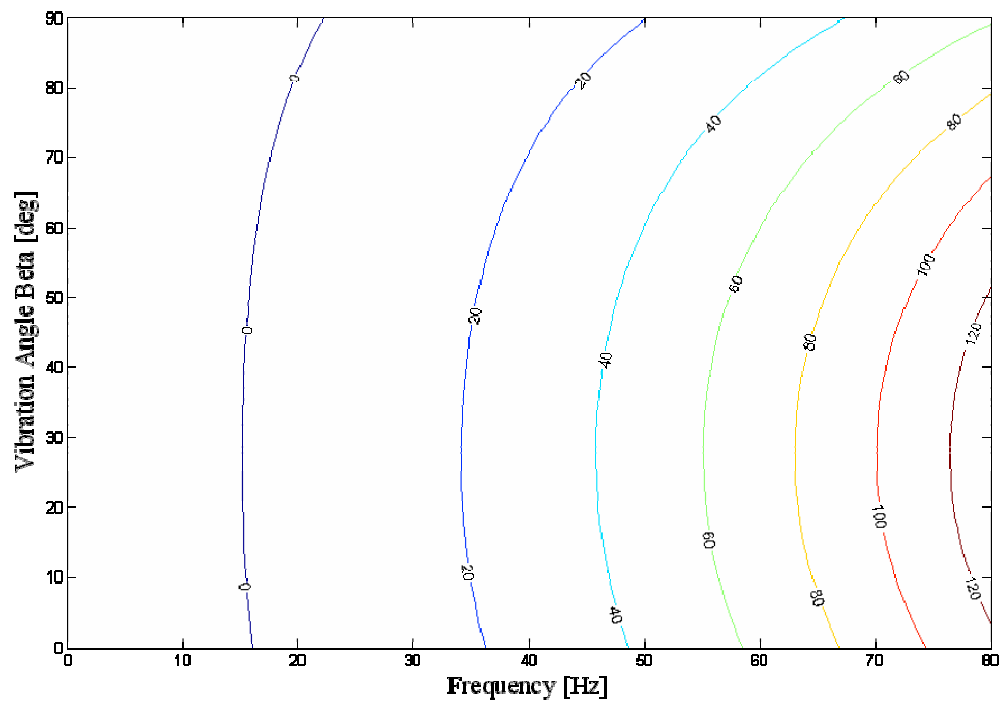


Figure 5.8 Acceleration in the x direction versus the frequency (f) and vibration angle (β) for cylindrical part on plane surface (contour lines).

A comparison of the acceleration in the x direction versus the vibration amplitude and the frequency is shown in the figures 5.9 and 5.10. These figures can be used to find the approximate transportation velocity. The used parameters are: $\alpha=16^\circ$, $\beta=15^\circ$, $\mu=0.5$ and $g=9.8m/s^2$. A non-linear behavior in function of the frequency is observed in these graphics; this result agrees with previous results. The behavior with respect to the vibration amplitude is linear and is significant in high and medium frequency regions.

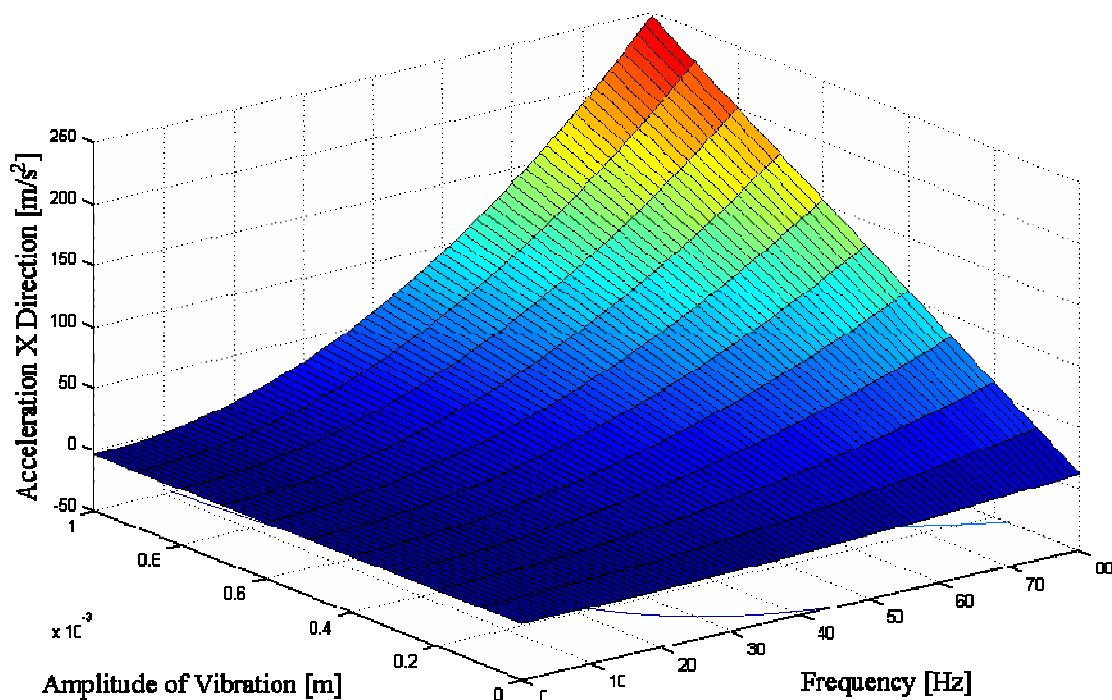


Figure 5.9 Acceleration in the x direction versus the frequency (f) and vibration amplitude for cylindrical part on plane surface (surface).

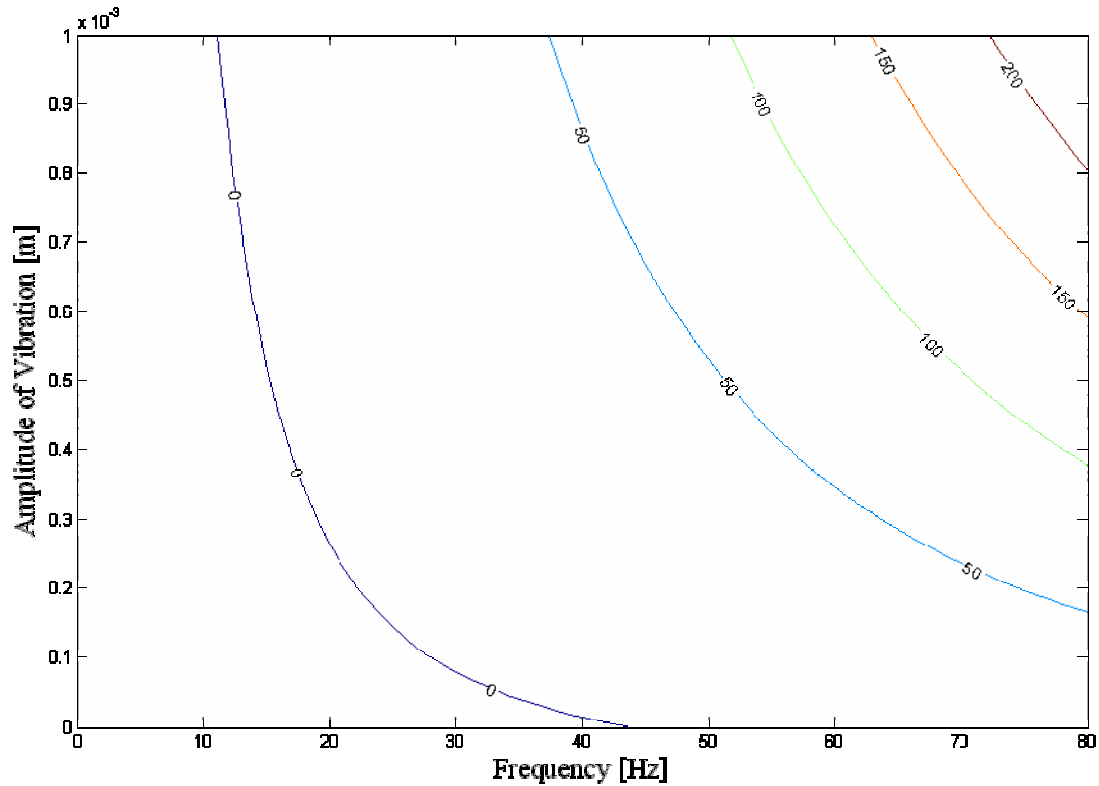


Figure 5.10 Acceleration in the x direction versus the frequency (f) and vibration amplitude for cylindrical part on plane surface (contour lines).

The acceleration in the y direction versus the angles of vibration force α and β is shown in the figure 5.11 and 5.12. The figures show an interval minimum for α from 0° to 20° and β from 0° to 45° . The used parameters are: $f=60\text{Hz}$, $A_0=5 \times 10^{-4}\text{m}$, $g=9.8\text{m/s}^2$ and $\mu=0.5$. The acceleration in the y direction is a loss motion originated by the non-unidirectional vibration force and track inclination angles.

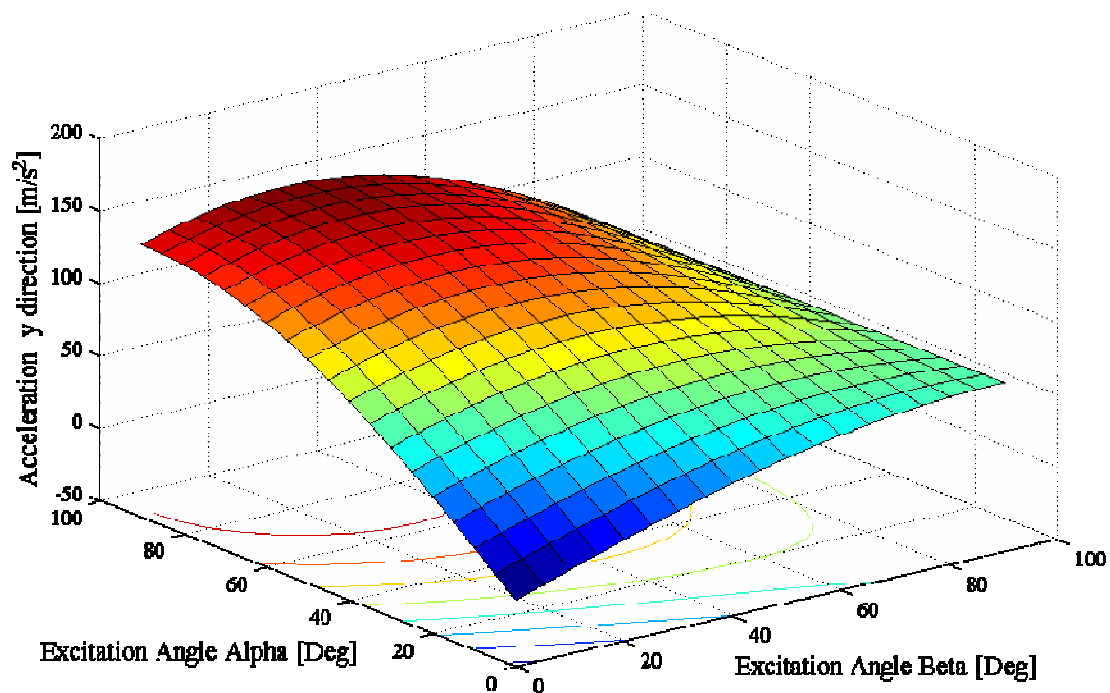


Figure 5.11 Acceleration in the y direction versus the excitation angles of the vibration force for cylindrical part on plane surface (surface).

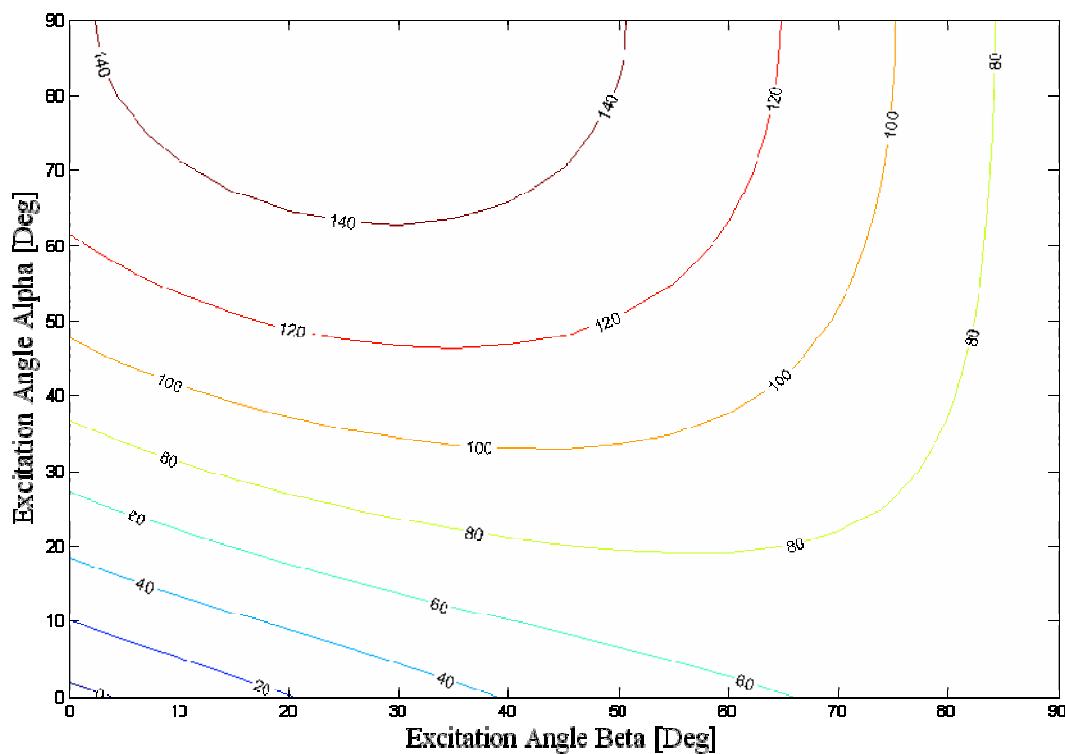


Figure 5.12 Acceleration in the y direction versus the excitation angles of the vibration force for cylindrical part on plane surface (contour lines).

The figures 5.13 and 5.14 show the acceleration in the y direction versus the angle β and the friction coefficient. The used parameters are: $f=60\text{Hz}$, $A_0=5 \times 10^{-4}\text{m}$, $g=9.8\text{m/s}^2$ and $\alpha=16^\circ$. The combined effect of the friction coefficient and the vibration angle is the displacement of the work range. The friction coefficient effect is a hyperbolic behavior of the surface. This effect is significant in the regions for small and high values of excitation angles.

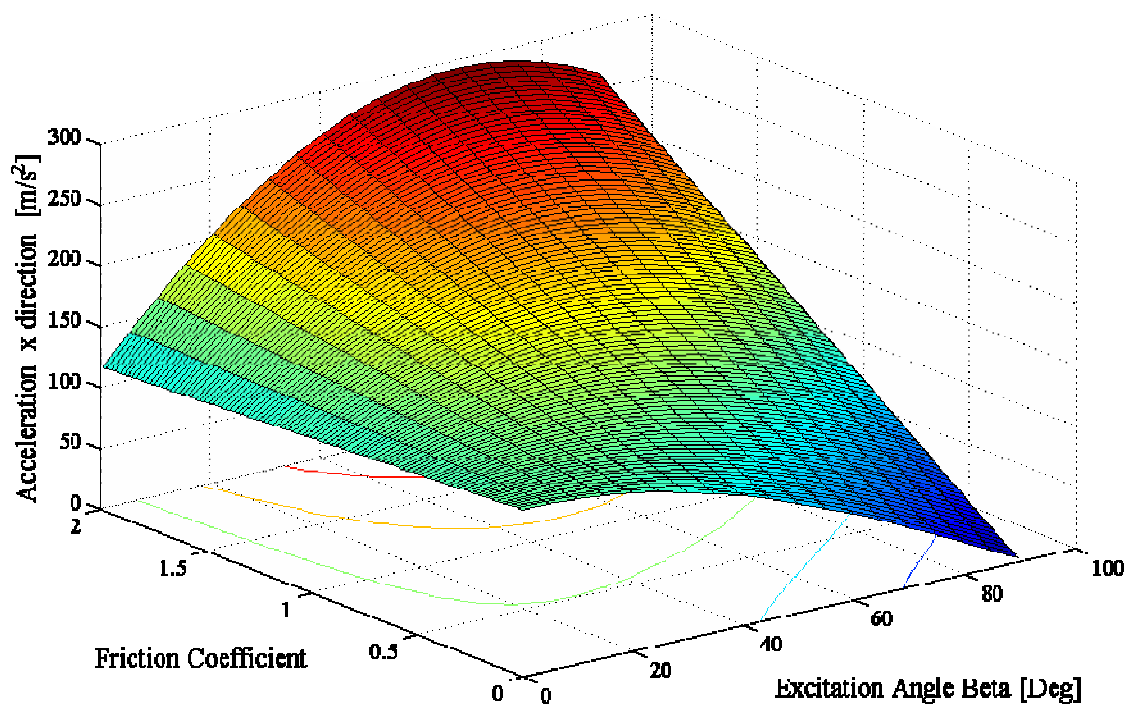


Figure 5.13 Acceleration in the y direction versus the excitation angle β and the friction coefficient for cylindrical part on plane surface (surface).

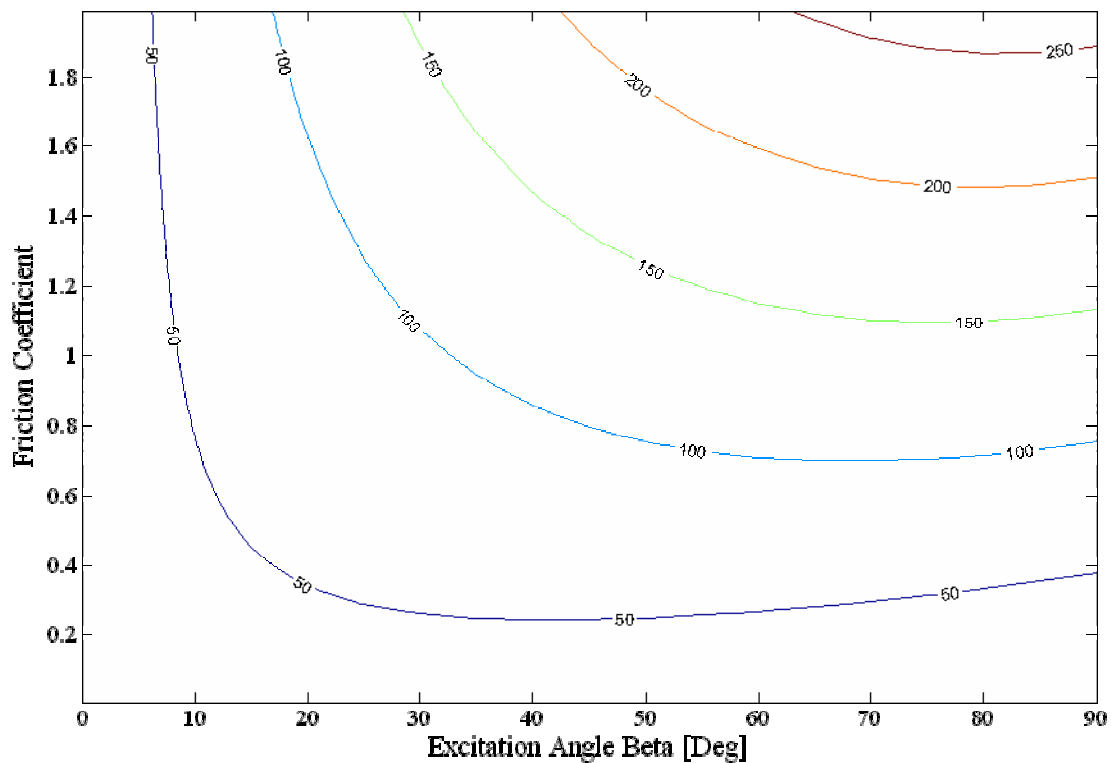


Figure 5.14 Acceleration in the y direction versus the excitation angle β and the friction coefficient for cylindrical part on plane surface (contour lines).

Acceleration in the y direction versus the angle β and the frequency is shown in the figures 5.15 and 5.16. These figures confirm the previous results. The interaction effect between β and the frequency is described as a translation of the work range. The used parameters are: $A_0 = 5 \times 10^{-4} m$, $g = 9.8 m/s^2$, $\mu = 0.5$ and $\alpha = 16^\circ$.

The y acceleration behavior is parabolic with respect to the frequency and sinusoidal with respect to the excitation angles. This acceleration increases the friction forces and decreases the rate of transportation. The optimal range is in small excitation angle values and frequency values in the intersection of high accelerations in the x direction and small accelerations in the y direction.

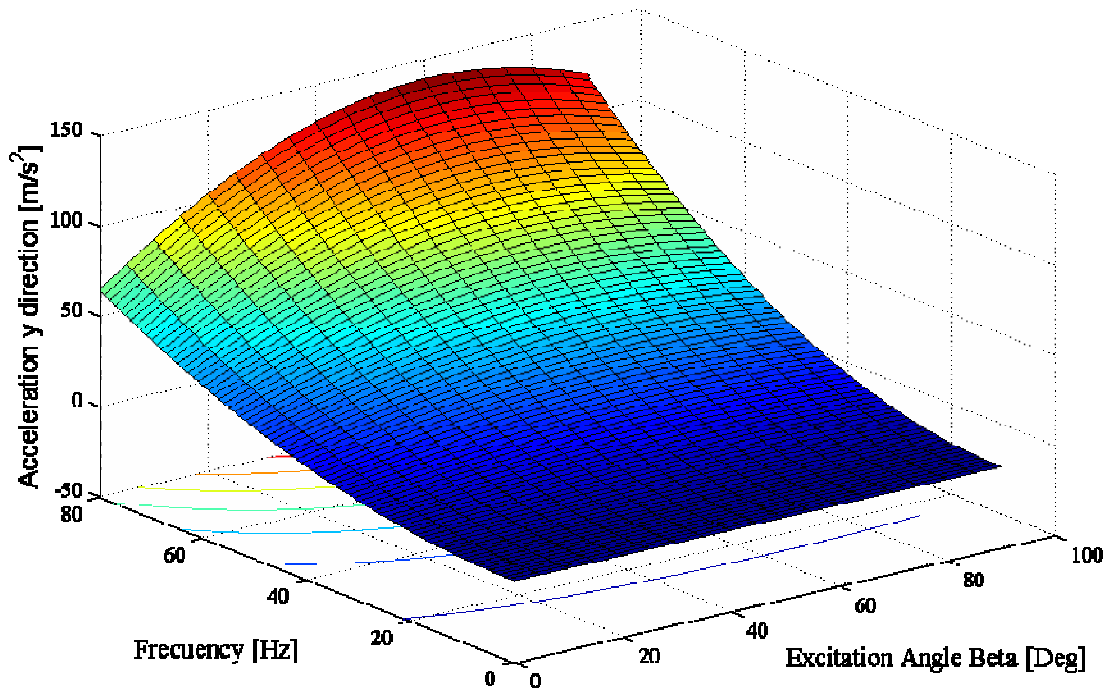


Figure 5.15 Acceleration in the y direction versus the excitation angle β and the frequency for cylindrical part on plane surface (surface).

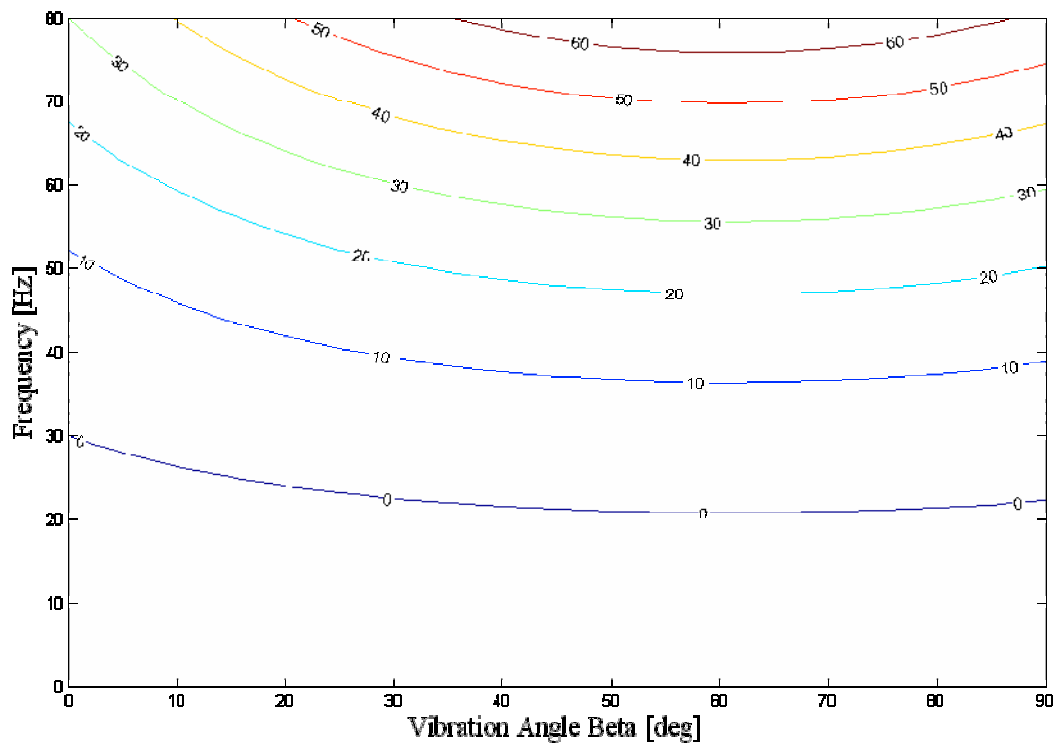


Figure 5.16 Acceleration in the y direction versus the excitation angle β and the frequency for cylindrical part on plane surface (contour lines).

The figures 5.17 and 5.18 show the variation of the acceleration in the y direction versus the frequency and the friction coefficient. The figure 5.18 shows the contour lines for this response surface. The interaction effect of these two factors is the curvature direction in the acceleration line. This curvature direction shows the weight of the frequency variation in a given range. The used parameters are: $A_0=5 \times 10^{-4} m$, $g=9.8 m/s^2$, $\beta=20^\circ$ and $\alpha=16^\circ$. The friction effects are significant in the small and high frequency regions. The friction coefficient has a linear effect while the frequency has a parabolic effect.

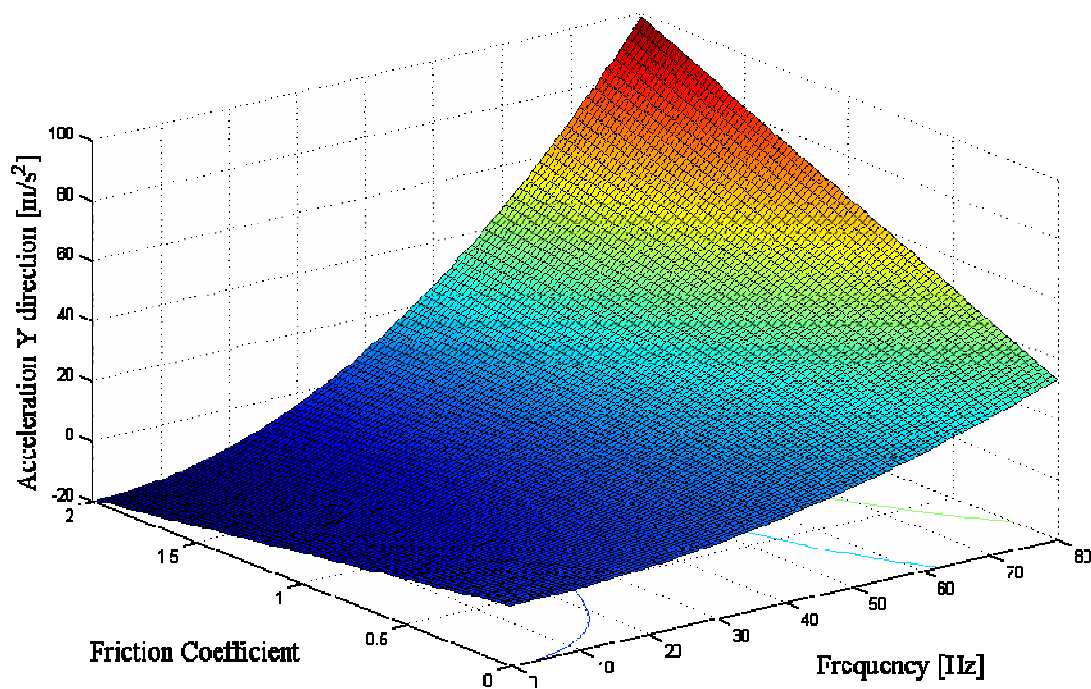


Figure 5.17 Acceleration in the y direction versus the frequency and the friction coefficient for cylindrical part on plane surface (surface).

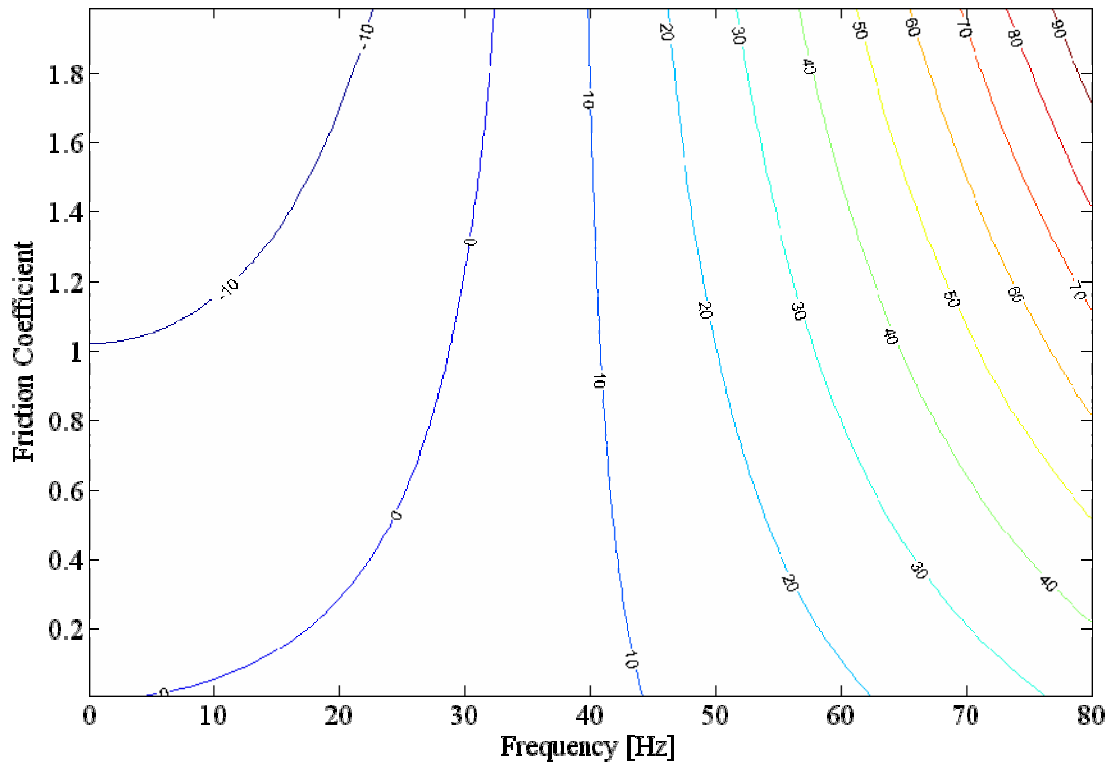


Figure 5.18 Acceleration in the y direction versus the frequency and the friction coefficient for cylindrical part on plane surface (contour lines).

The angular acceleration of the part versus the excitation angles α and β is shown in the figures 5.19 and 5.20. These figures show the variation of the angular acceleration and the effects of these two parameters. This acceleration is a consequence of all generated moments. The angular acceleration can be by rolling, sliding or both. The most general case is rolling plus sliding. The graphics show a sinusoidal behavior. The used parameters are: $A_0=5 \times 10^{-4}m$, $g=9.8m/s^2$, $f=60Hz$ and $\mu=0.5$.

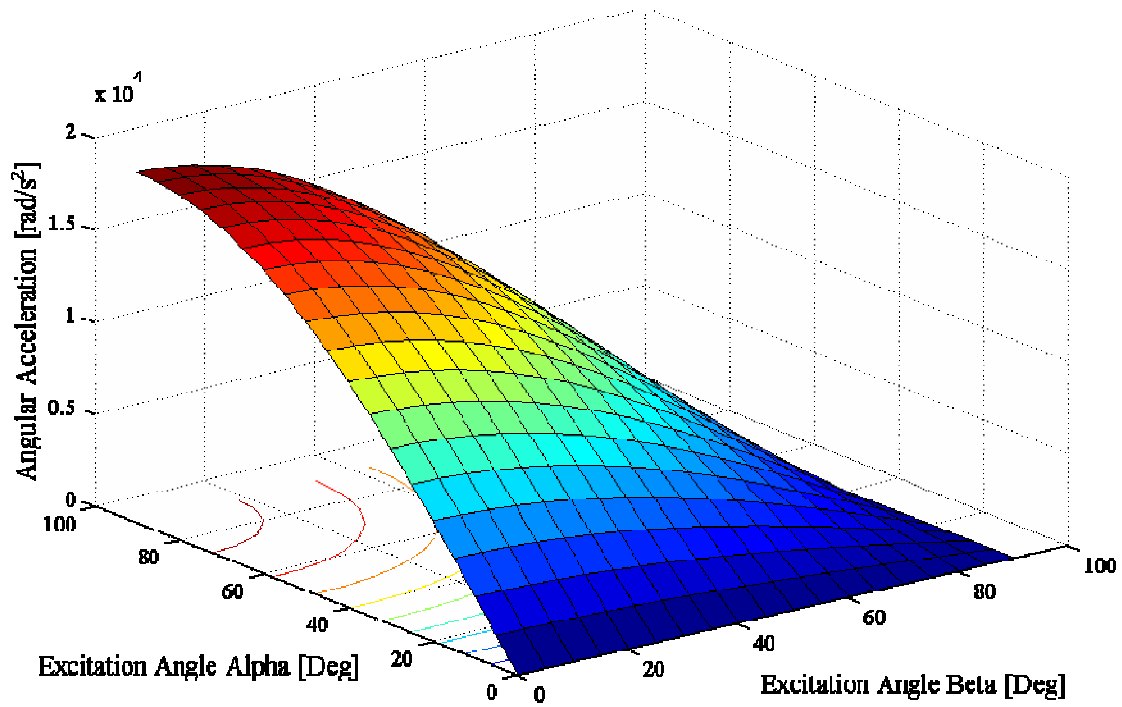


Figure 5.19 Angular acceleration versus the excitation angles α and β for cylindrical part on plane surface (surface).

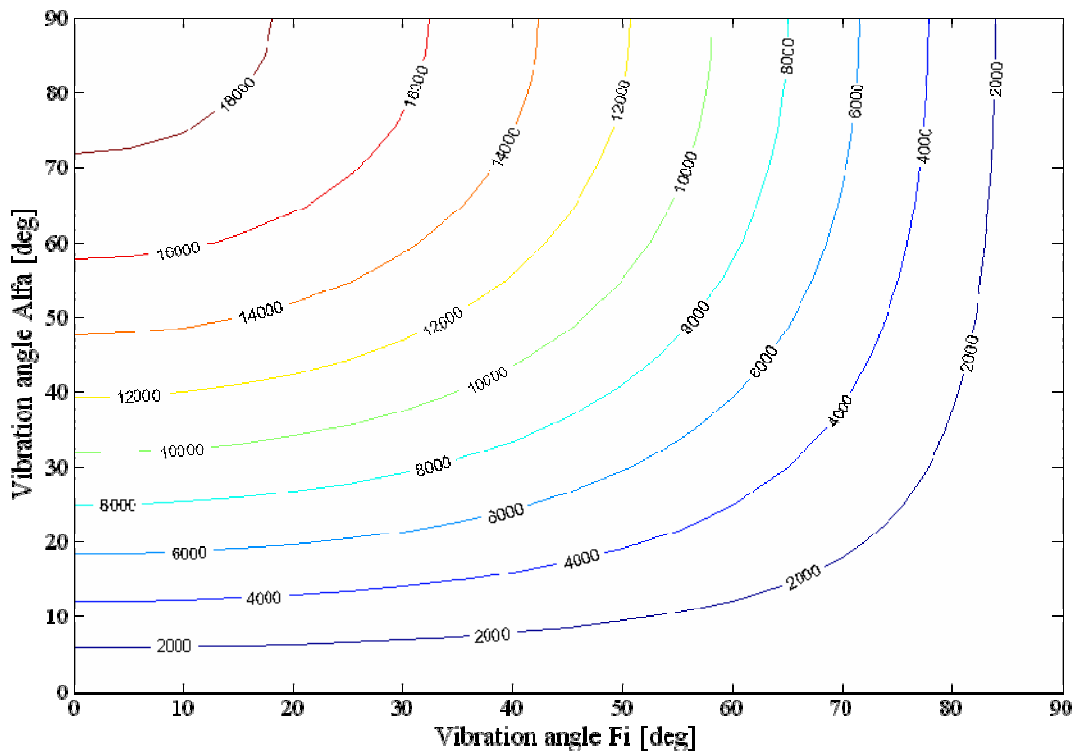


Figure 5.20 Angular acceleration versus the excitation angles α and β for cylindrical part on plane surface (contour lines).

Angular acceleration versus the frequency and the vibration angle β is presented in the figures 5.21. The used parameters are: $A_0=5 \times 10^{-4} m$, $g=9.8 m/s^2$, $\alpha=16^\circ$ and $\mu=0.5$. This graphic shows the interaction effect of the frequency and the vertical vibration angle on the angular acceleration. The frequency effect is parabolic and the effect of the excitation angle is sinusoidal. The angular acceleration increases if the frequency increases. Therefore, the work optimal frequency is the intersection of frequency curves for high accelerations in the x direction, small accelerations in the y direction and small angular accelerations.

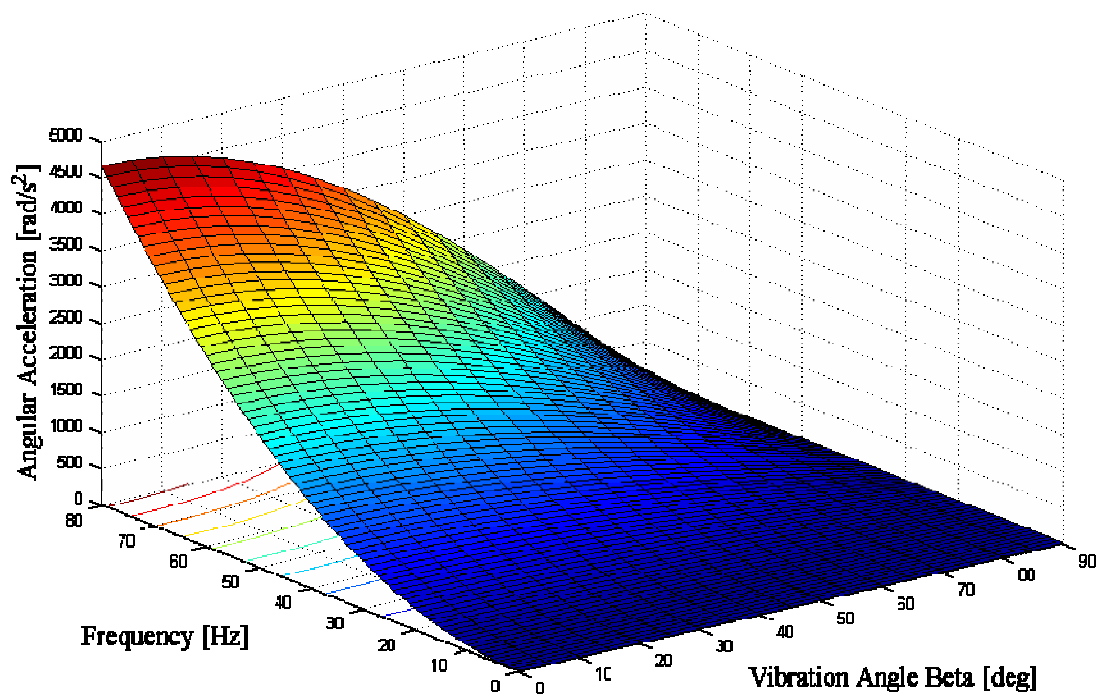


Figure 5.21 Acceleration in the y direction versus the excitation angles α and β for cylindrical part on plane surface.

5.3 Analysis of a Rectangular Part on the Narrow Track

The figure 3.8 in chapter 3 shows the parameters used for this analysis. The three-dimensional analysis for different conditions is presented in this section. The interactions between the parts themselves are negligible. The figure 5.22 shows the variation of the transportation velocity versus of frequency and vibration amplitude. The used parameters are: $\beta=5^\circ$, $\alpha=16^\circ$, $\delta=2^\circ$, $R=0.8m$, $a=0.15cm$, $b=1cm$, $h=5cm$, $\gamma=5^\circ$ and $\mu=0.3$.

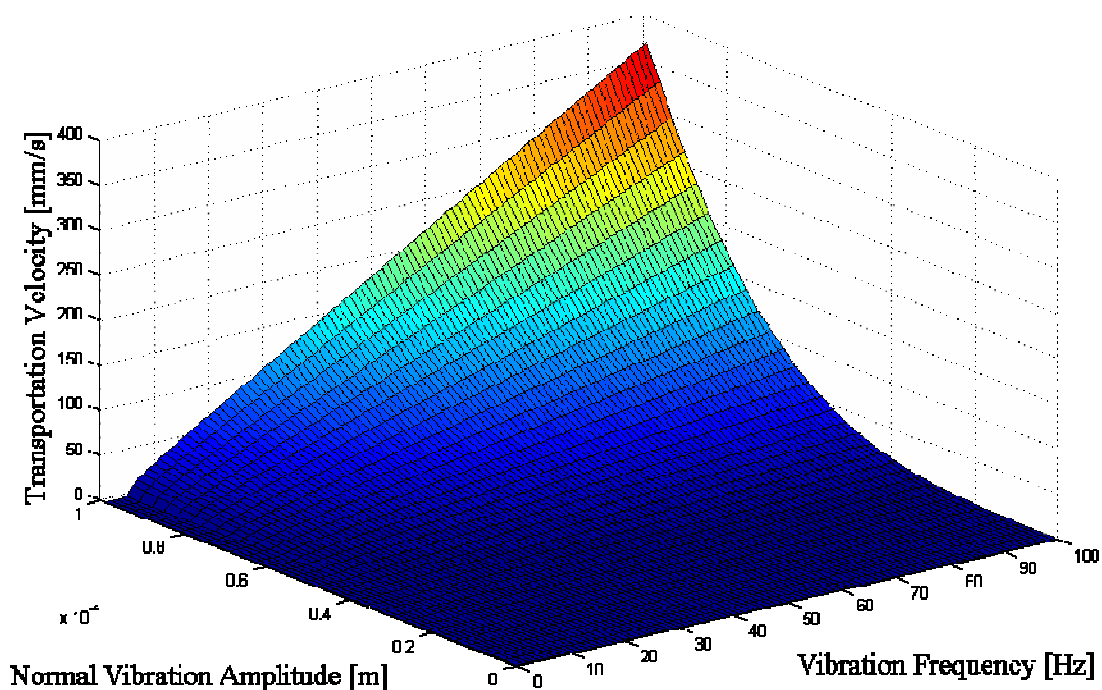


Figure 5.22 Transportation velocity versus frequency and amplitude of vibration.

The normal vibration amplitude is given by:

$$A_{0N} = A_0 \sin(\beta)$$

where A_{0N} is the normal amplitude, A_0 is the amplitude and β is the excitation angle.

The transportation velocity rises if the vibration frequency and normal amplitude rise.

This result can be observed from figure 5.22.

The transportation velocity in function of the excitation angle and the amplitude is shown in the figures 5.23. The used parameters are: $f=60\text{Hz}$, $\alpha=16^\circ$, $\delta=0^\circ$, $R=0.8\text{m}$, $a=0.15\text{cm}$, $b=1\text{cm}$, $h=5\text{cm}$, $\gamma=5^\circ$, $\delta=2^\circ$ and $\mu=0.3$. The maximum velocity is obtained in the region $A_0=[0.9-1]\text{mm}$, and $\beta=[0-25^\circ]$.

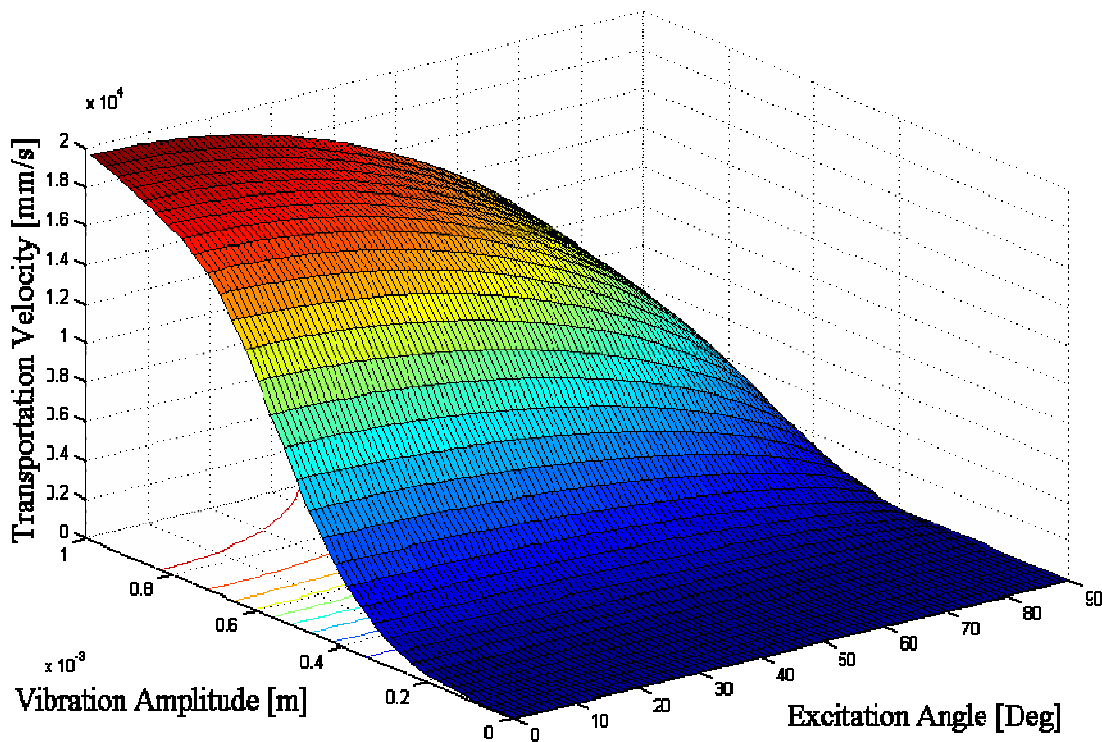


Figure 5.23 Transporting velocity versus inclination angle and vibration amplitude.

Figure 5.23 shows high transportation velocity values for high vibration amplitudes and small excitation angles. This graphic shows an optimal range for high vibration amplitudes values and small excitation angles values in the range of 0° to 40° . These values agree with the typical values presented in Boothroyd (1992).

In the figure 5.24 the variation of the transportation velocity in function of the frequency and inclination angle is shown. The used parameters are: $A_0=0.35\text{mm}$, $\alpha=16^\circ$, $\delta=0^\circ$, $R=0.6\text{m}$, $a=0.15\text{cm}$, $b=1\text{cm}$, $h=5\text{cm}$, $\gamma=5^\circ$ and $\mu=0.3$. The combined effect of the frequency and excitation angle is very high on the velocity, this is observed in the curvature of the contour curves.

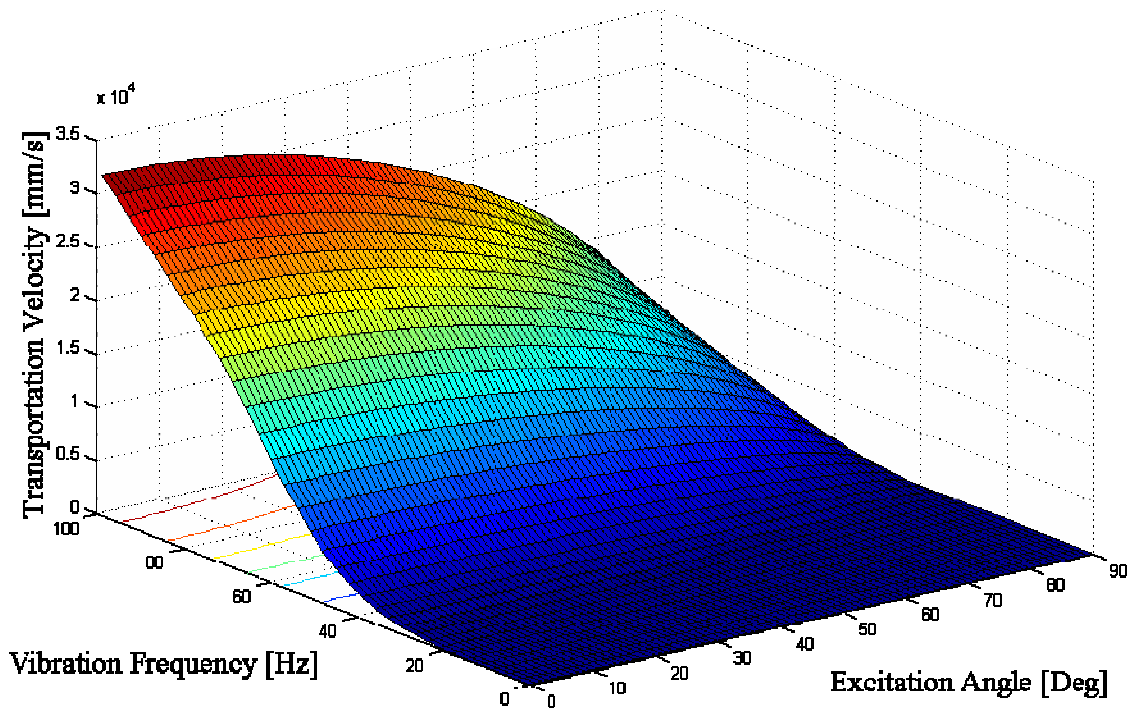


Figure 5.24 Transportation velocity versus frequency and excitation angle.

The obtained result of this graphic agrees with the previous results. The transportation velocity rises for high vibration frequency values and small excitation angles values. The range of optimal values is high vibration frequency values and excitation angle from 0° to 35° .

The figure 5.25 shows the variation of the transportation velocity in function of the excitation angles. The combined effect of the angles is inversely proportional to the velocity. The used parameters are: $A_0=1mm$, $f=60Hz$, $\delta=0^\circ$, $a=0.15cm$, $b=1cm$, $h=5cm$, $\gamma=0^\circ$, $R=0.8m$ and $\mu=0.3$.

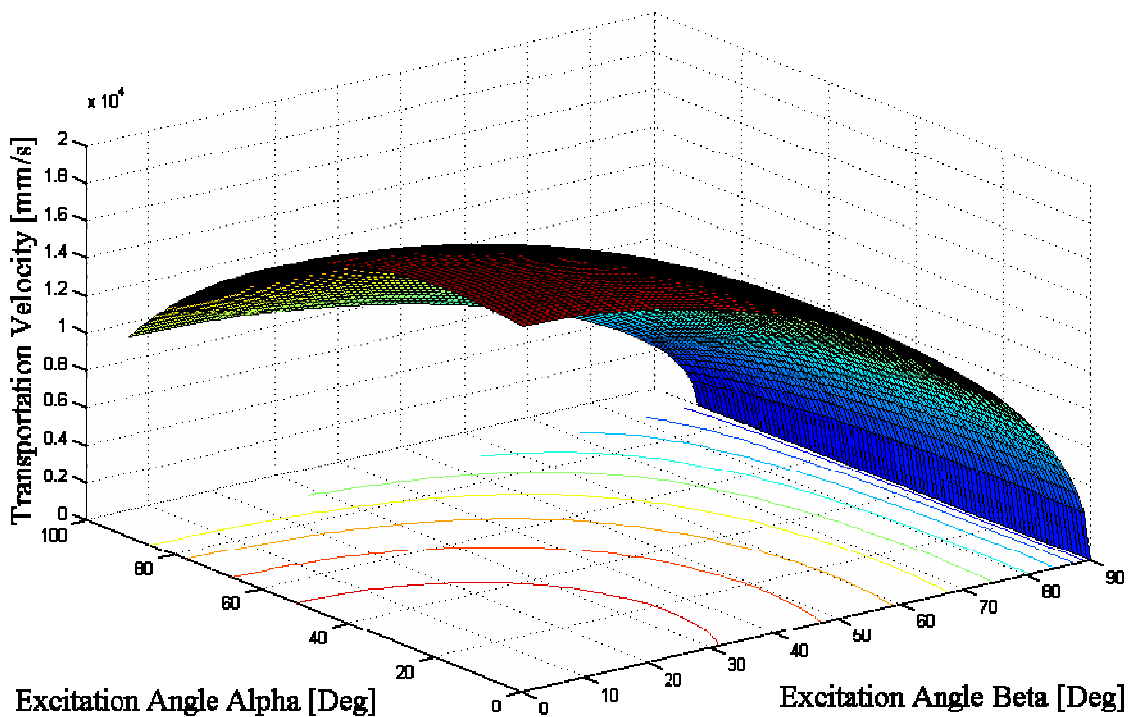


Figure 5.25 Transportation velocity versus excitation angles.

The results of this figure show an optimal region of excitation for the intervals from 0° to 45° for α and from 0° to 35° for β . These results agree with the real values and typical values given by Boothroyd (1992).

The figure 5.26 shows the transportation velocity versus the inclination angles. The effect of the angle δ is a small decrease in the velocity value. This decrease is consequence of the increase of the normal force between the wall and the part. The used parameters are: $A_0=1\text{mm}$, $f=60\text{Hz}$, $a=0.15\text{cm}$, $\alpha=0^\circ$, $\beta=5^\circ$, $b=1\text{cm}$, $h=5\text{cm}$, $\gamma=5^\circ$, $R=0.8\text{m}$ and $\mu=0.3$.

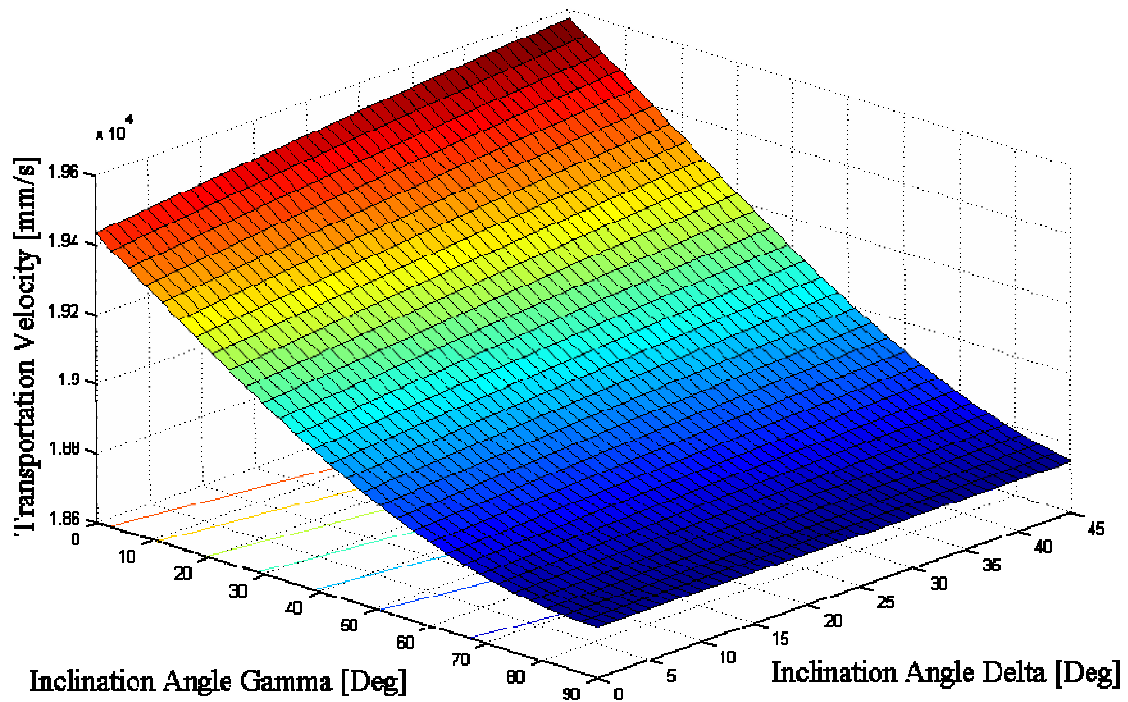


Figure 5.26 Transportation velocity versus excitation angles.

The figure 5.26 shows small transportation velocity values for high values of gamma due to the weight component rise which opposes the motion direction. The delta effect is small.

The figure 5.27 shows the variation of the transportation velocity versus the friction coefficient and the frequency. The friction effect is to decrease the velocity of transportation if the friction increases. The used parameters are: $Ao=1mm$, $\gamma=5^\circ$, $\delta=2^\circ$, $a=0.15cm$, $\alpha=16^\circ$, $\beta=5^\circ$, $b=1cm$, $h=5cm$ and $R=0.8m$.

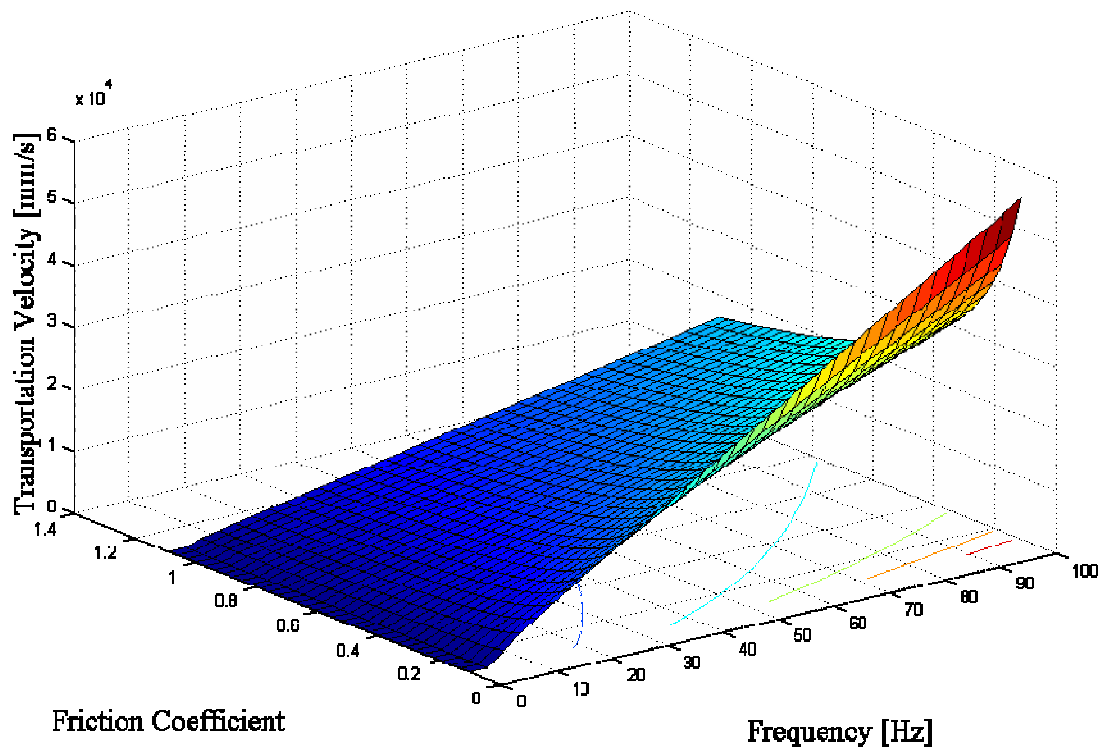


Figure 5.27 Transportation velocity versus friction coefficient and frequency.

The figure 5.27 shows high transportation velocity values for small values of the friction coefficient. This result is acceptable because the energy of motion decreases due to the friction forces. There is an ideal motion behavior if the friction forces are zero.

5.4 Comparison of Results

The figure 5.28 shows a comparison between the proposed model in this work versus the results obtained in the work of Wolfsteiner and Pfeiffer (2000). These results were obtained with the following parameters: $f=100\text{Hz}$, $\mu=0.3$, $\alpha=5^\circ$, $\beta=15^\circ$, $Ao=0.35\text{mm}$ and $\delta=0^\circ$, dimension of the part $5\text{cm} \times 1\text{cm} \times 0.15\text{cm}$.

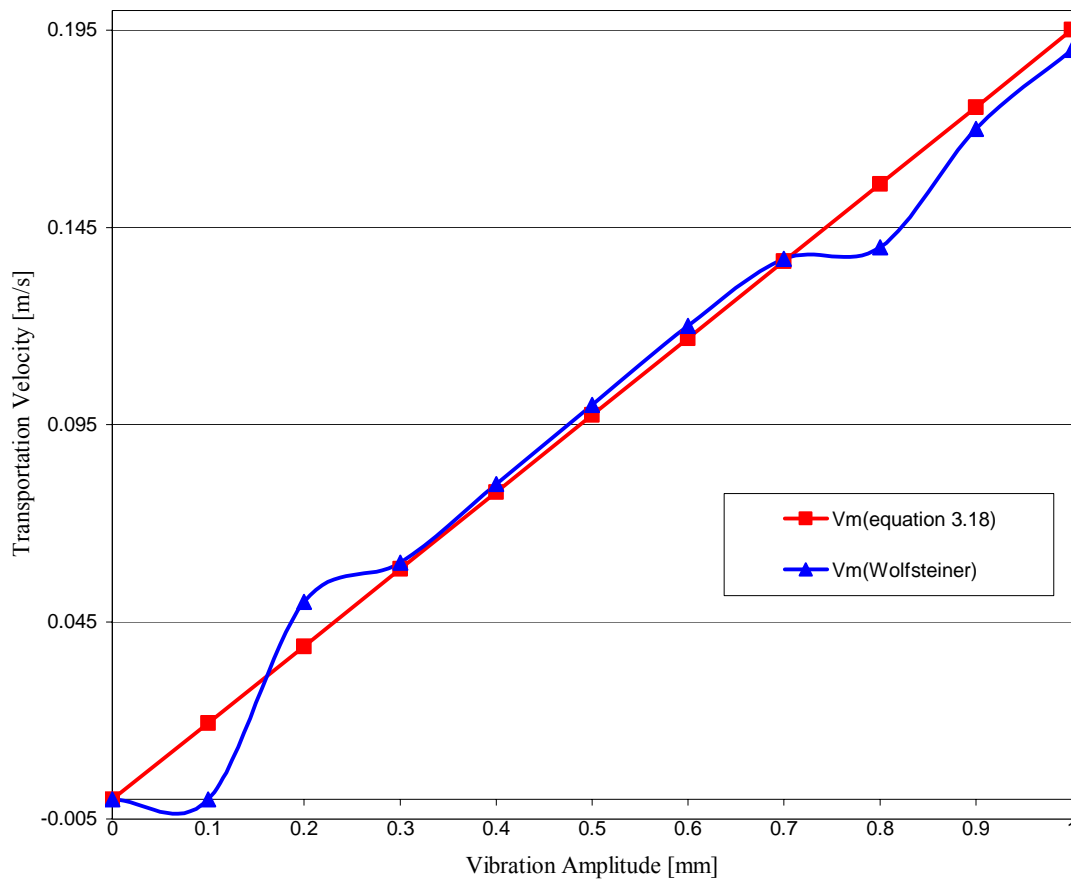


Figure 5.28 Comparison of results for transportation velocity (Wolfsteiner and Pfeiffer).

The velocity measured by Wolfsteiner and Pfeiffer was the real velocity. The velocity plotted is the average transportation velocity of the parts. The figure 5.28 shows that the proposed model is adequate to describe the physical phenomenon calculated with equation 3.18.

The figure 5.29 shows a comparison between the proposed model in this work versus the result obtained in the work of Boothroyd (1992). These results were obtained with the following parameters: $f=60\text{Hz}$, $\mu=0.3$, $\alpha=0^\circ$, $\gamma=0^\circ$ and $\delta=0^\circ$

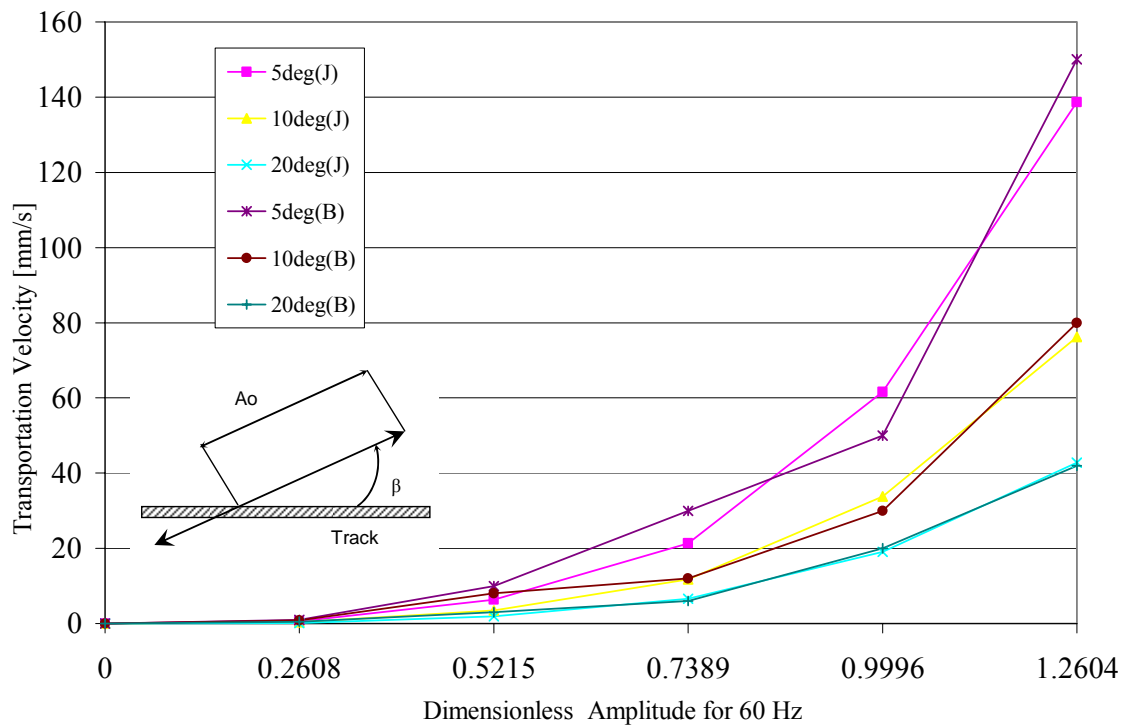


Figure 5.29 Comparison of results for the transportation velocity: B= Boothroyd (1992), J= Proposed Model.

The velocity plotted is the average transportation velocity of the parts. Boothroyd employed a two-dimensional model for the transportation velocity. The figure 5.29 shows that the proposed model using equation 3.18 is adequate to describe the physical phenomenon.

CHAPTER 6

Conclusions and Recommendations

6.1 Conclusions

- The presented model of the part feeder dynamics considered the main physical phenomena of the transportation process including multiple unilateral contacts based in the second Newtonian law and the Coulomb friction.
- The model shows that the kinematic parameters such as relative velocities and accelerations depend of interactions between geometric and vibrations parameters.
- The part is in contact if the normal force is compressive and the relative normal acceleration is zero or if the normal force is zero and the relative normal acceleration is greater that zero.
- The motion for a part in contact is separation or continual sliding. The condition for a unique solution depends of the friction.

- The transportation velocity of the rectangular part on the narrow track depends on the friction coefficient, vibration frequency, vibration amplitude, the track inclination angles, bowl radius, excitation angles, geometry and parts dimension.
- The screw theory is employed to model the physical phenomenon of the cylindrical part on the horizontal plane. This concept is adequate for complex restriction conditions.
- The combined effect of the friction coefficient and the vibration angle is the displacement of the work range; this result is shown in the figures 5.13 and 5.14. The friction coefficient effect is a hyperbolic behavior of the acceleration surface in the y direction. This effect is significant in the regions for small and high values of excitation angles.
- The y acceleration behavior is parabolic with respect to the frequency and sinusoidal with respect to the excitation angles, figure 5.13. This acceleration increases the friction forces and decreases the rate of transportation. The optimal range is in small excitation angle values and frequency values in the intersection of high accelerations in the x direction and small accelerations in the y direction.
- The angular acceleration increases if the frequency increases; this is shown in figure 5.21. Therefore, the work optimal frequency is the intersection of frequency curves for high accelerations in the x direction, small accelerations in the y direction and small angular accelerations.

- Figure 5.23 shows high transportation velocity values for high vibration amplitudes and small excitation angles. This graphic shows an optimal range for high vibration amplitudes values and small excitation angles values in the range of 0° to 40° .

6.2 Recommendations

For future work it is recommended to study the dynamic behavior for other parts types such as conic or complex geometry parts. Other activity is to employ the proposed model to determine the transporting velocity including many parts.

It is recommended to employ the screw theory for the analysis and simulation of a thin disc part on the feeder. Another future activity will be to improve of the model including deformation in the parts.

Bibliography

Andreas, Ugo and Casini, Paolo. 1999. "Dynamics of Three-Block Assemblies with Unilateral Deformable Contacts Part 1: Contact Modelling". *Earthquake Engineering and Structural Dynamics*, Vol. 28:1621-1636.

Andreas, Ugo and Casini, Paolo. 1999. "Dynamics of Three-Block Assemblies with Unilateral Deformable Contacts Part 2: Actual Application". *Earthquake Engineering and Structural Dynamics*. Vol. 28:1637-1649.

Boothroyd, Geoffrey. 1992. "Assembly Automation and Product Design". Marcel Dekker Inc.

Chang, Chau-Chin and Huston, S Ronald L. 2001. "Collisions of Multibody Systems". *Computational Mechanics 2001*, Vol.27: 436-444.

Dooner, David and Seireg, Ali A. 1995. "The Kinematic Geometry of Gearing". John Wiley and Son, Inc. New York.

Du, Winncy Y. 2001. "Motion Tracking of a Part on a Vibratory Feeder". *IEEE/ASME International Conference on the Advanced Intelligent Mechatronics Proceedings, Como Italy*: 75-80.

Gerstmayr Johannes and Schöberl. 2002. "A 3d Finite Element Approach to Flexible Multibody Systems". *Fifth World Congress on Computational Mechanics*. July 7-12, , Vienna Austria.

Huang, Chintien and Wang, Jin-Cheng. 2003. "The Finite Screw System Associated with the Displacement of a Line". *Journal of Mechanical Design*, 125: pp 105-109.

Kecskeméthy, A. Lange, C. and Grabner, G. 2001. "Object-Oriented Modeling of Multibody Dynamics Including Impacts". European Conference on Computational Mechanics, June 26-29, Cracow, Poland

Lipkin, H and Duffy, J. 2001. "Sir Robert Stawell Ball and Methodologies of Modern Screw Theory". J Mechanical Engineering Science Part C, Vol. 216 (1): 1-11.

Meirovitch, Leonard. 2001, "Fundamentals of Vibrations". McGraw Hill Inc, New York.

Pennock, Gordon and Oncu, B. A. 1992. "Application of Screw Theory to Rigid Body Dynamic". ASME Journal of Dynamic System , Measurement and Control, 114(2): 262-269.

Pennock, Gordon R. and Meehan, Patrick J. 2002. "Geometric Insight Into the Dynamics of a Rigid Body Using the Spatial Triangle of Screw". Journal of Mechanical Design, 124: pp 584-689.

Pfeiffer, Friedrich and Glocker, Christoph. 1993. "Multibody Dynamics with Unilateral Contacts". John Wiley and Son, Inc. New York.

Wolfsteiner, P and Pfeiffer, F. 2000. "Modeling, Simulation, and Verification of the Transporting Process in Vibratory Feeders". Z. Angew. Math. Mech. 80(1): 35-48.